5-2021

Quantum Dynamical Phenomena in Non-Hermitian and Magnomechanical Systems

Saeid Vashahri Ghamsari
University of Arkansas, Fayetteville

Quantum Dynamical Phenomena in Non-Hermitian and Magnomechanical Systems

A dissertation submitted in partial fulfillment
of the requirements for the degree of
Doctor of Philosophy in Physics

by

Saeid Vashahri-Ghamsari

University of Isfahan
Bachelor of Science in Physics, 2005
Shahid Beheshti University
Master of Science in Photonics, 2008

May 2021
University of Arkansas

This dissertation is approved for recommendation to the Graduate Council

Min Xiao, Ph.D.
Dissertation Director

Julio Gea-Banacloche, Ph.D.
Committee Member

Reeta Vyas, Ph.D.
Committee Member

Surendra Singh, Ph.D.
Committee Member

Mark Arnold, Ph.D.
Committee Member

ABSTRACT

In this dissertation, we have investigated quantum dynamics via three case studies. First, we studied a system of two coupled waveguides respectively carrying optical damping and optical gain in addition to squeezing elements in one or both waveguides. Such a system is expected to generate highly entangled light fields in the two waveguides. We, however, show that the degree of the created entanglement is significantly affected by the quantum noises associated with the amplification and dissipation. Because of the noise effect, one can only have nonzero entanglement for a limited time interval. Second, we generalized the first project by considering the gain saturation effect. The nonclassical properties of light are highly relevant to the gain saturation that influences the quantum noise. We explained the impact of gain saturation on a quantum light field dynamically evolving in the coupled system. In contrast to the ideal situation without gain saturation, one can achieve a steady state under the gain saturation. Moreover, gain saturation reduces the influence of amplification noise and thereby better preserves such quantum features as entanglement. We illustrate the effects of gain saturation by examining the time evolution of the Wigner function, the entanglement of the light fields, and the cross-correlation function between the two output modes. Significant differences exist between unsaturated and saturated situations, especially for low photon numbers. Finally, we studied a magnomechanical phonon laser beyond the steady-state that includes a microwave cavity with a ferromagnetic sphere installed in it. The system is simultaneously driven by a microwave field and a constant magnetic field. Using the decomposition of the time evolution operator, we linearize the equations of motion and solve them numerically. Our results show there is an oscillatory population inversion between the optical supermodes. However, it is possible to obtain stimulated phonons with relatively high numbers provided the system is operating in the resonant condition and the power of the drive field is higher than its threshold.

DEDICATION

To my wife, my mother, my sons, and to the memory of my father

ACKNOWLEDGEMENTS

The graduation carrier in the department of physics at the University of Arkansas is an invaluable experience in my life. First, I express my sincere thanks to my advisor, professor Min Xiao, for his continuous encouragement, support, and patience. I have enjoyed useful and helpful discussions with him. Professor Xiao helped me to obtain physical insight. And more importantly, he showed me the value of independence in the research.

I also acknowledge Professor Bing He, Universidad Mayor in Chile, for his continuous advice and support both when he was a visiting researcher at the University of Arkansas and also when he moved to Chile. In particular, I have benefitted from the mathematical techniques he taught me.

Likewise, I should thank all of my committee members. I enjoyed the useful course "Quantum Optics" that Professor Gea-Banacloche presented in the fall of 2018. I was pleased to take Electromagnetic Theory I and II with Professor Vyas and "Scientific Computation" with Professor Arnold. Also, I have invaluable experience in the undergraduate optics lab under the guidance of Professor Singh. Further, I wish to thank Professor Qing Lin at Huaqiao University, China, for helping me accomplish the numerical simulations.

I also should acknowledge Professor Claud Lacy, Professor William Oliver, and Professor Julia Kennefick for always accommodating my teaching requests and preferences as a TA. Their consideration has made my teaching experience very delightful.

Last but not least, I should express my heartfelt thanks to my wife for her support and support during my carrier. Without the help of my wife, I couldn't accomplish my research. Notably, she took care of my kids alone during the Covid-19 outbreak, which allowed me to focus on my research and dissertation writing.

TABLE OF CONTENTS

1 Introduction

Quantum dynamics describes the evolution of quantum operators over time. In particular, it deals with the motion, energy, and momentum exchanges of systems. Therefore, if a system interacts with its environment, the quantum dynamics provides information about the future of the system. Notably, if a system interacts with a thermal reservoir that introduces noise to the system, it is of interest to know how the system operators are impacted by this external unfavorable source.

Because of their mathematical complexities, quantum dynamical phenomena are neglected in many studies dealing with quantum systems. These systems are usually investigated under the assumption that the system does not evolve with time. In other words, it is assumed there is a steady-state for the system. However, this assumption is too optimistic for some particular systems, and they indeed evolve to a state much different from its initial state. The mathematical complexity mentioned above is mostly due to two distinct factors: (1) The noise that appears as a random drive force has a stochastic effect on the system. To avoid the stochastic effect, it is mostly assumed there is a steady-state for the system and the noise effects are ignored. (2) If one deals with a nonlinear interaction, the coupled equations of motion are nonlinear as well, and it is hard to solve such a system. In many nonlinear systems, to simplify the equations, it is assumed the system has a steady-state. Under this assumption, the nonlinear differential equations are converted to a system of algebraic equations whose solution is much more straightforward. These two cases are realistic in many circumstances. However, when one deals with the quantum features of light like the entanglement, one cannot ignore the noise effect, and the only way of including the noise is a dynamical approach. Also, there are situations at which the noise does not play an important role, but still there is no steady state for the system.

In this dissertation, we investigate three case studies that need a quantum dynamical description:

- The first is a coupled waveguide system, one of which carries optical gain and the other has an optical loss. This is a particular case of the so-called $\mathscr{PT}$-symmetric systems [1], a relatively new field of study that started in the late 1990s. If we are interested in the pure quantum features of light like entanglement, it is important to know if the noise impacts it. To answer this question, we should consider the system as a quantum dynamical case.

- The second case is the extension of the first system to a regime that the optical gain is saturated. The saturation effect itself is a dynamical phenomenon.

- The third is a "magnomechanical phonon laser" [2], which is a nonlinear system including a microwave cavity and a ferromagnetic element inside it. The system is simultaneously driven by a time-dependent microwave field and a constant magnetic field. Until recently, most schemes of phonon lasers are studied under the steady-state approximation (for example, see [3]), because this assumption allows one to linearize the relevant differential equations by converting each quantum operator to a classical steady-state value plus a small quantum fluctuation term. However, more explorations have shown such a description yields incorrect results [4]. In this thesis, we use a method called "decomposition of the evolution operator" that linearizes the relevant equations without the need for a steady-state assumption.

This chapter provides the necessary information needed for studying the systems mentioned above. In section 1.1, we introduce the notion of $\mathscr{PT}$-symmetric needed for chapter 2. Next, we illustrate the classical as well as quantum noise in section 1.2. Section 1.3 describes the method of the decomposition of the evolution operator that we use in chapter 4. As we will

study a magnomechanical phonon laser in chapter 4, in section 1.4, we provide a summary of the magnomechanical systems.

1.1 Parity-time symmetry formalism

1.1.1 Background

According to the axioms of quantum mechanics, the corresponding operators of physical observables should be Hermitian [5]. The Hermiticity of operators guarantees that the spectrum of energy to be real and the time evolution to be unitary. The energy of such systems is conservative. The conservation of energy is a fundamental concept for each closed system. However, in some situations, one is interested in a subspace of the closed system. The subsystem (we call it the open system) can exchange energy with its environment, which is the rest of the original system [6].

In the early decades of the twentieth century, George Gamow applied a phenomenological approach to the study of such an open system, say alpha decay of the nucleus [7]. Later, Lindblad proposed a more formal basis for describing the dynamics of open quantum systems [8]. According to the more rigorous approaches developed later, if a quantum system is coupled to its environment, the dynamics of the system becomes non-Hermitian [9]. Moreover, the dynamics features quantum jumps that introduce noise to the system. Without considering the noise, all commutation relations of the quantum operators would be invalid [6].

Intuitively, for studying "microscopic systems" one should consider the noise. However, for "macroscopic systems", a mean-field approach is widely used in which the quantum dissipation is encapsulated in a "non-Hermitian effective Hamiltonian" [10, 6]. The mean-field approach simplifies the analysis and reduces the number of degrees of freedom needed for describing the system. As we will see in this section, one can use the non-Hermitian effective Hamiltonian

for macroscopic optical systems like coupled gain-loss waveguides and resonators as long as the classical features of light are concerned [11]. Nonetheless, as we will see in chapters 2 and 3, the effective Hamiltonian approach fails to yield correct results when we investigate the non-classical features of light, such as entanglement. Although we deal with a macroscopic system in this case, we should apply a formalism that takes the noise into account.

1.1.2 Parity-time symmetry in quantum mechanics

In 1998, Bender and his colleagues showed a wide range of non-Hermitian Hamiltonian demonstrate an entirely real spectrum of energy provided the Hamiltonian, $\hat{H} = \hat{p}^2/2m + \hat{V}(x)$, respects the parity-time ($\mathscr{P}\mathscr{T}$) symmetry [1, 12]. In the mathematical language, $[\hat{H}, \hat{\mathscr{P}}\hat{\mathscr{T}}] = 0$. The parity operator reverses the coordinate position by mirror reflection ($\hat{x} \to -\hat{x}$ and $\hat{p} \to -\hat{p}$), whereas the time-reversal operator flips the direction of time evolution ($i \to -i$) [13]. If $\hat{V}(x) = \hat{V}^*(-x)$, the aforementioned commutation relation is satisfied [14]. This means the real (imaginary) part of the potential should be an even (odd) function. One should notice that the mentioned commutation relation is a necessary (but not sufficient) condition for the realness of the eigenvalues. To ensure an entirely real spectrum, not only the commutation relation must be satisfied, but also parameters of the non-Hermitian Hamiltonian must be restricted within certain threshold values [6, 10, 13, 15].

We clarify this extra constraint by investigating a couple of examples. Suppose we have a toy model for which $\hat{H} = \hat{p}^2 - (ix)^N$, where N is a real number [1]. The potential satisfies $\hat{V}^*(-x) = -\big(-i(-x)\big)^N = -(ix)^N = \hat{V}(x)$, and hence $[\hat{H}, \hat{\mathscr{P}}\hat{\mathscr{T}}] = 0$ for all values of N. However, as Figure 1(a) shows, the spectrum undergoes a $\mathscr{P}\mathscr{T}$-symmetry phase transition as N varies. For $N > 2$, the Hamiltonian possesses unbroken $\mathscr{P}\mathscr{T}$-symmetry with a pure real-valued spectrum. If $N < 2$, the spectrum becomes partially complex with finite (or, none if $N < 1$) real values and

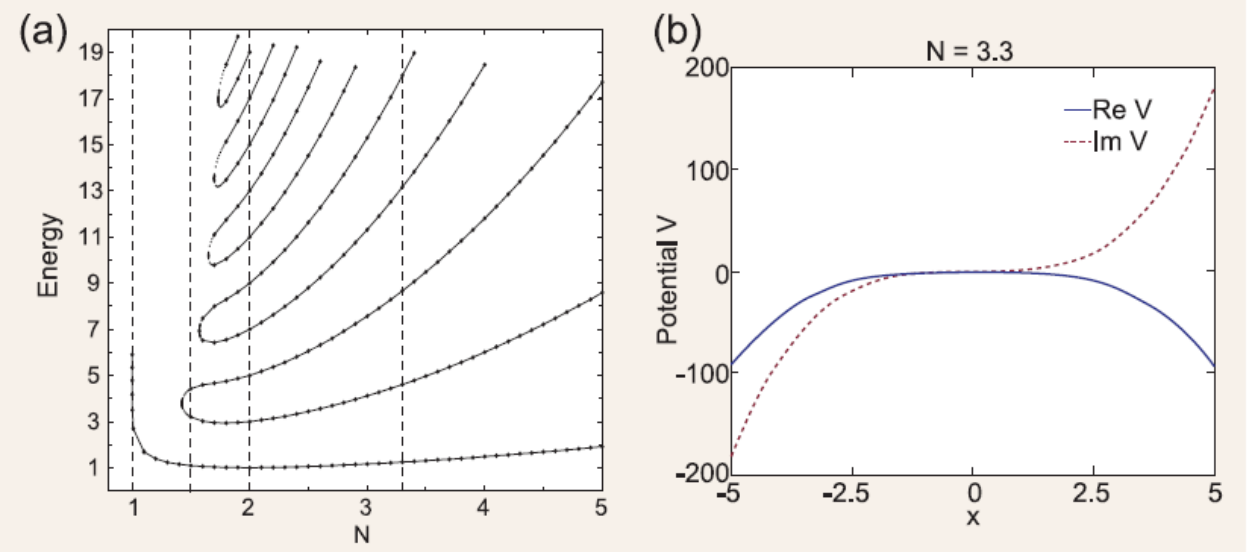

Figure 1.1: $\mathscr{P}\mathscr{T}$-symmetry phase transitions for $\hat{H} = \hat{p}^2 - (ix)^N$. (a) For $N > 2$, the spectrum of energy is pure real and the system is in the $\mathscr{P}\mathscr{T}$-symmetry phase. If $N < 2$, the spectrum is partially complex with finite (or, when $N < 1$, none) real eigenvalues and infinite pairs of complex conjugate ones. This the range at which the system is in the $\mathscr{P}\mathscr{T}$-broken phase. At $N = 2$, the system changes its phase. (b) Real and imaginary parts of the potential [15].

infinite "pairs" of complex conjugate values. The threshold value $N = 2$ is a phase transition point across which the system switches from a $\mathscr{P}\mathscr{T}$-symmetry to $\mathscr{P}\mathscr{T}$-broken [15]. This point is called "exceptional point" and possesses unique features specially in optics [16].

At the exceptional point, the eigenvalues as well as the eigenvectors coalesce [6, 10, 15]. This is in contrast to the common degeneracy in quantum mechanics for which two or more different measurable states of a quantum system share the same eigenvalue [5]. We explain the coalescence by considering the following Hamiltonian of a two-component system (i.e., a gain-loss coupled system):

$$\hat{H} = \begin{pmatrix} -ig & J \\ J & ig \end{pmatrix} \tag{1.1}$$

where J is the coupling parameter and g $(-g)$ is the gain (loss). Let $g/J < 1$. We define $\theta =$

$\sin^{-1}(g/J)$ so the following equations look nicer. Then, the eigenvalues of the Hamiltonian are $E_{1,2} = \pm J\cos(\theta)$ and the bi-orthogonal eigenvectors are $|\varphi_{1,2}\rangle = \left(1, \pm e^{\pm i\theta}\right)^T$. This regime is called the exact $\mathscr{P}\mathscr{T}$-symmetry phase for which the two eigenmodes are distributed over the gain and loss sites. In this case, neither of the eigenmodes experiences a net gain or loss.

At the exceptional point where $J = g$, we have $E_1 = E_2 = 0$ and $|\varphi_1\rangle = |\varphi_2\rangle = \left(1, i\right)^T$, i.e., we have only one eigenvalue and one eigenvector.

For $g/J > 1$, if we redefine $\theta = \cosh^{-1}(g/J)$, then the eigenvalues and eigenvectors are $E_{1,2} = \pm iJ\sinh(\theta)$ and $|\varphi_{1,2}\rangle = \left(1, ie^{\pm\theta}\right)^T$, respectively. This regime is called $\mathscr{P}\mathscr{T}$-broken regime at which one mode enjoys amplification and the other undergoes dissipation [6, 15].

1.1.3 $\mathscr{P}\mathscr{T}$-symmetry in optics

The realization of $\mathscr{P}\mathscr{T}$-symmetry in quantum mechanics is challenging because of the fundamental difficulties arising from the operators [17]. On the other hand, if we compare the Schrödinger equation with the paraxial wave equation in optics, we notice they are mathematically isomorphic, and hence the $\mathscr{P}\mathscr{T}$-symmetric formalism can be generalized to optics (let $\hbar = 1$) [11]:

$$i\frac{\partial\Psi(x,t)}{\partial t} = \Big[-\frac{1}{2m}\frac{d^2}{dx^2} + V(x)\Big]\Psi(x,t), \tag{1.2}$$

$$i\frac{\partial E(x,z)}{\partial z} = \Big[-\frac{1}{2k_0 n_0}\frac{d^2}{dx^2} + k_0\big(n_R(x) + in_I(x)\big)\Big]E(x,z). \tag{1.3}$$

In equation 1.3, the propagation distance z along the optical axis replaces time, $E(x,z)$ is the transverse electric field, k_0 is the free space wave vector, n_0 is the background index, and $n(x) = k_0\big(n_R(x) + in_I(x)\big)$ is the complex refractive index that plays the role of potential. If the paraxial wave satisfies the condition $n(x) = n^*(-x)$, the optical system is $\mathscr{P}\mathscr{T}$-symmetric . If the sign of

Im[$n(x)$] is negative (positive), it represents optical gain (loss). The manipulation of refractive index (and therefore gain and loss) is much easier in optics than engineering the potential in quantum mechanics [13].

For the first time, El-Ghanainy and his colleagues proposed the idea of $\mathscr{P}\mathscr{T}$-symmetry in optics [11]. They applied this formalism to a coupled gain-loss waveguide system with equal rates of gain and loss, whose result is a coupled of differential equations similar to equation (1.3), one with a positive imaginary part of the refractive index and the other with a negative imaginary part. After more theoretical works [18, 19, 20, 21], $\mathscr{P}\mathscr{T}$-symmetry was verified in a coupled gain-loss waveguide system with complex optical potentials [22, 14]. In these pioneering experimental studies of $\mathscr{P}\mathscr{T}$-symmetry , spontaneous $\mathscr{P}\mathscr{T}$-symmetry breaking and power oscillations violating left–right symmetry were observed. It is notable that these two experimental cases are "passive" $\mathscr{P}\mathscr{T}$-symmetric systems [23] for which there is no optical gain, but one waveguide is passive and the other is neutral. In [22] it is shown the imposed complex refractive index distribution satisfies the $\mathscr{P}\mathscr{T}$-symmetry requirement.

In addition to two coupled waveguides, $\mathscr{P}\mathscr{T}$-symmetry has also been demonstrated in other systems such as coupled silica microtoroids [24, 25], microring resonators [26], and photonic crystal cavities [27, 28, 29]. The subsequent theoretical and experimental studies on this field have shown interesting features that are difficult to implement with non-$\mathscr{P}\mathscr{T}$-symmetric optical systems. To mention a few, we should refer to loss-induced transparency [22], power oscillations [18, 14], unidirectional invisibility [30, 31, 32], and $\mathscr{P}\mathscr{T}$-symmetric lasers [33]. The study of $\mathscr{P}\mathscr{T}$-symmetric formalism is not restricted to optics; similar research activities have been extended to other physical settings such as electronics [34], microwaves [35], mechanics [36], acoustics [37], and atomic systems [38, 39, 40, 41].

These studies are based on the paraxial wave equation for which light is a classical field. But in 2012 Agarwal used a second quantization formalism to investigate the spontaneous generation of photons in the transmission of quantum fields in a coupled gain-loss waveguide system [42]. This approach treats light as a quantum field and takes the noise into account. We will follow this approach in chapters 2 and 3.

1.2 Noise in Open Quantum Systems

1.2.1 Classical versus Quantum Noise

A physical system with a few degrees of freedom coupled to an environment or bath with many (possibly, infinite) degrees of freedom is called open. The coupling of the system to the bath inevitably changes the time evolution of the system operators compared to the same ideal isolated system. This change in the time evolution happens in classical as well as in quantum systems [43].

In general, there are two types of interactions between the system and the bath: (1) external control fields that drive the evolution of the system, (2) Uncontrolled interactions such as the thermal motion of the bath elements, or the background magnetic field of the environment. The latter interactions lead to deviations between the targetted and the actual time evolutions and a loss of coherence [44]. We call the uncontrolled interactions noise as they cause unfavorable results.

The origin of the classical noise is the fluctuations in the motion of particles and the variation of the number of particles within a given volume. A well-known example is a Brownian motion of particles (say, the pollen grains) in a fluid. The particles not only experience damping due to the viscous fluid, but they also undergo a zigzag motion around the average path. Langevin introduced a random drive force (noise) that explains the zigzag motion [45, 46]. Quantum noise, on the other hand, is due to the Heisenberg uncertainty relations between two non-commuting

operators. As an example, consider an electron in a potential well. Although there is no classical fluctuation and hence no classical noise, the uncertainty relation does not allow the confined electron to remain motionless. The operator

$$\hat{j} = \frac{e}{m}\hat{p}, \tag{1.4}$$

is proportional to the current. Knowing the Fourier transform of $\langle \hat{j}(0)\hat{j}(t)\rangle$, one can find the frequency spectrum of the quantum fluctuation. If $|\psi(0)\rangle$ is the wavefunction in the Heisenberg picture, the expectation value of an arbitrary operator $\hat{O}$ is defined as

$$\langle \hat{O}(t)\rangle = \langle \psi(0)|\exp[i\hat{H}t]\hat{O}(0)\exp[-i\hat{H}t]|\psi(0)\rangle. \tag{1.5}$$

where we assumed $\hbar = 1$. Then we can write $\langle \hat{j}(t)\hat{j}(0)\rangle$ as a sum over a complete set of states, which can be chosen as energy eigenstates:

$$\langle \hat{j}(t)\hat{j}(0)\rangle = \left(\frac{e}{m}\right)^2 \sum_n \exp\big[-i\big(\big(E_n - E_0\big)t\big)\big]|\langle \psi_n|\hat{p}|\psi_0\rangle|^2. \tag{1.6}$$

This spectrum has only positive frequencies, i.e., frequencies corresponding to transitions from ground states to excited states. If excited states are occupied too, positive as well as negative frequencies will appear in the spectrum. If $\hat{j}(t)$ and $\hat{j}(0)$ are interchanged, the correlation function with the electron in the ground state would have negative frequencies instead of positive frequencies. Therefore,

$$\langle \hat{j}(0)\hat{j}(t)\rangle \neq \langle \hat{j}(t)\hat{j}(0)\rangle. \tag{1.7}$$

The electron is a charged particle. Thus the momentum fluctuation is a source of electromagnetic radiation and hence a source of quantum noise [45].

1.2.2 Quantum Heisenberg-Langevin Equation

We need a generic model for describing the quantum noise. Therefore, we should introduce a model for the system and the bath. In addition, we need to make some assumptions. We assume that the bath is an assembly of harmonic oscillators. This is a reasonable assumption specially for the quantum optical systems, because in this case the bath is the electromagnetic field, which is truly an assembly of harmonic oscillators [47]. The oscillators of the bath must satisfy the following conditions in order to make a solid model for the quantum noise:

- There should be a smooth, dense spectrum of oscillator frequencies (for the electromagnetic field, naturally the normal modes in a large volume demonstrate a smooth, dense frequency spectrum);
- The coupling of the system to the bath operators should be linear in the bath harmonic oscillator operators;
- The coupling coefficients of the system to the bath operators must be a smooth function of the frequencies.

Let the total Hamiltonian is

$$\hat{H} = \hat{H}_{sys} + \hat{H}_B + \hat{H}_{int}, \tag{1.8}$$

where

$$\hat{H}_B = \int_{-\infty}^{\infty} d\omega\, \omega\, \hat{f}^{\dagger}(\omega)\hat{f}(\omega) \tag{1.9}$$

is the bath Hamiltonian and

$$\hat{H}_{int} = i\int_{0}^{\infty} d\omega\, \kappa(\omega)\big[\hat{c} - \hat{c}^{\dagger}\big]\big[\hat{f}^{\dagger}(\omega) + \hat{f}(\omega)\big] \tag{1.10}$$

is the interaction Hamiltonian. $\hat{f}(\omega)$ is a boson annihilation operator of the bath satisfying $\left[\hat{f}(\omega),\hat{f}^{\dagger}(\omega')\right] = \delta(\omega-\omega')$ and $\hat{c}$ is a system operator. We assume that for the bare system we have $\hat{c}(t)\rightarrow\hat{c}(t)e^{-i\omega_0 t}$ where ω_0 is the resonance frequency of the system and $\hat{f}(\omega)\rightarrow\hat{f}(\omega)e^{-i\omega t}$. The system with this resonance frequency is coupled to a band of frequencies of the bath centered around ω_0. So, virtually one can redefine the limits of the integral as

$$\int_{\omega_0-\vartheta}^{\omega_0+\vartheta} d\omega \ldots \tag{1.11}$$

with cutoff $\vartheta \ll \omega_0$. There are several time scales that should be separated. One is the optical frequency ω_0 which is much larger than the cutoff. The cutoff itself is much larger than the typical frequencies of the system dynamics. It is also much larger than the frequency scale induced by the system-bath coupling, i.e., the decay rates. Moreover, we assume a smooth system-bath coupling $\kappa(\omega)$ in the frequency interval. So, we set $\kappa(\omega)\rightarrow\sqrt{\gamma/2\pi}$, which is a constant within the interval. This is called Markov approximation. Physically, a quantum Markovian description is an approximation where the environment is modeled as a heat bath with a short correlation time and weakly coupled to the system [48].

Now we can apply the rotating wave approximation and ignore fast oscillating terms $e^{\pm i(\omega+\omega_0)t}$. In addition, we assume that the time scales of the system are much smaller than $1/\vartheta$ in the weak coupling limit where γ is rather small. This means we can set the limits of integral from $-\infty$ to ∞. Putting all these approximations together, we can rewrite the interaction Hamiltonian as

$$\hat{H}_{int} = \frac{i}{\sqrt{2\pi}}\int_{-\infty}^{\infty} d\omega\,\sqrt{\gamma}\left[\hat{f}^{\dagger}(\omega)\hat{c}-\hat{c}^{\dagger}\hat{f}(\omega)\right] \tag{1.12}$$

If we apply the Heisenberg equations of motion for the bath operators and an arbitrary

system operator $\hat{a}$, we obtain

$$\frac{d\hat{f}(\omega)}{dt} = -i\omega\,\hat{f}(\omega) + \sqrt{\frac{\gamma}{2\pi}}\hat{c}, \tag{1.13}$$

whose solution is

$$\hat{f}(\omega) = e^{-i\omega(t-t_0)} + \sqrt{\frac{\gamma}{2\pi}}\int_{t_0}^{t} e^{-i\omega(t-t')}\hat{c}(t')dt' \tag{1.14}$$

and

$$\frac{d\hat{a}}{dt} = -i\big[\hat{a},\hat{H}_{sys}\big] + \sqrt{\frac{\gamma}{2\pi}}\int_{-\infty}^{\infty} d\omega\,\Big\{\hat{f}^{\dagger}(\omega)[\hat{a},\hat{c}] - [\hat{a},\hat{c}^{\dagger}]\hat{f}(\omega)\Big\} \tag{1.15}$$

We define

$$\hat{f}_{in}(t) = \frac{1}{\sqrt{2\pi}}\int d\omega\, e^{-i\omega(t-t_0)}\hat{f}_0(\omega). \tag{1.16}$$

Noting that

$$\int_{-\infty}^{\infty} d\omega\, e^{-i\omega(t-t')} = 2\pi\delta(t-t') \tag{1.17}$$

we conclude that

$$\big[\hat{f}_{in}(t),\hat{f}_{in}^{\dagger}(t')\big] = \delta(t-t'). \tag{1.18}$$

Inserting (1.14) in (1.15) and using (1.18), we obtain the following equation called quantum Langevin equation [47]:

$$\frac{d\hat{a}}{dt} = -i\big[\hat{a},\hat{H}_{sys}\big] - \big[\hat{a},\hat{c}^{\dagger}\big]\Big(\frac{\gamma}{2}\hat{c} + \sqrt{\gamma}\,\hat{f}_{in}(t)\Big) + \Big(\frac{\gamma}{2}\hat{c}^{\dagger} + \sqrt{\gamma}\,\hat{f}_{in}^{\dagger}(t)\Big)\big[\hat{a},\hat{c}\big]. \tag{1.19}$$

1.2.3 The Stochastic Schrödinger Equation

There is also an alternative formulation in terms of a master equation for a reduced system density operator together with the quantum fluctuation regression theorem, but we don't use it in this thesis. The mathematical basis for these two methods is quantum stochastic calculus, which is a non-commutative analog of Ito's stochastic calculus [47]. Gardiner and Collett demonstrated the

connection between the more physically motivated Heisenberg-Langevin equations and the more mathematically precise "quantum stochastic differential equations" [49]. In particular, Gardiner developed a formulation called "quantum stochastic Schrödinger equation" for the time evoultion operator $\hat{U}(t) = \exp\big(-i\big[\hat{H}_B + \hat{H}_{sys}\big]t\big)$ of the system interacting with Bose fields $\hat{f}(t)$ and $\hat{f}^\dagger(t)$. These operators satisfy the following commuatation relations (with respect to the vacuumm state $|0\rangle$) [46]:

$$\langle \hat{f}(t)\hat{f}^\dagger(t')\rangle = \delta(t-t'), \tag{1.20}$$

$$\langle \hat{f}^\dagger(t)\hat{f}(t')\rangle = \langle \hat{f}(t)\hat{f}(t')\rangle = \langle \hat{f}^\dagger(t)\hat{f}^\dagger(t')\rangle = 0. \tag{1.21}$$

We define

$$\hat{B}(t) = \int_0^t \hat{f}(s)\,ds. \tag{1.22}$$

A quantum stochastic calculus is based on the following increment:

$$d\hat{B}(t) = \hat{B}(t+dt) - \hat{B}(t). \tag{1.23}$$

The corresponding Ito's rules for for these increment are

$$\begin{aligned} \big[d\hat{B}(t)\big]^2 = \big[d\hat{B}^\dagger(t)\big]^2 = 0, \\ d\hat{B}(t)d\hat{B}^\dagger(t) = dt, \\ d\hat{B}^\dagger(t)d\hat{B}(t) = 0. \end{aligned} \tag{1.24}$$

Putting all this information together, we obtain the Ito form of the quantum stochastic Schrödinger equation [46]:

$$d\hat{U}(t) = \Big\{\Big(-i\hat{H} - \frac{1}{2}\gamma\,\hat{c}^\dagger\hat{c}\Big)\,dt + \sqrt{\gamma}\,d\hat{B}^\dagger(t)\,\hat{c} - \sqrt{\gamma}\,d\hat{B}(t)\,\hat{c}^\dagger\Big\}, \tag{1.25}$$

whose formal solution is

$$\hat{U}(t) = \hat{T}\exp\int_0^t \Big(-i\hat{H}\,ds + \sqrt{\gamma}\,d\hat{B}^\dagger(s)\,\hat{c} - \sqrt{\gamma}\,d\hat{B}(s)\,\hat{c}^\dagger\Big), \tag{1.26}$$

where $\hat{T}$ is the time ordering operator. For a system operator $\hat{a}$, we define a Heisenberg operator as $\hat{a}(t) = \hat{U}^{\dagger}(t)\hat{a}\hat{U}(t)$. Then,

$$\begin{aligned} d\hat{a}(t) &\equiv \hat{a}(t+dt) - \hat{a}(t) \\ &= \hat{U}^{\dagger}(t+dt,t)\hat{a}(t)\hat{U}(t+dt,t) - \hat{a}(t) \\ &= -i\big[\hat{a}, \hat{H} - i\sqrt{\gamma}\, d\hat{B}(t)\,\hat{c}^{\dagger} + i\sqrt{\gamma}\, d\hat{B}^{\dagger}(t)\,\hat{c}\big]dt \\ &+ \frac{\gamma}{2}\Big(2\hat{c}^{\dagger}\hat{a}\hat{c} - \hat{a}\hat{c}^{\dagger}\hat{c} - \hat{c}^{\dagger}\hat{c}\hat{a}\Big)dt \end{aligned} \tag{1.27}$$

This equation is an alternative to the Langeving equation, and we will use it in the next chapters to investigate the time evolution of the operators of the system coupled to a bath.

1.3 The Time Decomposition Method in Nonlinear Systems

1.3.1 Background and motivation

In quantum optics, sometimes we deal with a cavity system biased by an electromagnetic wave (classical or quantum), and meanwhile, it is coupled to a heat bath that introduces noise to the system. Also, there might be an element inside the cavity that generates nonlinear effects such as Kerr nonlinearity [50], optomechanical interaction [51], or magnomechanical interaction [52]. The equation of motion of such a system has nonlinear terms, and generally it is hard to solve it.

In many practical cases, the external drive field is strong and can be treated classically. Therefore, if $\hat{a}$ is an operator of the system, it is possible to convert it to a classical steady-state plus a quantum fluctuation term: $\hat{a} \rightarrow \alpha_s + \delta\hat{a}$. This is the common approach to linearize the nonlinear differential equations, and it is applied to many cases (see, for example, [53] and the review article [51]). However, if the external field is weak (for example, a single photon field [54]), one cannot use a steady-state approximation. There is another method, called time-evolution decomposition,

developed by B. He, that applies to strong as well as weak bias fields [54, 55, 56, 57]. This method linearizes the differential equations without breaking an operator to a steady-state and a fluctuation term. Also, it simplifies the calculation of the expectation value of an arbitrary function of the field operators without need of solving the master equation. These merits make this method a good alternative to the conventional method of linearizing, especially when we are interested in the dynamical behavior of the system such as the dynamical phonon laser in a magnomechanical system (chapter 4).

1.3.2 The decomposition of the time evolution operator

Suppose the total Hamiltonian of a system is composed of two "time-dependent" parts that in general do not commute with each other:

$$\hat{H} = \hat{H}_1(t) + \hat{H}_2(t), \quad [\hat{H}_1(t), \hat{H}_2(t)] \neq 0. \tag{1.28}$$

The time evolution operator is

$$\hat{U}(t) = \hat{T} \exp\Big(-i \int_0^t d\tau \, \big[\hat{H}_1(\tau) + \hat{H}_2(\tau)\big]\Big). \tag{1.29}$$

Also, one can decompose the evolution operator as follows:

$$\hat{T} \exp\Big(-i \int_0^t d\tau \, \big[\hat{H}_1(\tau) + \hat{H}_2(\tau)\big]\Big) = \hat{T} \exp\Big(-i \int_0^t d\tau \, \hat{V}_2(t,\tau)\hat{H}_1(\tau)\hat{V}_2^{\dagger}(t,\tau)\Big) \hat{T} \exp\Big(-i \int_0^t d\tau \, \hat{H}_2(\tau)\Big), \tag{1.30}$$

where $\hat{V}_2(t,\tau) = \hat{T} \exp\Big(-i \int_\tau^t d\tau' \hat{H}_2(\tau')\Big)$, and

$$\hat{T}\exp\Big(-i\int_0^t d\tau\,\big[\hat{H}_1(\tau)+\hat{H}_2(\tau)\big]\Big)=$$
$$\hat{T}\exp\Big(-i\int_0^t d\tau\,\hat{H}_1(\tau)\Big)\hat{T}\exp\Big(-i\int_0^t d\tau\,\hat{V}_1^{\dagger}(\tau,0)\hat{H}_2(\tau)\hat{V}_1(\tau,0)\Big), \quad (1.31)$$

where $\hat{V}_1(\tau,0)=\hat{T}\exp\Big(-i\int_0^\tau d\tau'\hat{H}_1(\tau')\Big)$.

Typically, it is straightforward to simplify $\hat{V}_1^{\dagger}(\tau,0)\hat{H}_2(\tau)\hat{V}_1(\tau,0)$. Thereby, the total evolution operator can be decomposed to a product like $\hat{U}_1\hat{U}_2$.

The proof of the decomposition method is as follows. We prove equations (1.30) and (1.31) using two different methods [54]:

- The unitary operator $\hat{T}\exp\Big(-i\int_0^t d\tau\,\big(\hat{H}_1(\tau)+\hat{H}_2(\tau)\big)\Big)$ is the product of the infinitely small elements

  $$\hat{U}(t_i)=\exp\big[-i\hat{H}_1(t_i)\delta t-i\hat{H}_2(t_i)\delta t\big],$$

  where $\delta t=\lim_{N\to\infty}t/N$ and $0\leqslant t_i\leqslant t$. Within the small period δt, one can decompose the small element $\hat{U}(t_i)$ into $\hat{U}_2(t_i)\hat{U}_1(t_i)=\hat{U}_1(t_i)\hat{U}_2(t_i)$, where $\hat{U}_i(t_k)=\exp\big[-i\hat{H}_i(t_k)\delta t\big]$, for any pairs of $\hat{H}_1(t)$ and $\hat{H}_2(t)$ as the cross terms due to their non-commutativity are negligible.

Then,

$$
\begin{aligned}
& \hat{T}\exp\Big(-i\int_0^t d\tau\,\big[\hat{H}_1(\tau)+\hat{H}_2(\tau)\big]\Big) \\
= \;& \hat{U}_2(t_{N-1})\hat{U}_1(t_{N-1})\hat{U}_2(t_{N-2})\hat{U}_1(t_{N-2})\cdots\hat{U}_2(t_2)\hat{U}_1(t_2)\hat{U}_2(t_1)\hat{U}_1(t_1)\hat{U}_2(t_0)\hat{U}_1(t_0) \\
= \;& \hat{U}_2(t_{N-1})\hat{U}_1(t_{N-1})\hat{U}_2^\dagger(t_{N-1}) \\
\times \;& \underbrace{\hat{U}_2(t_{N-1})\hat{U}_2(t_{N-2})}_{\hat{V}_2(t,t_{N-2})}\hat{U}_1(t_{N-2})\underbrace{\hat{U}_2^\dagger(t_{N-2})\hat{U}_2^\dagger(t_{N-1})}_{\hat{V}_2^\dagger(t,t_{N-2})} \\
\times \;& \underbrace{\hat{U}_2(t_{N-1})\hat{U}_2(t_{N-2})\hat{U}_2(t_{N-3})}_{\hat{V}_2(t,t_{N-3})}\hat{U}_1(t_{N-3})\underbrace{\hat{U}_2^\dagger(t_{N-3})\hat{U}_2^\dagger(t_{N-2})\hat{U}_2^\dagger(t_{N-1})}_{\hat{V}_2^\dagger(t,t_{N-3})} \\
\times \;& \cdots \\
\times \;& \underbrace{\underbrace{\hat{U}_2(t_{N-1})\hat{U}_2(t_{N-2})\cdots\hat{U}_2(t_1)\hat{U}_2(t_0)}_{\hat{V}_2(t,0)}\hat{U}_1(t_0)\underbrace{\hat{U}_2^\dagger(t_0)\hat{U}_2^\dagger(t_1)\cdots\hat{U}_2^\dagger(t_{N-2})\hat{U}_2^\dagger(t_{N-1})}_{\hat{V}_2^\dagger(t,0)}}_{\exp\left[-i\hat{V}_2(t,0)\hat{H}_1(t_0)\hat{V}_2^\dagger(t,0)\delta t\right]} \\
\times \;& \underbrace{\hat{U}_2(t_{N-1})\hat{U}_2(t_{N-2})\cdots\hat{U}_2(t_1)\hat{U}_2(t_0)}_{\hat{V}_2(t,0)}. \qquad (1.32)
\end{aligned}
$$

Except for the bottom row, each row after the last equals sign in equation (1.32) is the small element $\exp\big[-i\hat{V}_2(t,t_k)\hat{H}_1(t_k)\hat{V}_2^\dagger(t,t_k)\delta t\big]$.

- The exponentials $\hat{T}\exp\big[-i\int_0^t d\tau\big(\hat{H}_1(\tau)+\hat{H}_2(\tau)\big)\big]$ and $\hat{T}\exp\big[-i\int_0^t d\tau\,\hat{H}_1(\tau)\big]$ are the solutions to the follwoing differential equations:

$$\frac{d\hat{U}}{dt} = -i\big(\hat{H}_1(t)+\hat{H}_2(t)\big)\hat{U}(t) \qquad (1.33)$$

and

$$\frac{d\hat{V}_1}{dt} = -i\hat{H}_1(t)\hat{V}_1(t), \qquad (1.34)$$

respectively. The initial condition for the differential equations is $\hat{U}(0)=\hat{V}_1(0)=I$, the identity operator. The solution of equation (1.34) is

$$\hat{V}_1(t) = \hat{T}\exp\Big[-i\int_0^t d\tau\,\hat{H}_1(\tau)\Big]. \qquad (1.35)$$

We define $\hat{W}(t) = \hat{V}_1^\dagger(t)\hat{U}(t)$, whose differential with respect to t is

$$\frac{d\hat{W}}{dt} = -\hat{V}_1^\dagger \frac{d\hat{V}_1}{dt}\hat{V}_1^\dagger\hat{U} + \hat{V}_1^\dagger\frac{d\hat{U}}{dt} =$$
$$i\hat{V}_1^\dagger\hat{H}_1\hat{V}_1\hat{V}_1^\dagger\hat{U} - i\hat{V}_1^\dagger(\hat{H}_1+\hat{H}_2)\hat{U} = -i\hat{V}_1^\dagger\hat{H}_2\hat{V}_1\hat{V}_1^\dagger\hat{U} = -i\hat{V}_1^\dagger\hat{H}_2\hat{V}_1\hat{W}. \quad (1.36)$$

Its solution is

$$\hat{W}(t) = \hat{T}\exp\Big[-i\int_0^t d\tau\hat{V}_1^\dagger(\tau)\hat{H}_2(\tau)V_1(\tau)\Big], \quad (1.37)$$

where we have used the abbreviations $\hat{V}_i(t,0) \equiv \hat{V}_i(t)$ and $\hat{W}(t,0) \equiv \hat{W}(t)$.

Evidently, equations (1.30) and (1.31) can be generalized to any number of Hamiltonian. For example, if we have a Hamiltonian like $\hat{H} = \hat{H}_0 + \hat{H}_s + \hat{H}_{int} + \hat{H}_B$ that includes the free oscillation, the system Hamiltonian, the interaction Hamiltonian, and the bath Hamiltonian, the decomposition of the evolution operator $\hat{U}(t)$ converts it to a product of separated time evolutions: $\hat{U}_0(t)\hat{U}_s(t)\hat{U}_{int}(t)\hat{U}_B(t)$. Therefore, if there is a nonlinear Hamiltonian in the total time evolution operator, we can easily separate it out of the total. Then, we can use a Taylor expansion for the nonlinear time evolution operator and only keep the smallest term. Thereby, we can linearize the equations of motion obtained using equation (1.27) without converting a system operator to a steady-state term plus a fluctuation term. In chapter 4, we will see a practical example.

In addition to the above merit, to calculate the expectation values of the system operators, we do not need to solve the master equation and find the total density matrix $\rho(t)$, as a function of time [54]. Suppose the total density matrix $\hat{\rho}(t)$ for the combination of the system and reservoir at $t = 0$ is $\hat{\rho}(0) = \hat{\rho}_s(0)\otimes\hat{\rho}_R$, where $\hat{\rho}_s(0)$ is the initial density matrix of the system and $\hat{\rho_R}$ is the density matrix of the bath or reservoir. We assume that the bath does not evolve with time because the bath is not affected by the system due to its large size. We can write the expectation value of a

system operator using $\hat{U}(t,0)$ as

$$\begin{aligned}\langle \hat{O}_S \rangle &= \mathrm{Tr}_S[\hat{O}_S \hat{\rho}(t)] \\ &= \mathrm{Tr}_S[\hat{O}_S \hat{U}_0(t,0)\mathrm{Tr}_R\big(\hat{U}(t,0)\hat{\rho}(0)\otimes\hat{\rho}_R\hat{U}^\dagger(t,0)\big)\hat{U}_0^\dagger(t,0)] \\ &= \mathrm{Tr}_{S,R}[\hat{U}^\dagger(t,0)\hat{U}_0^\dagger(t,0)\hat{O}_S\hat{U}_0(t,0)\hat{U}(t,0)\hat{\rho}(0)\otimes\hat{\rho}_R].\end{aligned} \tag{1.38}$$

In many practical cases, the Hamiltonian has a free part whose time evolution operator can be factor out, so that $\hat{U}_0(t,0) = \exp\{-i(\omega_c \hat{a}^\dagger \hat{a} + \omega_m \hat{b}^\dagger \hat{b})t\}$. In such cases, for any operator $\hat{O}_S = \hat{f}(\hat{c}_i, \hat{c}_i^\dagger)$, the transformation by $\hat{U}_0(t,0)$ only adds a phase $e^{-i\omega_i t}$ ($e^{i\omega_i t}$), where $i = c$ or m, to $\hat{c}_i$ ($\hat{c}_i^\dagger$). Then we can find the expectation value using the transformation $\hat{U}^\dagger(t,0)\hat{f}(\hat{c}_i, \hat{c}_i^\dagger)\hat{U}(t,0) = \hat{f}\big(\hat{U}^\dagger(t,0)\hat{c}_i\hat{U}(t,0), \hat{U}^\dagger(t,0)\hat{c}_i^\dagger\hat{U}(t,0)\big)$ over the total initial state of system plus reservoir, with the phase absorbed in $\hat{c}_i$ ($\hat{c}_i^\dagger$). The reduction of calculating the system observables to finding the transformed basic system operators $\hat{U}^\dagger(t,0)\hat{c}_i\hat{U}(t,0)$ is the main advantage of the decompositon of the time evolution. We can similarly determine the more complicated averages such as $\langle \hat{O}_1(t+\tau)\hat{O}_2(\tau)\rangle$, which is generally calculated using the quantum regression formula [54].

1.4 Magnomechanical Systems

In chapter 4, we will investigate a magnomechanical phonon laser, which is a hybrid quantum system. Here we introduce a summary about the magnomechanical systems. More technical details, including the Hamiltonian of the system, remain for chapter 4.

A cavity magnomechanical system consists of a microwave cavity and a ferromagnetic material (usually a yttrium iron garnet (YIG) sphere) installed in it [58]. The system, which can be biased by an external magnetic or/and electromagnetic field, works based on the collective spin excitations in the ferromagnetic sample, called magnons [59]. Upon the bias, the magnons coherently couple to the microwave photons through the magnetic dipole interaction and couple to

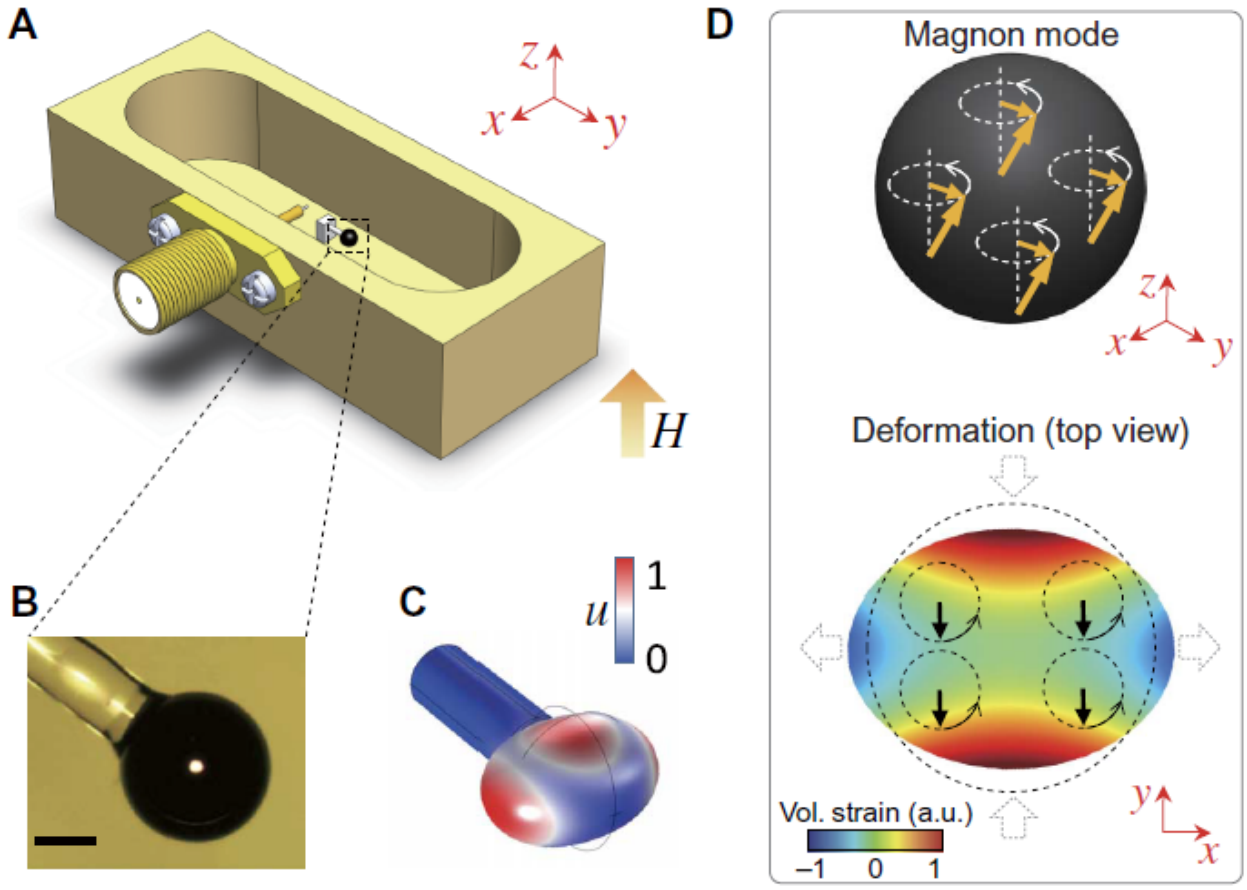

Figure 1.2: (a) The device consists of a copper cavity and a YIG sphere. A microwave magnetic field along the y-direction) is applied. Another uniform external magnetic field is applied along the z-direction to bias the YIG sphere for magnon-photon coupling. (b) The image of the highly polished 250-mm-diameter YIG sphere that is glued to a 125-mm-diameter supporting silica fiber. (c) Simulated mechanical displacement of the $S_{1,2,2}$ phonon mode in the YIG sphere that has the strongest magnomechanical interaction with the uniform magnon mode. (d) The top panel shows the uniform magnon excitation in the YIG sphere. The bottom panel illustrates how the dynamic magnetization of magnon (vertical black arrows) deforms (compresses along the y-direction) the YIG sphere (and vice versa), which rotates at the magnon frequency. The color scale represents the corresponding volumetric strain fields that the dynamic magnetization of magnon induces [52].

the phonons generated due to the eformation of the YIG via the magnetostrictive interaction (the change of the dimension of a substance that is exposed to a magnetic field) [60]. The magnetostriction occurs in all pure substances. However, even in strongly magnetic materials, the change of dimension is about 10^{-5} [61]. One can attribute the magnetostriction to three types of interactions

depending on the distance between the constituent ions: exchange intercation, dipole-dipole interaction, and spin-orbit interaction [52]. The magnetostriction force, thus, deforms the YIG sphere in strong magnetic fileds, converting it to a mechanical oscillator. Since the magnon frequency can be easily adjusted by the external field and the YIG sphere has a long coherence time, a low decay rate, and a high spin density ($4.2 \times 10^{21}\text{cm}^{-3}$), one can control the oscillations of the YIG sphere with high tunability. Figure 1.2 demonstrates a typical magnomechanical system. The device consists of a three-dimensional copper cavity and a YIG sphere. The YIG sphere is placed near the maximum microwave magnetic field (along the y-direction) of the cavity TE_{011} mode. A uniform external magnetic field is applied along the z-direction to bias the YIG sphere for magnon-photon coupling. In Figure 1.4(d), the top panel shows the uniform magnon excitation in the YIG sphere. The bottom panel illustrates how the dynamic magnetization of magnon (vertical black arrows) deforms the YIG sphere, which rotates at the magnon frequency [52].

Highly tunable magnomechanical systems are good alternatives for electro- and optomechanical systems [51] for which to couple the phonon to optical or microwave photons, mechanisms such as radiation force [62], electrostatic force [63], and piezoelectric force [64] have been applied. Such interaction mechanisms intrinsically lack fine tunability [52].

Due to their high tunability and long coherence, the cavity magnomechanical system has become a promising platform for implementing various novel phenomena, such as the bistability of cavity-magnon polaritons [65], magnon gradient memory [66], cavity spintronics [67], magnomechanical phonon laser [2], and cooperative polariton dynamics [68]. Furthermore, it was experimentally shown that the magnons in the small YIG sphere can couple to the optical photons [69], phonons [52], and superconducting qubits [70].

In this thesis, we will investigate the magnomchanical phonon laser in the dynamical

regime. Previously, it is studied in the steady-state approximation [2], but as we will see, its behavior in the dynamic case is totally different.

2 Continuous-variable entanglement generation in a system of coupled gain-loss waveguides

2.1 Introduction

Quantum information is a branch of science in which the quantum states are used as a tool to store or convey information. In particular, the quantum states of light are a fertile field for quantum information processing because light is an excellent carrier of information and also with today's technology it is possible to prepare such quantum states of light [71, 72]. The most advanced experimental demonstrations of quantum information systems at this time include trapped ions [73], linear optics [74], superconductors [75, 76], and quantum dots in semiconductors [77, 78, 79]. The basic idea behind quantum information processing is to use the laws of quantum mechanics to enhance the capabilities of transferring or manipulating data. The subject has three branches [80]:

- **Quantum cryptography:** the use of quantum mechanics to allow the presence of an eavesdropper to be detected when confidential information is being transferred between two parties.
- **Quantum computing:** the use of quantum mechanics to boost the computational power of a computer.
- **Quantum teleportation:** the use of quantum mechanics to transfer the quantum state of one particle to another.

Quantum teleportation relies profoundly on the properties of entangled states. In this chapter, we focus on generating the entangled states of light using a system of two coupled gain-loss

waveguide. As we will see in the next section, this is a special case of entanglement called "continuous variable".

In section 2.2, we start with the definition of the entangled states. We will introduce the discrete and continuous variable entanglement and will discuss the pros and cons of each one. Since the Gaussian states are the most well-known state of light proper for the continuous variable entanglement, we will explain these states and also how it is possible to quantify the degree of entanglement for such states. As quantum dynamics plays the main role in this thesis, we will consider the quantum noise effect in all subsequent sections because it may radically change the dynamics of the system. In section 2.3, we will explain why we have chosen a coupled gain-loss waveguide system as a potential device for generating entangled states, and in particular, what is the role of $\mathscr{P}\mathscr{T}$-symmetry . Then, in section 2.4 we introduce the Hamiltonian and the equations of motion. In section 2.5, we explain how the photon number and the waveguide mode correlation evolve with and without quantum noise effect. Finally, in section 2.6, we analyze the entanglement as a function of time if we add a squeezing element to either of the waveguides or to both of them.

2.2 Quantum information processing with continuous variables

2.2.1 The notion of quantum entanglement

Entanglement is one of the most counter-intuitive aspects of the quantum world that has no classical counterpart. In simple words, a multi-partite system is said to be in an entangled state if its wave function (or, more generally, its state vector) cannot be factorized into a product of the wave functions of the individual parts [80]. A well-known entangled state is the singlet (triplet) spin

state [5]:

$$|\psi\rangle = \frac{1}{\sqrt{2}}\big(|\uparrow\downarrow\rangle \pm |\downarrow\uparrow\rangle\big). \tag{2.1}$$

This state cannot be written as products of $|\uparrow\rangle \otimes |\downarrow\rangle$. To study the entanglement rigorously, consider a multi-partite system consisting of N subsystems. In the classical mechanics, we apply a phase space formalism to describe such a system. Then, the total (pure) state space of the system is the *Cartesian* product of the N subsystem spaces. This means the total state is the product space of N "separate" systems. In quantum mechanics, on the other hand, the total Hilbert space $\mathscr{H}$ is a *tensor* product of the subsystem spaces:

$$\mathscr{H} = \mathscr{H}_1 \otimes \mathscr{H}_2 \otimes \cdots \otimes \mathscr{H}_N. \tag{2.2}$$

Using the superposition principle, we can write the total state of the whole system as

$$|\psi\rangle = \sum_{\mathrm{i}_1,\ldots,\mathrm{i}_N} C_{\mathrm{i}_1,\ldots,\mathrm{i}_N} |\mathrm{i}_1\rangle \otimes |\mathrm{i}_2\rangle \otimes \cdots \otimes |\mathrm{i}_N\rangle. \tag{2.3}$$

In general, we cannot write the total state as a product of states of the individual subsystem:

$$|\psi\rangle \neq |\psi_1\rangle \otimes |\psi_2\rangle \otimes \cdots \otimes |\psi_N\rangle. \tag{2.4}$$

In other words, we cannot generally assign a single state vector to each individual subsystem. In such a case, we say that the (pure) state is *entangled* [81, 82].

In practical cases, we deal with mixed states instead of pure states. The definition of entanglement for such states differs from that of the pure state. A mixed state of N subsystems is entangled if we cannot write its density matrix as a convex combination of product states:

$$\rho \neq \sum_{\mathrm{i}} p_{\mathrm{i}}\, \rho_1^{\mathrm{i}} \otimes \cdots \otimes \rho_N^{\mathrm{i}}. \tag{2.5}$$

Those pure and mixed systems whose states do not satisfy equations (2.4) and (2.5), respectively, are called "separable" [82].

2.2.2 Continuous versus discrete variables

Nowadays, there are two main approaches to quantum information processing [83]:

1. The "digital" approach, in which the information is encoded in quantum systems with discrete degrees of freedom (qubits (quantum bits) or qudits). The qubits are quantum systems with two distinguishable states (we can call them 0 and 1). Examples of qubits are the two polarization states of a single photon, spin-1/2 electrons or nuclei, and two lowest energy levels of quantum dots or quantized superconducting circuits (see Table (2.1)). The qbits can not only represent pure 0 and 1 states, but they can also take on superposition states, in which the system is in both the 0 and 1 state at the same time. This "entanglement" is a consequence of the superposition principle of quantum mechanics.

2. The "analog" approach, in which the quantum correlations are encoded in continuous variable (CV) degrees of freedom like the quadrature amplitudes of a quantized harmonic oscillator that play the role of position and momentum. The quantized modes of bosonic systems such as the electromagnetic field, vibrational modes of solids, atomic ensembles, nuclear spins in a quantum dot, Josephson junctions, and Bose-Einstein condensates are some examples of continuous variables.

The first real success in the quantum information processing with continuous variables came with the experimental realization of quantum teleportation for optical fields. The next breakthrough was the successful definition of the notion of universal quantum computation using the continuous variables, suggesting that such variables are as capable as conventional qubits [84].

The main merit of the continuous-variable quantum information is that it is more practical. The preparing, unitarily shaping, and measuring entangled quantum states are achievable in

Table 2.1: Some physical realizations of qubits [80]

Quantum system	Physical property	$\|0\rangle$	$\|1\rangle$
Photon	linear polarization	Horizontal	Vertical
Phonon	Circular polarization	Left	Right
Nucleus	Spin	Up	Down
Electron	Spin	Up	Down
Two-level atom	Excitation state	Ground state	Excited state
Josephson junction	Electric charge	N Cooper pairs	$N+1$ Cooper pairs
Superconducting loop	Magnetic flux	Up	Down

.

quantum optics using continuous quadrature amplitudes of the quantized electromagnetic field. For example, by homodyne detection and feedforward techniques, we provide the tools for measuring a quadrature with near-unit efficiency or for displacing an optical mode in phase space, respectively. Moreover, the quantum optical implementations based on the continuous variables are highly efficient because of their unconditionalness. The entangled states typically generated from the nonlinear optical interaction processes in an unconditional fashion. This unconditionalness is hard to obtain in discrete-variable qubit-based setups using single-photon states. In such a case, preparing the desired state by the nonlinear optical interaction depends on a particular (coincidence) measurement results that forbid the unwanted (in particular, vacuum) contributions in the outgoing state vector. The disadvantage of the unconditionalness is that the low quality of the entanglement of the prepared states. We know that one should use the squeezed light to generate continuous-variable entangled states. However, high quality and performance require large squeezing, which is technologically demanding [84].

To summarize, the continuous-variable implementations always work efficiently and unconditionally, but they are never perfect. On the other hand, the discrete-variable counterparts entangled states are generated only under special circumstances (conditioned upon rare successful events) but in principle, they are perfect. Also, when we send optical quantum states through noisy channels (optical fibers, for example), the continuous-variable states accumulate noise and emerge at the receiver as contaminated versions of the input states. But one can reliably send the discrete-variable quantum information encoded in single-photon states if they are not absorbed during transmission [84].

2.2.3 Gaussian states

The primary tool for analyzing continuous-variable quantum information processing is Gaussian states, which are continuous-variable states represented in terms of Gaussian functions [85]. The Gaussian states not only are practically easier to generate, but they are also easy to describe. The ground state and thermal states of bosonic systems are examples of Gaussian states that are created in linear amplification and loss processes. Generally, nonlinear operations can be approximated to a high degree of accuracy by Gaussian transformations. For instance, squeezing is a process that decreases the variance of one continuous variable (say, position, or electric field) while increasing the variance of the conjugate variable (momentum, or magnetic field). Linear squeezing is Gaussian, and nonlinear squeezing can mostly be approximated to first order by a linear Gaussian process [83].

Here we introduce a list of well-known Gaussian states [83, 86]:

- **The vacuum state.** The vacuum state $|0\rangle$ is a ubiquitous Gaussian state with zero photon. It is the eigenstate of the annihilation operator with zero eigenvalue: $\hat{a}|0\rangle = 0$. The wave-

function of the harmonic oscillator in the ground state is proportional to $\exp[-\alpha x^2]$, which is Gaussian.

- **The thermal state.** Every Gaussian state can be decomposed into thermal states. Therefore, the thermal state is the most fundamental (mixed) Gaussian state. The density matrix of the thermal state in the basis of Fock state is ($\hbar = 1$)

$$\rho_T = \sum_n p_n \, |n\rangle\langle n|, \quad p_n = \frac{\langle n\rangle^n}{\big(1+\langle n\rangle\big)^{n+1}}, \quad \langle n\rangle = \frac{1}{\big[\exp(\beta\omega)-1\big]}, \tag{2.6}$$

where ω is the angular frequency of the thermal field and $\beta = 1/(k_{\rm B}T)$. The quadrature distribution of the theramal state is

$$\langle X|\rho_T|X\rangle = \frac{1}{\sqrt{\pi\big(1+2\,\langle n\rangle\big)}} \exp\left(-\frac{X^2}{1+2\,\langle n\rangle}\right), \tag{2.7}$$

which is Gaussian.

- **The coherent state.** The coherent state, generated by the displacement operator $D(\alpha) = \exp\left(\alpha\hat{a}^\dagger - \alpha^*\hat{a}\right)$, is Gaussian:

$$|\alpha\rangle = \exp\Big(-\frac{1}{2}|\alpha|^2\Big)\sum_n^\infty \frac{\alpha^n}{\sqrt{n!}}|n\rangle. \tag{2.8}$$

- **The squeezed state.** The squeezed vacuum state is defined as $|\varepsilon\rangle = \hat{S}(\varepsilon)|0\rangle$ where $\varepsilon = re^{i\theta}$ and $\hat{S}(\varepsilon) = \exp\left(\frac{1}{2}\varepsilon\,\hat{a}^{\dagger 2} - \frac{1}{2}\varepsilon^*\hat{a}^2\right)$. Here, r is the squeezing parameter and θ is its phase. The representation of the squeezed state is the quadrature space is

$$\psi_\varepsilon(X) = \langle X|\varepsilon\rangle = \psi_0 \, \exp\left(-\frac{1}{2}X^2\frac{\cosh r - {\rm e}^{i\theta}\sinh r}{\cosh r + {\rm e}^{i\theta}\sinh r}\right), \tag{2.9}$$

which is Gaussian. There is another type of squeezed state called "displaced" or coherent squeezed state. That one is also Gaussian.

There are more examples of Gaussian states, but we suffice to the above cases, which are the most important ones.

2.2.4 Entanglement of a Gaussian state

Knowing that entanglement is the key resource in quantum information processing protocols, it is of interest to quantify the degree of entanglement. In particular, we are interested in quantifying the degree of entanglement for the CV Gaussian sates [87]. Several proposals have been offered for this purpose [88, 89, 90], but in this thesis we will apply the logarithmic negativity [91, 86], which is specially useful for two-mode Gaussian states. To introduce the idea, we start with the mathematical description of Gaussian states in the Hilbert space.

A well-known bosonic CV system is the quantized electromagnetic field. The quantization procedure of the field shows we can model it as a collection of noninteracting quantum harmonic oscillators with different frequencies. We refer to each oscillator as a "mode" of the system. We investigate the discrete number of modes to avoid the difficulties of the quantum field theory. Mathematically, we describe a CV system of N canonical bosonic modes by a Hilbert space $\mathscr{H} = \bigotimes_{k=1}^{N} \mathscr{H}_k$ resulting from the tensor product structure of infinite-dimensional Hilbert spaces $\mathscr{H}_k$'s, each of them associated to a single-mode. The Hamiltonian of the complete system of the electromagnetic field is [85]

$$\hat{H} = \sum_{k=1}^{N} \hat{H}_k = \sum_{k=1}^{N} \omega_k \Big(\hat{a}_k^\dagger \hat{a}_k + \frac{1}{2} \Big), \tag{2.10}$$

in which the creation and annihilation operators satisfy the bosonic commutation relations:

$$\big[\hat{a}_k, \hat{a}_l^\dagger \big] = \delta_{k,l}. \tag{2.11}$$

The quadratures of the electromagnetic field (corresponding to the position and momentum) are defined as

$$\hat{q}_k = \frac{\big(\hat{a}_k + \hat{a}_k^\dagger\big)}{\sqrt{2}}, \quad \hat{p}_k = \frac{\big(\hat{a}_k - \hat{a}_k^\dagger\big)}{i\sqrt{2}}. \tag{2.12}$$

Let define a compact notation for $\hat{q}_k$'s and $\hat{p}_k$'s:

$$\hat{\mathbf{X}} = \left(\hat{q}_1, \hat{p}_1, \hat{q}_2, \hat{p}_2, \ldots, \hat{q}_N, \hat{p}_N\right)^T, \tag{2.13}$$

where T stands for transpose. Then, for example, $\hat{X}_3$ refers to $\hat{q}_2$. We define the covariance matrix (CM) elements as

$$V_{i,j} = \frac{1}{2}\langle \hat{X}_i \hat{X}_j + \hat{X}_j \hat{X}_i \rangle - \langle \hat{X}_i \rangle \langle \hat{X}_j \rangle. \tag{2.14}$$

For a two-mode system, the covariance matrix takes the form

$$V = \begin{pmatrix} \begin{pmatrix} a_{11} & a_{12} \\ a_{21} & a_{22} \end{pmatrix} & \begin{pmatrix} c_{11} & c_{12} \\ c_{21} & c_{22} \end{pmatrix} \\ \begin{pmatrix} c'_{11} & c'_{21} \\ c'_{12} & c'_{22} \end{pmatrix} & \begin{pmatrix} b_{11} & b_{12} \\ b_{21} & b_{22} \end{pmatrix} \end{pmatrix} \equiv \begin{pmatrix} A & C \\ C^T & B \end{pmatrix}. \tag{2.15}$$

Let define new variables Δ and η as follows:

$$\Delta = \det A + \det B - 2 \det C \tag{2.16}$$

and

$$\eta = \sqrt{\frac{\Delta - \sqrt{\Delta^2 - 4 \det V}}{2}}, \tag{2.17}$$

where "det" stands for determinant. Then, the necessary and sufficient conditions for entanglement of the concerned Gaussian state is

$$\eta < \frac{1}{2}. \tag{2.18}$$

We can use a more elegant definition for the entanglement called logarithmic negativity [85, 86, 91, 92]:

$$E_N = \max[0, -\ln 2\eta] \tag{2.19}$$

Therefore, if $-\ln 2\eta > 0$, the Guassian state is entangled. In section 2.6 we apply this measure to quantify the degree of entanglement.

2.3 Macroscopic entanglement with a hybrid $\mathscr{PT}$-symmetric gain-loss waveguide system

As indicated in the previous section, light is an excellent carrier of quantum information as it interacts weakly with the environment. On the other hand, preparing, manipulating, and measuring the CV states of light is more accessible than the discrete photonic qubits. Also, the CV quantum states are often Gaussian states, the manipulation of which is available in current experimental technology. Besides, quantitative description of all properties of the Gaussian states is possible. These benefits motivate one to explore the ways of generating entangled Gaussian states.

Entanglement involving light fields with high intensities is an example of the so-called "macroscopic entanglement". In addition to their possible applications [84, 83], macroscopic entangled light fields are essential to fundamental physics; see, e.g., the experimental [93, 94] and theoretical studies [95, 96, 97, 98].

In this thesis, we deal with such light fields in a coupled optical waveguides alternately carrying gain and loss media. Recently, a wide range of experimental [22, 14, 31, 99, 25, 24] and theoretical [11, 20, 100, 101, 30, 102, 103, 104, 105, 106, 107, 108, 109, 110, 111] researches have been accomplished on these non-Hermitian systems. One advantage of these systems is that one can change the light transmission patterns by simply adjusting the intensity of coupling between their components. For example, the light field amplitudes under the balanced gain and loss, where the system can manifest a $\mathscr{PT}$-symmetry , will be quickly amplified once the coupling intensity is tuned below the gain-loss rate. Intuitively, one can apply this mechanism to realize entangled output light fields with high intensities by adding a squeezing element into one of the coupled components. One can also see the interest in the entanglement following the relevant non-Hermitian dynamics in many-body systems [112].

In most previous studies, the light fields in $\mathscr{P}\mathscr{T}$-symmetric systems are treated as classical electromagnetic fields. When dealing with the entanglement of the light fields, one will encounter an indispensable factor accompanying their amplification and dissipation—the quantum noises acting as the random drives from the associated reservoirs. The quantum noises must exist as they preserve the proper commutation relations for the evolved light field operators [47]. So far, only a few recent studies have considered the effects of the quantum noise in optical $\mathscr{P}\mathscr{T}$-symmetric systems [42, 113, 114], including the hybrid ones with other physical elements such as Kerr nonlinearity added into the systems [50, 4, 115].

As is well known, quantum entanglement is fragile under the influence of the noises from the environment [116, 117]. However, how they affect the entanglement generated by $\mathscr{P}\mathscr{T}$-symmetric systems remains an open question. In this thesis, we will clarify such effects of quantum noises by quantitatively examining their influence on the entanglement. The comparison between the generated macroscopic entanglement in the absence and presence of quantum noise due to the amplification and/or dissipation enables one to understand their effects in $\mathscr{P}\mathscr{T}$-symmetric systems more deeply.

2.4 Hamiltonian and the dynamics of the system

Because of inevitable interactions with their environments, most physical systems are open and their dynamics is non-Hermitian . The system of two coupled waveguides carrying optical gain and loss respectively as in Figure 2.1 is an example of such open systems. Waveguide $A(B)$ carries a gain (loss) medium, in which the single-mode field $\hat{a}(\hat{b})$ propagates. We do not care about the mechanisms of gain and loss, and hence we have not shown the relevant pumping needed for a gain medium. Here we only consider the propagation of the light fields at a normal group

velocity v_g, neglecting the possible superluminal propagation of the evanescent wave as described in [118, 119].

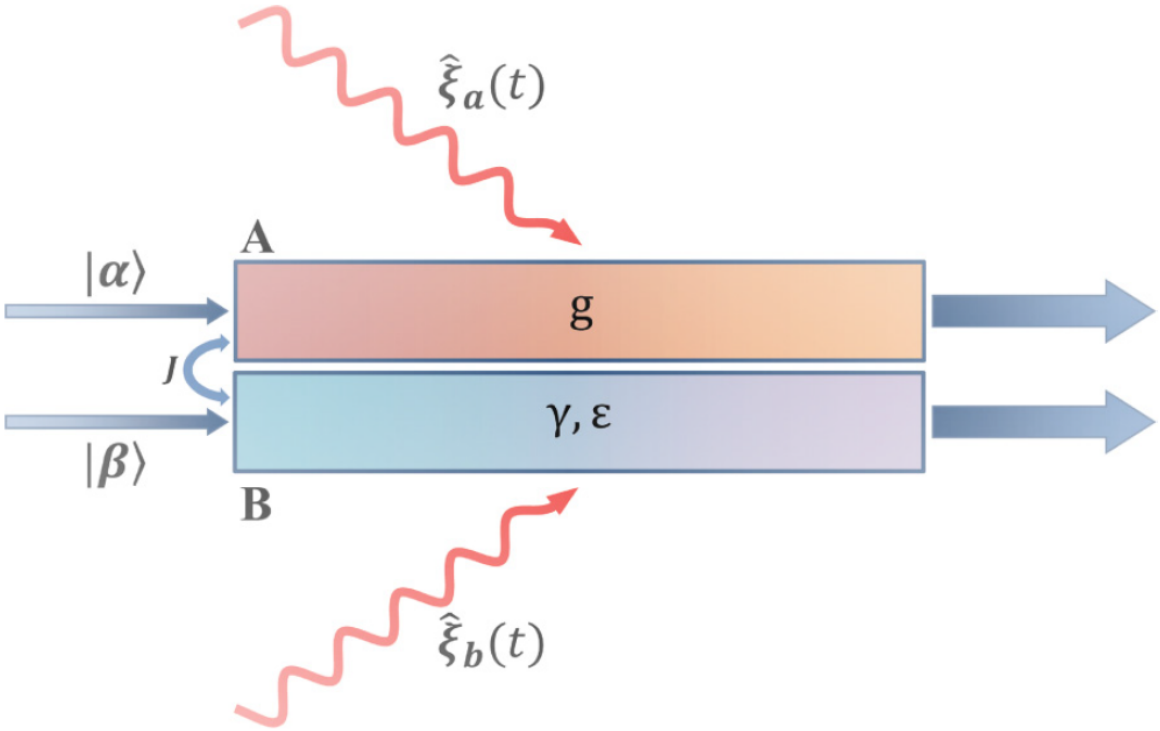

Figure 2.1: Setup of the hybrid $\mathscr{P}\mathscr{T}$-symmetric system: the coupled gain-loss waveguide system with an added squeezing element into the loss channel without showing the pumping fields used for the amplification. The input light fields are in coherent states.

The two light fields couple from one to another waveguide via the evanescent wave, and one can adjust the effective coupling intensity, J, by the gap distance. The magnitudes of the gain rate g and loss rate γ are decided by the media used, and the optical gain can be realized by doping erbium ions into various materials [120]. Moreover, in the current model we neglect the gain saturation by assuming a high saturation intensity for the gain medium. When the gain and loss are balanced ($g = -\gamma$), as mentioned in chapter 1, the necessary condition for $\mathscr{P}\mathscr{T}$-symmetry is satisfied. In this case, we can either use an effective non-Hermitian Hamiltonian that does not take

the noise into account or a Hermitian Hamiltonian that includes the stochastic terms describing the noise. First we introduce the effective non-Hermitian Hamiltonian which explicitly shows the $\mathscr{P}\mathscr{T}$-symmetry :

$$\hat{H}_{\mathrm{PT}} = ig\hat{a}^\dagger\hat{a} - ig\hat{b}^\dagger\hat{b} + J\left(\hat{a}^\dagger\hat{b} + \hat{a}\hat{b}^\dagger\right), \tag{2.20}$$

which can be diagonalized as

$$\begin{aligned}
&\left(\hat{a}^\dagger \hat{b}^\dagger\right)\begin{pmatrix} ig & J \\ J & -ig \end{pmatrix}\begin{pmatrix} \hat{a} \\ \hat{b} \end{pmatrix} \\
&= \left(\hat{q}^\dagger \hat{p}^\dagger\right)\begin{pmatrix} \frac{-ig+\sqrt{J^2-g^2}}{J} & \frac{-ig-\sqrt{J^2-g^2}}{J} \\ 1 & 1 \end{pmatrix}^{-1} \\
&\times \begin{pmatrix} ig & J \\ J & -ig \end{pmatrix}\begin{pmatrix} \frac{-ig+\sqrt{J^2-g^2}}{J} & \frac{-ig-\sqrt{J^2-g^2}}{J} \\ 1 & 1 \end{pmatrix}\begin{pmatrix} \hat{q} \\ \hat{p} \end{pmatrix} \\
&= \left(\hat{q}^\dagger \hat{p}^\dagger\right)\begin{pmatrix} -\sqrt{J^2-g^2} & 0 \\ 0 & \sqrt{J^2-g^2} \end{pmatrix}\begin{pmatrix} \hat{q} \\ \hat{p} \end{pmatrix} \\
&= \left(-\sqrt{J^2-g^2}\right)\hat{q}^\dagger\hat{q} + \left(\sqrt{J^2-g^2}\right)\hat{p}^\dagger\hat{p}
\end{aligned} \tag{2.21}$$

This Hamiltonian is invariant under the simultaneous parity transformation $\hat{a} \leftrightarrow \hat{b}$ and time inversion transformation $i \leftrightarrow -i$, hence the term $\mathscr{P}\mathscr{T}$-symmetry . The Hamiltonian comes from the dynamical equations in the previous studies of classical $\mathscr{P}\mathscr{T}$-symmetric systems, where the system modes $\hat{a}$ and $\hat{b}$ are replaced by the corresponding classical fields. When $g < J$ ($\mathscr{P}\mathscr{T}$-symmetric regime), this Hamiltonian's eigenvalues are real and the transmitting light intensities (proportional to $\langle\hat{a}^\dagger\hat{a}(t)\rangle$ and $\langle\hat{b}^\dagger\hat{b}(t)\rangle$) in both waveguides demonstrate periodic oscillations in time. When $g > J$ ($\mathscr{P}\mathscr{T}$-symmetry broken regime), the eigenvalues become imaginary, and the intensities of the transmitting light fields change from oscillatory to exponentially growing. The

transition takes place at $g = J$, the exceptional point.

As indicated before, the non-Hermitian Hamiltonian in equation (2.20) does not possess the quantum noise elements, so one cannot apply it to study the noise-sensitive phenomena such as quantum entanglement. One approach for overcoming the shortcoming is to adopt a stochastic Hamiltonian. We suppose that the reservoir is modeled as an ensemble of oscillators with the positive energy. But for the light amplification we consider an ensemble of oscillators with the negative energy as discussed in [47]. The reservoirs are in the vacuum states at zero temperature. With respect to the self oscillation Hamiltonian (we assume the angular frequency for the light propagating in both waveguides is ω_0)

$$\hat{H}_0 = \omega_0\, \hat{a}^\dagger \hat{a} + \omega_0\, \hat{b}^\dagger \hat{b} \tag{2.22}$$

of the waveguide modes and that of the reservoirs

$$\hat{H}_R = -\int d\omega\; \omega\; \hat{f}_a^\dagger(\omega)\hat{f}_a(\omega) + \int d\omega\; \omega\; \hat{f}_b^\dagger(\omega)\hat{f}_b(\omega), \tag{2.23}$$

the general coupling Hamiltonian between the system and reservoirs takes the following:

$$\begin{aligned}
\hat{H}_{\text{int}} &= i\int_{-\infty}^{\infty} d\omega\, \sqrt{2g/(2\pi)}\big(\hat{f}_a(\omega)\mathrm{e}^{i\omega t} + \hat{f}_a^\dagger(\omega)\mathrm{e}^{-i\omega t}\big) \\
&\times \big(\hat{a}^\dagger \mathrm{e}^{i\omega_0 t} - \hat{a}\mathrm{e}^{-i\omega_0 t}\big) \\
&+ i\int_{-\infty}^{\infty} d\omega\, \sqrt{2\gamma/(2\pi)}\big(\hat{f}_b(\omega)\mathrm{e}^{-i\omega t} + \hat{f}_b^\dagger(\omega)\mathrm{e}^{i\omega t}\big) \\
&\times \big(\hat{b}^\dagger \mathrm{e}^{i\omega_0 t} - \hat{b}\mathrm{e}^{-i\omega_0 t}\big).
\end{aligned} \tag{2.24}$$

Applying the rotation wave approximation (RWA) that neglects the fast oscillating terms in the equation (2.24), the coupling Hamiltonian becomes

$$\begin{aligned}
\hat{H}_{\text{int}} &= i\sqrt{2g}\{\hat{a}^\dagger \hat{f}_a^\dagger(t) - \hat{a}\hat{f}_a(t)\} \\
&+ i\sqrt{2\gamma}\{\hat{b}^\dagger \hat{f}_b(t) - \hat{b}\hat{f}_b^\dagger(t)\},
\end{aligned} \tag{2.25}$$

where

$$\hat{f}_a(t) = \frac{1}{\sqrt{2\pi}} \int_{-\infty}^{\infty} d\omega\, \hat{f}_a(\omega) \mathrm{e}^{i(\omega-\omega_0)t},$$
$$\hat{f}_b(t) = \frac{1}{\sqrt{2\pi}} \int_{-\infty}^{\infty} d\omega\, \hat{f}_b(\omega) \mathrm{e}^{-i(\omega-\omega_0)t}. \tag{2.26}$$

The noise operators satisfy

$$\langle \hat{f}_c(t) \hat{f}_c^{\dagger}(t') \rangle = \delta(t-t') \tag{2.27}$$

for $c = a, b$. The other commutation relations become zero. The coupling between the waveguides is described by

$$\hat{H}_c = J\left(\hat{a}^{\dagger}\hat{b} + \hat{a}\hat{b}^{\dagger}\right). \tag{2.28}$$

To entangle the light fields, one needs to add a squeezing element into the waveguide system. The action of the squeezing element with parameter $\varepsilon = r\exp(i\theta)$ is described by the following Hamiltonian (when it is added into waveguide B):

$$\frac{i}{2}\left[\varepsilon\, \mathrm{e}^{-i\omega_p t}(\hat{b}^{\dagger})^2 - \varepsilon^* \mathrm{e}^{i\omega_p t}(\hat{b})^2\right] \tag{2.29}$$

This Hamiltonian is based on the undepleted pump approximation for a process of second harmonic generation in a nonlinear crystal with certain symmetry (for example, LiNbO3) [121]. A similar use of squeezing element was also proposed for engineering the quantum properties of other systems (see, e.g., [122]). Noting that in the interaction picture

$$\mathrm{e}^{i\hat{H}_0 t}\hat{b}^2 \mathrm{e}^{-i\hat{H}_0 t} = \hat{b}^2 \mathrm{e}^{-2i\omega_0 t}, \tag{2.30}$$

if we set $\omega_p = 2\omega_0$, then the total Hamiltonian reads

$$\hat{H} = J\left(\hat{a}^{\dagger}\hat{b} + \hat{a}\hat{b}^{\dagger}\right) + \frac{i}{2}\left[\varepsilon(\hat{b}^{\dagger})^2 - \varepsilon^*(\hat{b})^2\right]$$
$$+ i\sqrt{2g}\left[\hat{a}^{\dagger}\hat{f}_a^{\dagger}(t) - \hat{a}\,\hat{f}_a(t)\right] + i\sqrt{2\gamma}\left[\hat{b}^{\dagger}\hat{f}_b(t) - \hat{b}\,\hat{f}_b^{\dagger}(t)\right]. \tag{2.31}$$

The dynamical evolution due to the total Hamiltonian determines all properties of the light fields propagating in the concerned system. Let define

$$\hat{B}_c(t) = \int_0^t \hat{f}_c(\tau)\, d\tau \tag{2.32}$$

Then, if we use equation (1.27), i.e.,

$$\begin{aligned}
\mathrm{d}\hat{c}(t) &= \hat{U}^\dagger(t+\mathrm{d}t)\hat{c}(t)\hat{U}(t+\mathrm{d}t) - \hat{c}(t) \\
&= i\Big[J\left(\hat{a}^\dagger\hat{b} + \hat{a}\hat{b}^\dagger\right) + \frac{i}{2}\Big(\varepsilon\,(\hat{b}^\dagger)^2 - \varepsilon^*(\hat{b})^2\Big),\ \hat{c}\Big]\,\mathrm{d}t \\
&= -\sqrt{2g}\left[\hat{a}^\dagger\mathrm{d}\hat{B}_a^\dagger - \hat{a}\,\mathrm{d}\hat{B}_a,\ \hat{c}\right] - \sqrt{2\gamma}\left[\hat{b}^\dagger\mathrm{d}\hat{B}_b - \hat{b}\,\mathrm{d}\hat{B}_b^\dagger,\ \hat{c}\right] \\
&+ g\big(2\hat{a}\hat{c}\hat{a}^\dagger - \hat{c}\hat{a}\hat{a}^\dagger - \hat{a}\hat{a}^\dagger\hat{c}\big)\mathrm{d}t + \gamma\big(2\hat{b}^\dagger\hat{c}\hat{b} - \hat{c}\hat{b}^\dagger\hat{b} - \hat{b}^\dagger\hat{b}\hat{c}\big)\mathrm{d}t,
\end{aligned} \tag{2.33}$$

we obtain a system of linear differential equations for the operators $\hat{a}$ and $\hat{b}$ and their Hermitian conjugates:

$$\frac{\mathrm{d}}{\mathrm{d}t}\begin{pmatrix}\hat{a}\\ \hat{a}^\dagger\\ \hat{b}\\ \hat{b}^\dagger\end{pmatrix} = \begin{pmatrix} g & 0 & -iJ & 0\\ 0 & g & 0 & iJ\\ -iJ & 0 & -\gamma & \varepsilon\\ 0 & iJ & \varepsilon^* & -\gamma\end{pmatrix}\begin{pmatrix}\hat{a}\\ \hat{a}^\dagger\\ \hat{b}\\ \hat{b}^\dagger\end{pmatrix} + \begin{pmatrix}\sqrt{2g}\,\hat{f}_a^\dagger\\ \sqrt{2g}\,\hat{f}_a\\ \sqrt{2\gamma}\,\hat{f}_b\\ \sqrt{2\gamma}\,\hat{f}_b^\dagger\end{pmatrix} \tag{2.34}$$

To solve the dynamical equations more efficiently and avoid complex entries in the matrix, it is convenient to work with the quadratures of the light fields (for $c = a, b$) and quantum noises defined as

$$\begin{aligned}
\hat{q}_c &= \frac{1}{\sqrt{2}}\big(\hat{c} + \hat{c}^\dagger\big), \\
\hat{p}_c &= -\frac{i}{\sqrt{2}}\big(\hat{c} - \hat{c}^\dagger\big), \\
\hat{Q}_c &= \frac{1}{\sqrt{2}}\Big(\hat{f}_c(t) + \hat{f}_c^\dagger(t)\Big), \\
\hat{P}_c &= -\frac{i}{\sqrt{2}}\Big(\hat{f}_c(t) - \hat{f}_c^\dagger(t)\Big).
\end{aligned} \tag{2.35}$$

Then, we obtain

$$\frac{\mathrm{d}}{\mathrm{d}t}\begin{pmatrix}\hat{q}_a\\ \hat{p}_a\\ \hat{q}_b\\ \hat{p}_b\end{pmatrix}=\begin{pmatrix}g & 0 & 0 & J\\ 0 & g & -J & 0\\ 0 & J & -\gamma+\frac{1}{2}(\varepsilon+\varepsilon^*) & -\frac{i}{2}(\varepsilon-\varepsilon^*)\\ -J & 0 & -\frac{i}{2}(\varepsilon-\varepsilon^*) & -\gamma-\frac{1}{2}(\varepsilon+\varepsilon^*)\end{pmatrix}\begin{pmatrix}\hat{q}_a\\ \hat{p}_a\\ \hat{q}_b\\ \hat{p}_b\end{pmatrix}+\begin{pmatrix}\sqrt{2g}\,\hat{Q}_a\\ -\sqrt{2g}\,\hat{P}_a\\ \sqrt{2\gamma}\,\hat{Q}_b\\ \sqrt{2\gamma}\,\hat{P}_b\end{pmatrix}, \tag{2.36}$$

which can be written in a compact form:

$$\frac{\mathrm{d}}{\mathrm{d}t}\hat{\mathbf{X}}(t)=M\hat{\mathbf{X}}(t)+\hat{\mathbf{F}}(t), \tag{2.37}$$

where

$$\hat{\mathbf{X}}(t)=\left(\hat{q}_a(t),\hat{p}_a(t),\hat{q}_b(t),\hat{p}_b(t)\right)^T, \tag{2.38}$$

$$\hat{\mathbf{F}}(t)=\left(\sqrt{2g}\,\hat{Q}_a(t),-\sqrt{2g}\,\hat{P}_a(t),\sqrt{2\gamma}\,\hat{Q}_b(t),\sqrt{2\gamma}\,\hat{P}_b(t)\right)^T, \tag{2.39}$$

and, for $\varepsilon=r\exp(i\theta)$,

$$M=\begin{pmatrix}g & 0 & 0 & J\\ 0 & g & -J & 0\\ 0 & J & -\gamma+r\cos\theta & -r\sin\theta\\ -J & 0 & -r\sin\theta & -\gamma-r\cos\theta\end{pmatrix} \tag{2.40}$$

is called the dynamic matrix. If we can find $\hat{\mathbf{X}}(t)$, we can quantify the degree of entanglement.

The general form of the solution is

$$\hat{\mathbf{X}}(t)=\mathrm{e}^{Mt}\hat{\mathbf{X}}(0)+\int_0^t\mathrm{e}^{M(t-t')}\hat{\mathbf{F}}(t')\,\mathrm{d}t'. \tag{2.41}$$

The eigenvalues of the dynamic matrix do not depend on the phase of the squeezing pa-

rameter:

$$\begin{aligned}
\lambda_1 &= \frac{1}{2}\Big(g+r-\gamma-\sqrt{-4J^2+(g-r+\gamma)^2}\Big),\\
\lambda_2 &= \frac{1}{2}\Big(g+r-\gamma+\sqrt{-4J^2+(g-r+\gamma)^2}\Big),\\
\lambda_3 &= \frac{1}{2}\Big(g-r-\gamma-\sqrt{-4J^2+(g+r+\gamma)^2}\Big),\\
\lambda_4 &= \frac{1}{2}\Big(g-r-\gamma+\sqrt{-4J^2+(g+r+\gamma)^2}\Big).
\end{aligned} \tag{2.42}$$

Therefore, we expect the solution is independent of the phase of the squeezing parameter, too. Since the dynamic matrix is time-independent, we can easily convert the matrix exponential in equation (2.41) to a matrix and write the general form of the solution as

$$\begin{pmatrix} \hat{q}_a(t)\\ \hat{p}_a(t)\\ \hat{q}_b(t)\\ \hat{p}_b(t) \end{pmatrix} = \begin{pmatrix} r_{11} & r_{12} & r_{13} & r_{14}\\ r_{21} & r_{22} & r_{23} & r_{24}\\ r_{31} & r_{32} & r_{33} & r_{34}\\ r_{41} & r_{42} & r_{43} & r_{44} \end{pmatrix} \begin{pmatrix} \hat{q}_a(0)\\ \hat{p}_a(0)\\ \hat{q}_b(0)\\ \hat{p}_b(0) \end{pmatrix} + \int_0^t \mathrm{d}\tau \begin{pmatrix} s_{11} & s_{12} & s_{13} & s_{14}\\ s_{21} & s_{22} & s_{23} & s_{24}\\ s_{31} & s_{32} & s_{33} & s_{34}\\ s_{41} & s_{42} & s_{43} & s_{44} \end{pmatrix} \begin{pmatrix} \hat{Q}_a(\tau)\\ \hat{P}_a(\tau)\\ \hat{Q}_b(\tau)\\ \hat{P}_b(\tau) \end{pmatrix}. \tag{2.43}$$

Here r_{ij} is a function of t only, while s_{ij} is a function of t and τ. To find r_{ij} and s_{ij}, first we diagonalize the matrix M and then use the fact that if $M = UDU^{-1}$, then $\mathrm{e}^M = U\mathrm{e}^D U^{-1}$ [123].

We cannot perform the integration in the second line of equation (2.43), because here we deal with operators, not functions. In other words, it does not make sense to assign a particular value, say, to $\hat{Q}_a$ at $t = 0$ or at any other time. What has a physical meaning is the expectation values of the operators with respect to the proper states. In the current problem, we suppose that the light

fields are coherent states: $|\alpha,\beta\rangle = |\alpha\rangle \otimes |\beta\rangle$. The reservoir is in the vacuum state $|0,0\rangle$. Then, we can find the expectation values of the operators of equation (2.14). The expectation values of the homogeneous part are calculated with respect to the input coherent states, while those of the inhomogeneous part are found with respect to the total reservoir state. As examples, here we have found

$$\begin{aligned}
\big\langle \alpha,\beta \big| \hat{q}_a(0) \big| \alpha,\beta \big\rangle &= \frac{1}{\sqrt{2}}\big(\alpha+\alpha^*\big), \\
\big\langle \alpha,\beta \big| \{\hat{p}_b(0),\hat{q}_a(0)\} \big| \alpha,\beta \big\rangle &= -i\big(\alpha+\alpha^*\big)\big(\beta-\beta^*\big), \\
\big\langle \alpha,\beta \big| \hat{p}_b(0)^2 \big| \alpha,\beta \big\rangle &= \frac{1}{2}\Big(1-\beta^2+2\beta\beta^*-\beta^{*2}\Big).
\end{aligned} \tag{2.44}$$

where $\{\}$ stands for anti-commutation. The noise operators satisfy the following relations:

$$\begin{aligned}
\big\langle 0,0 \big| \hat{Q}_a(\tau)\hat{Q}_a(\tau') \big| 0,0 \big\rangle &= \frac{1}{2}\delta(\tau-\tau'), \\
\big\langle 0,0 \big| \hat{P}_a(\tau)\hat{P}_a(\tau') \big| 0,0 \big\rangle &= \frac{1}{2}\delta(\tau-\tau'), \\
\big\langle 0,0 \big| \hat{Q}_b(\tau)\hat{Q}_b(\tau') \big| 0,0 \big\rangle &= \frac{1}{2}\delta(\tau-\tau'), \\
\big\langle 0,0 \big| \hat{P}_b(\tau)\hat{P}_b(\tau') \big| 0,0 \big\rangle &= \frac{1}{2}\delta(\tau-\tau').
\end{aligned} \tag{2.45}$$

The other commutation relations become zero.

Interestingly, after simplification, we notice that all matrix elements are independent of the input field intensities, i.e., they are independent of α and β. As examples, here we have found the general form of two elements of the covariant matrix (CM) defined in equation (2.15):

$$\begin{aligned}
a_{11} &= r_{11}^2 + r_{12}^2 + r_{13}^2 + r_{14}^2 + \int_0^t \Big[s_{11}^2 + s_{12}^2 + s_{13}^2 + s_{14}^2 \Big]\, \mathrm{d}\tau, \\
a_{12} &= r_{11}r_{21} + r_{12}r_{22} + r_{13}r_{23} + r_{14}r_{24} + \int_0^t \Big[s_{11}s_{21} + s_{12}s_{22} + s_{13}s_{23} + s_{14}s_{24} \Big]\, \mathrm{d}\tau
\end{aligned} \tag{2.46}$$

Thereby, we can find all elements of the covariant matrix. These CM elements can be experimentally measured [124].

2.5 Evolution of the photon number and the waveguide mode correlation

A main purpose of this chapter is to find out how the quantum noises will affect the entanglement generated with the setup in Figure 2.1. To see this, one could compare the values of the entanglement found as the results of the evolutions according to the Hamiltonian in equations (2.20) and in (2.31), respectively. As indicated before, the only difference between these two is an extra quantum noise drive term, $\hat{\mathbf{F}}(t)$, which consists of the components of pure random variables. By intuition, such random drives from the environment could only modify the dynamics of the system without changing the evolution patterns of the measurable quantities so much, as it has been found from the photon number evolutions in a $\mathscr{P}\mathscr{T}$-symmetric system without squeezing [42].

A relevant question is whether the added squeezing will make a considerable difference. To answer the question, we examine how the output light fields' intensities evolve according to the full dynamical equation, i.e., (2.41). Previously, the evolved light intensities in a $\mathscr{P}\mathscr{T}$-symmetric system without squeezing have been studied for single photon and vacuum state as inputs [42]. Due to the noise associated with the amplification, the output field intensity is found not to be zero even when the input field is in a vacuum state. After adding a squeezing element, we find that the photon numbers can be enhanced further, in addition to the effect of the gain medium at the rate g.

Figure 2.2 shows the photon numbers plotted for a setup with the squeezing element in the damping waveguide, indicating that the photon numbers will be intensified by increasing the squeezing parameter r. The phase factor θ in the squeezing parameter has no effect as mentioned before. The contribution from the homogeneous part in equation (2.41) will become much more significant with the increase of r. Therefore, the relative difference between the light intensities obtained by using the Hamiltonians (2.20) and (2.31), respectively, becomes smaller than that in

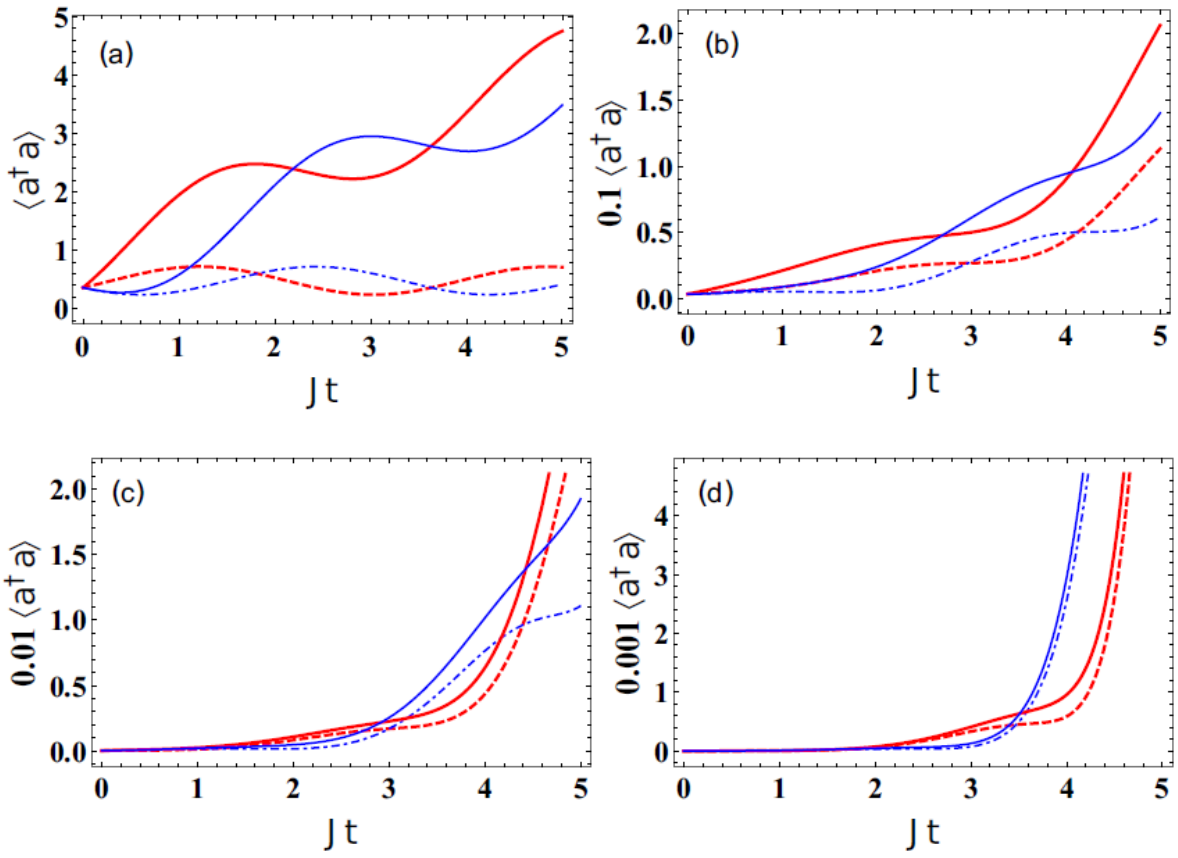

Figure 2.2: The light intensity I_a and I_b (proportional to the respective photon numbers) out of the gain and loss waveguide, represented by red and blue curves, respectively, as compared with the corresponding quantities $I_{a,h}$, and $I_{b,h}$ calculated without the noise drives (the dashed red and blue curves). Here the dimensionless time gt is used to indicate how long the light fields evolve in the waveguides. We set the parameters as $\theta = 0$, $J = 1.9g$, and $g = -\gamma$. The squeezing parameter: (a) $r = 0$, (b) $r = 0.5g$, (c) $r = g$, and (d) $r = 1.5g$. The input coherent states are given as $\alpha = \beta = 0.6$.

the previously studied situation without the squeezing; compare Figure 2.2(a) with Figure 2.2(d). However, at small values of r, there is a significant difference between the intensities with and without considering the quantum noise effects. As is seen from Figures 2.2(a)–2.2(d), the corresponding photon numbers are indeed enhanced by the amplification noise. Similar to the situation of a simple $\mathscr{P}\mathscr{T}$-symmetric system without squeezing [42], one sees that the quantum noises simply modify the output light intensity quantitatively, but their evolution patterns remain unchanged.

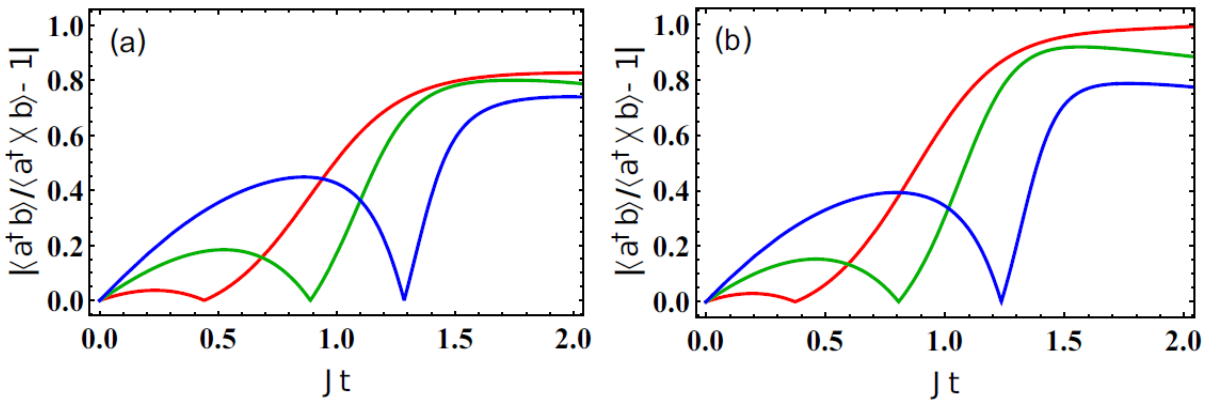

Figure 2.3: The correlation function $|\langle\hat{a}^\dagger\hat{b}\rangle - \langle\hat{a}^\dagger\rangle\langle\hat{b}\rangle|$ calculated with $J = 1.9g$. We set $g = -\gamma$ and $\theta = 0$. Three different values of squeezing, $r = 0$ (blue), $r = g$ (green), and $r = 1.5g$ (red), are considered for the squeezing element in the damping waveguide. The input coherent states are given as $\alpha = \beta = 0.6$. Panel (a) shows the mode correlation without considering the quantum noise effect, and panel (b) demonstrates the mode correlation under the full dynamics.

As another example, we look at a nonlocal quantity, the correlation function defined as $|\langle\hat{a}^\dagger\hat{b}\rangle - \langle\hat{a}^\dagger\rangle\langle\hat{b}\rangle|$, assuming that the squeezing element is inside the damping waveguide. Apparently, such a correlation function, which evolves with time, might be similar to the entanglement of the light fields. Figure 2.3 illustrates the evolution of such a correlation function for three different values of the squeezing parameter. Panel (a) shows the mode correlation without considering the quantum noise effect, and panel (b) demonstrates the mode correlation under the full dynamics. As expected, the correlation becomes stronger with a larger squeezing parameter r. One also sees that the inclusion of quantum noise drive only slightly modifies the amplitude of the correlation without changing the time evolution pattern. In particular, it is interesting that by including the noise drives sometimes one can have a stronger correlation. Then it is natural for one to consider whether this phenomenon reflects a similar pattern for the corresponding entanglement between the output light fields.

2.6 Entanglement of output fields

By the elements used in Figure 2.1, it seems that highly entangled intense light fields is possible as the light fields keep amplified in the $\mathscr{P}\mathscr{T}$-symmetric broken regime. The degrees of the entanglement of Gaussian states can be measured by the logarithmic negativity, equation (2.19):

$$E_N = \max[0, -\ln 2\eta]$$

Assuming the input light fields as coherent states, one finds an important property of such entanglement measured by equation (2.19). Referring to equation (2.14), one sees that the first term depends on the mode operators as well as the noise drives, whereas the second term only depends on the mode operators (the expectation values of the noise operators in it are zero). After subtracting the latter from the former, the CM elements become irrelevant to the intensity of the input fields. Consequently, the intensity of the input coherent states will be irrelevant to the generated entanglement, the degree of which is mainly influenced by the noise drives leading to the inhomogeneous part in equation (2.41).

In what follows, we will examine the output entanglement with three different configurations: the squeezing element in the damping waveguide, in the amplification waveguide, and in both waveguides.

2.6.1 Squeezing element in the damping waveguide

The first configuration we study is a coupled gain-loss waveguide system with an added squeezing element to the damping waveguide as shown in Figure 2.1. In our calculations, we fix the phase factor θ because its variation does not affect the results. The output fields will become strongly entangled without adding the noise drive term $\hat{\mathbf{F}}(t)$ that gives the inhomogeneous part in equa-

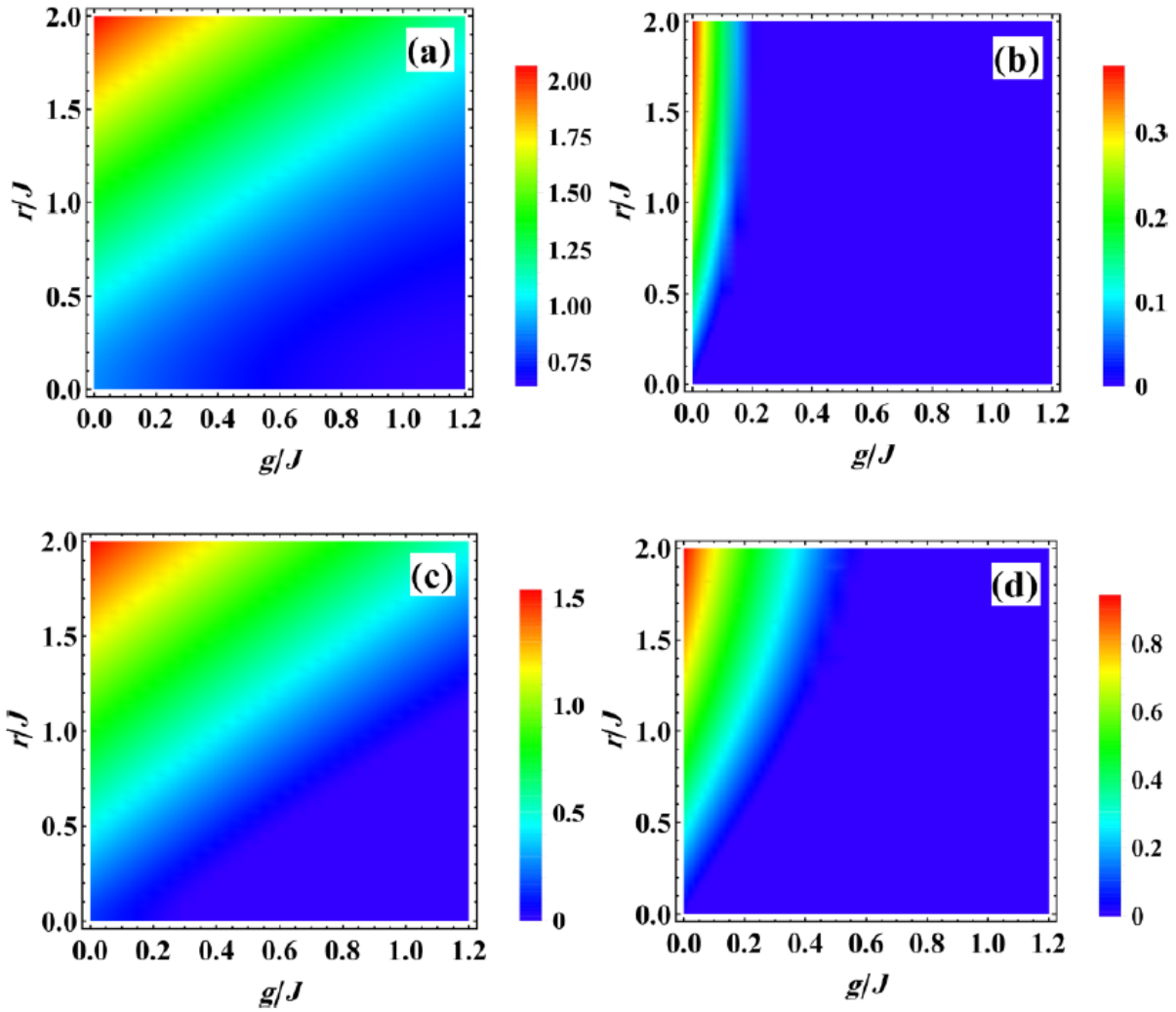

Figure 2.4: Distribution of the entanglement (in terms of E_N) without (with) involving the quantum noises when a squeezing element is added into the damping waveguide is shown in panels (a) and (c) [(b) and (d)]. We set $\theta = 0$ and compare the entanglement at $Jt = 1$. For panels (a) and (b) we take $\gamma/J = 0.6$ and for panels (c) and (d) we choose $\gamma/J = 0.1$.

tion (2.41). Figures 2.4(a) and 2.4(c) show that the degree of entanglement simply increases as r/J . Highly entangled fields with huge photon number are thus seemingly possible by choosing the proper system parameters. One should notice that the distributions of entanglement in Figures 2.4(a) and 2.4(c) are qualitatively the same for different damping rates, but the degrees of entanglement differ quantitatively.

The inclusion of the quantum noises associated with the amplification and dissipation will totally change the aforementioned scenario. Now one will find that the entanglement vanishes throughout the time except when g/J is very small. Without loss of generality, we demonstrate the realistic entanglement distribution at a particular time as in Figures 2.4(b) and 2.4(d) (two different values of the damping rate γ/J are also considered). The interplay of the quantum noises with the squeezing element under the full dynamics causes such distinct entanglement distributions from the corresponding ones without considering the noises. In contrast to the previous situation, here the distribution of the nonzero entanglement changes qualitatively with the damping rates γ/J and the degree of entanglement changes quantitatively as well, so that the lower loss rate yields the higher entanglement.

To illustrate the effects of the quantum noises more clearly, we extend the range of g/J to the negative values in Figure 2.5, so that the obtained entanglement distributions also cover the situation when both waveguides contain dissipation medium. In Figure 2.5(a), where the quantum noises are not included, the values of E_N distribute continuously from the positive to the negative range of g/J . The corresponding entanglement is shown to grow with the damping rate $\gamma/J = -g/J$, but that is impossible to occur. Such an unphysical result constitutes an evidence that quantum noises are indispensable in the study of entanglement. On the contrary, the realistic entanglement obtained under the noise effects in Figure 2.5(b) takes a discontinuous transition on the boundary $g/J = 0$ because the dynamics of system changes across the boundary. In this situation, the higher loss rate in the range of negative g/J results in the lower entanglement that is a physically reasonable result.

The noises associated with the amplification and dissipation act simultaneously with the squeezing that entangles the light fields, and their effects dominate over the latter when g/J and

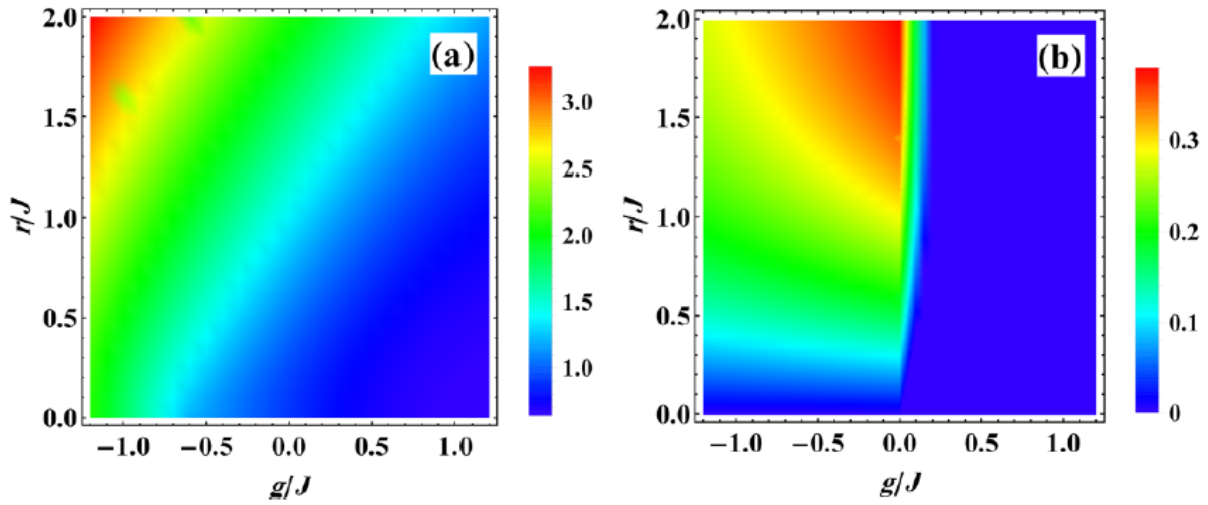

Figure 2.5: Distribution of the entanglement (in terms of E_N) for the setup of Figure 2.1. The negative values of g/J represent a situation where both waveguides are filled with damping medium. The quantum noises are neglected in panel (a) but are included in panel (b). The system parameters are the same as those in Figure 2.4. In panel (b), the value of E_N is discontinuous at $g/J = 0$ because for $g/J > 0$ the amplification and dissipation noises act, but for $g/J < 0$ only the dissipation noise acts in both waveguides.

γ/J become large. The different components in the noise drive vector contribute to the evolved modes via the respective elements in the dynamic matrix M. If the gain and loss are balanced, the impact of the amplification noise and the dissipation noise will be equal provided no squeezing element is added to the system (one can see that from the relevant elements of the dynamic matrix M). However, a squeezing element can interplay with the relevant noises, and if it is placed in the damping waveguide, the influence of the dissipation noise will be enhanced. Mathematically, such interplay has more contribution from the dissipation noise operator $\hat{f}_b(t)$, which is inside the drive terms in equation (2.41), to the CM elements. This also explains the fact that the entanglement is less influenced under the lower loss rate γ/J since the intensity of the dissipation noise [decided by $\sqrt{\gamma}$ in equation (2.31)] becomes lower. On the other hand, regardless of how small the damping

rate is, the entanglement will vanish quickly at a high gain rate even if the squeezing is large because the high gain rate leads to a significant effect of amplification noise, which can erase the entanglement.

Meanwhile, by comparing Figures 2.3 with 2.4, one concludes that the existence of correlations between the two system modes does not guarantee their entanglement. The correlation under the full dynamics can be even stronger than the corresponding one without considering the noises, but the noises weaken the entanglement and, under some circumstances, they will erase the entanglement completely. The entanglement has to be determined by the relations between the CM elements involving the light field correlations, and hence its existence is much more restricted.

2.6.2 Squeezing element in the amplifying waveguide

If the squeezing element is inserted into the amplifying waveguide, the dynamic matrix will change to

$$M = \begin{pmatrix} g + r\cos\theta & r\sin\theta & 0 & J \\ r\sin\theta & g - r\cos\theta & -J & 0 \\ 0 & J & -\gamma & 0 \\ -J & 0 & 0 & -\gamma \end{pmatrix}. \tag{2.47}$$

The dynamical evolutions of thewaveguide modes, as given by equation (2.41), will be changed accordingly. In what follows, we will examine how the entanglement between the two waveguide modes will change as the location of the squeezing element is swapped to the amplifying waveguide.

In Figure 2.6(a), we illustrate the numerically simulated entanglement evolutions in the absence of the quantum noise effects. One sees that the entanglement will monotonically grow to high degrees with time. This is, however, not true in reality since the quantum noise must be

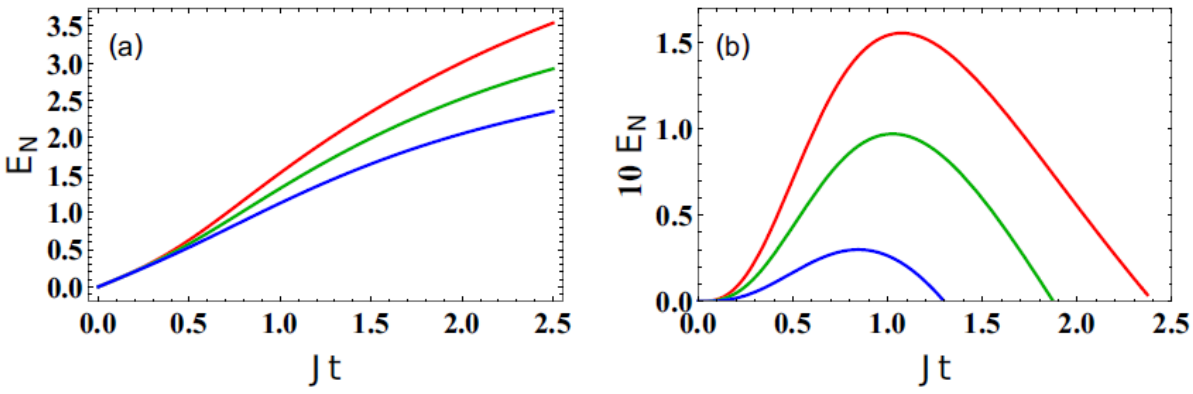

Figure 2.6: Time evolution of the entanglement due to a squeezing element in the amplifying waveguide. Here $g/J = 0.6$, $\gamma/J = 0.6$, and $\theta = 0$. The red (upper), green (middle), and blue (lower) curves are associated with $r/J = 2$, $r/J = 1.7$, and $r/J = 1.4$, respectively. Panel (a) shows the entanglement evolutions found with the non-Hermitian Hamiltonian in equation (2.20) (i.e.,without involving the quantum noise effects), together with the squeezing action. Panel (b) demonstrates the entaglement under the full dynamics. The entanglement grow in the absence of quantum noise, but it decays to zero by involving the noise effects.

considered in a real process. Figure 2.6(b), including the quantum noise effects, shows that the entanglement will be finally erased, so there is an optimum evolution time to obtain maximum entanglement (or, an optimum length for the waveguide). The degrees of the achieved entanglement is nonetheless higher than the situation of placing the squeezing into the damping waveguide, those illustrated in Figures 2.4(b) and 2.4(d). Moreover, the nonzero entanglement can exist in the broader range of the parameter space; compare Figure 2.7(b) with Figure 2.4(b).

In this configuration, the squeezing enhances the effect of the amplification noise, but the effect of the noise accompanying the light field dissipation is kept almost invariant. One can confirm this fact from Figures 2.7(b) and 2.7(d). In Figure 2.7(d), the loss rate is reduced by 6 times to have the dissipation noise weakened accordingly. However, neither the degree of entanglement nor the range of nonzero E_N is obviously changed. This is in contrast to a considerable change

from Figure 2.4(b) to 2.4(d). Such difference also implies that, given a gain rate g/J that is not very large, the dissipation noise is more detrimental to the concerned entanglement.

An important feature that should be illustrated with the time evolutions is that the entanglement evolved under the full dynamics undergoes the entanglement sudden death (ESD) [117]; see Figure 2.6(b). Beyond the moments of ESD when it disappears, the entanglement will stay zero forever (for bipartite entanglement of Gaussian states, the logarithmic negativity is a well-defined quantity). By the scenario in Figure 2.6, one concludes that the quantum noises control the actual time evolution pattern of the entanglement.

2.6.3 Squeezing elements in both waveguides

Next, we consider the setup with the squeezing elements added into both waveguides. In this situation, the dynamic matrix of the system becomes

$$M = \begin{pmatrix} g + r\cos\theta & r\sin\theta & 0 & J \\ r\sin\theta & g - r\cos\theta & -J & 0 \\ 0 & J & -\gamma + r\cos\theta & r\sin\theta \\ -J & 0 & r\sin\theta & -\gamma - r\cos\theta \end{pmatrix}. \tag{2.48}$$

Under the condition $g = -\gamma$, the system exhibits a $\mathscr{P}\mathscr{T}$ symmetry like the Hamiltonian in equation (2.20). In this configuration, the degree of entanglement will be even higher than those of the two previous configurations if the quantum noises are absent; see Figures 2.8(a) and 2.8(c). It is within the expectation since the squeezing elements act in both waveguides. Also, in the presence of the quantum noises, the degree of the entanglement is higher than those in the two other configurations as demonstrated in Figures 2.8(b) and 2.8(d). Moreover, the range of nonzero E_N becomes broader as compared to Figures 2.4(b) and 2.4(d). Now both the amplification noise and the dissipation

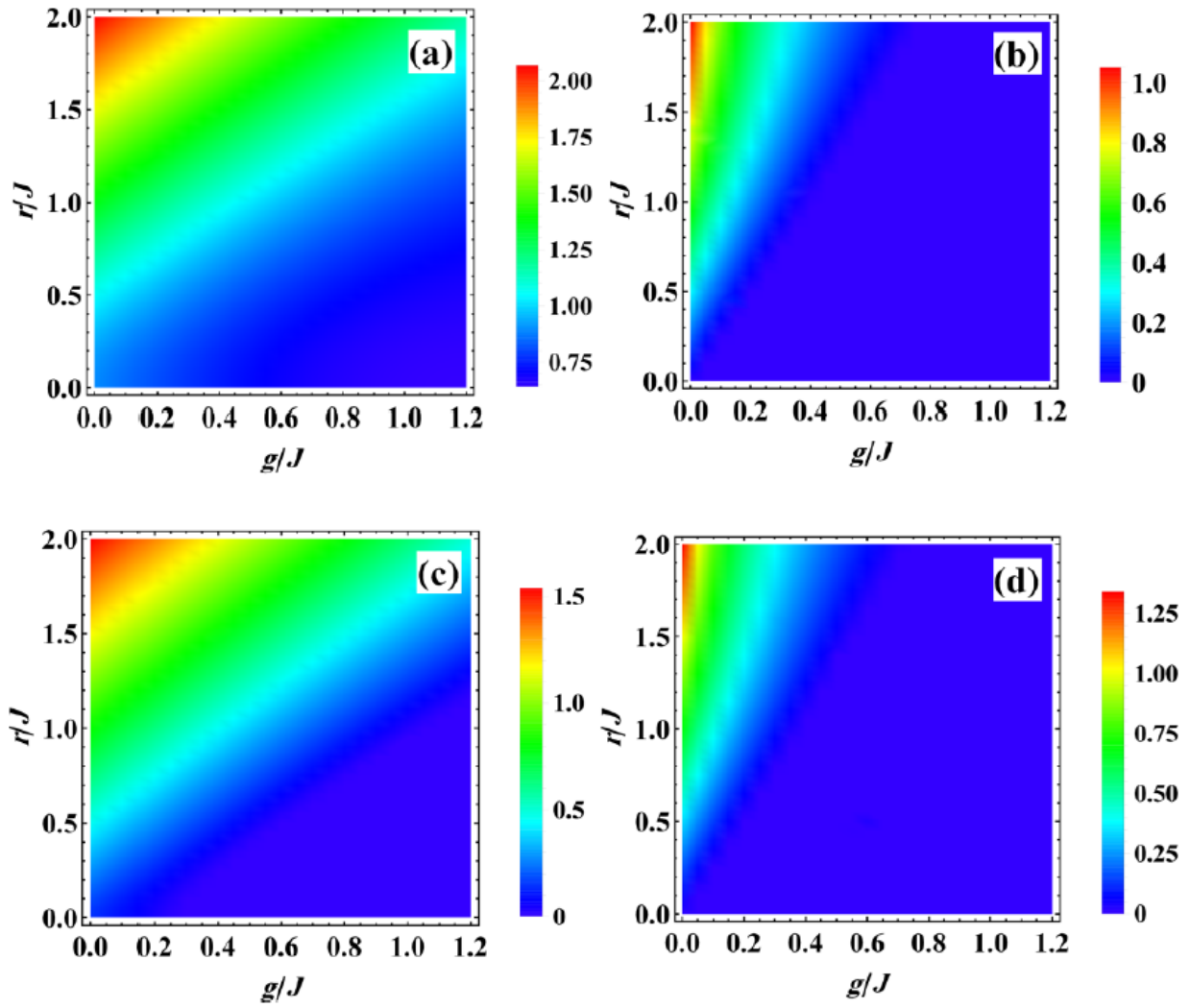

Figure 2.7: Panels (a) and (c): the entanglement distribution (in terms of E_N) from a squeezing element in the amplifying waveguide without involving the noise effects. Panels (b) and (d): the corresponding entanglement distribution including the quantum noise effects. Here we choose $\theta = 0$ and $Jt = 1$. In panels (a) and (b) we set $\gamma/J = 0.6$, and in panels (c) and (d) we have $\gamma/J = 0.1$.

noise are relevant to the evolved entanglement as their effects are enhanced by the squeezing elements in both waveguides. A consequence is that the generated entanglement is dependent on the loss rate γ/J as well as on the gain rate g/J . In spite of such enhanced noise effects, the stronger squeezing effect from doubled elements can overcome their influence to create a higher entangle-

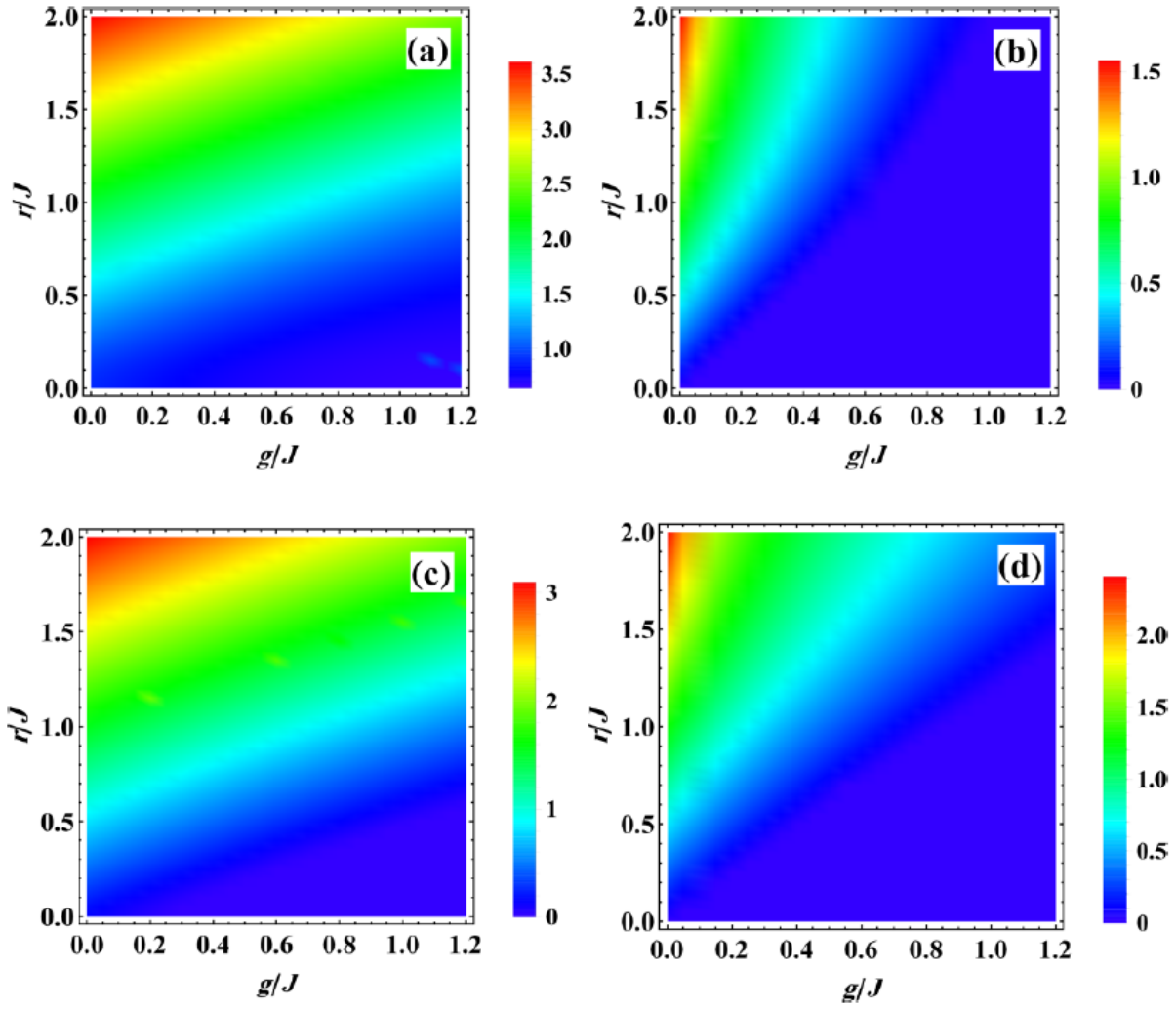

Figure 2.8: Distribution of entanglement (in terms of E_N) generated by placing identical squeezing elements into both waveguides. We set $\theta = 0$, and $Jt = 1$. In panels (a) and (c), the entanglement values are calculated without considering quantum noises, and in panels (b) and (d), the entanglement values are found under the full dynamics. In panels (a) and (b), we set $\gamma/J = 0.6$, and in panels (c) and (d), we set $\gamma/J = 0.1$.

ment of the light fields. The time evolutions of the entanglement are similar to those in Figure 6 and will not be explicitly shown again.

2.6.4 Summary and conclusion

We have studied how quantum noises influence the CV entanglement generated by a hybrid $\mathscr{P}\mathscr{T}$-symmetric setup. By intuition, the existing quantum noises associated with amplification and dissipation would only modify the entanglement generated by the system slightly. Then, according to the prediction by the non-Hermitian Hamiltonian in equation (2.20), highly entangled, high-intensity light fields can be readily created by such a setup, especially by the system operating in the $\mathscr{P}\mathscr{T}$-symmetry broken regime ($g/J > 1$) where the light fields can simultaneously be amplified and entangled. However, the quantum noises can completely erase the entanglement, rendering its evolution totally different from those of photon numbers and field-mode correlations. The results obtained by the full dynamics indicate that certain amounts of the entanglement can still be achieved, though they are weaker than those predicted without considering the quantum noises. In particular, placing the squeezing element inside the waveguide amplifying the propagating light field enables one to realize light fields with considerable CV entanglement, given the gain rate g/J that is not too large. The possible experimental realization of such systems relies on finding a material or a method to purely amplify and squeeze the input light simultaneously. The importance of studying this model setup is to clarify that quantum noises must be considered in $\mathscr{P}\mathscr{T}$-symmetric optical systems for engineering the quantum properties of light fields. Also, we should emphasize that in this setup we assumed that the gain rate in constant. In the next chapter, we will see if we consider the nonlinear gain saturation effect, the time evolution pattern of entanglement radically changes.

3 Effects of gain saturation on the quantum properties of light in the non-Hermitian gain-loss coupler

3.1 Introduction

As we discussed in the previous chapters, non-Hermitian optical systems have unique properties and many applications in communication, computing, biochemistry, and environmental sensing. The most influential parameters of these systems are the gain and loss rates. Peculiar features that are either difficult or impossible to be implemented by Hermitian optical systems exist in the non-Hermitian entities given various combinations of their gains and losses. For the ideal models, the gain and loss coefficients do not depend on the intensity of the light propagating in the systems. However, in almost all amplifying media, optical gain is a function of the field intensity, so that the intensity of the propagating beam does not increase forever. When the intensity of light reaches a steady state, the gain reduces to its "saturated" value. Although the saturation effect has been examined in some classical non-Hermitian optical systems [25, 125, 126, 127, 128, 129, 130, 131], the dynamical nature of gain saturation in the quantum regimes has remained mostly unexplored [132]. Notably, since the variation of gain coefficient affects the quantum noise associated with the amplification, one expects that the saturation of gain can significantly influences the quantum-noise-sensitive properties of light such as entanglement.

So far, the majority of non-Hermitian optical systems are studied under the assumption that the light is a classical electromagnetic field, and the gain and loss coefficients are intensity-independent (non-saturable), and the quantum noises due to amplification and dissipation are negligible. In this chapter, we dispense with these assumptions by adopting a full quantum dynamical

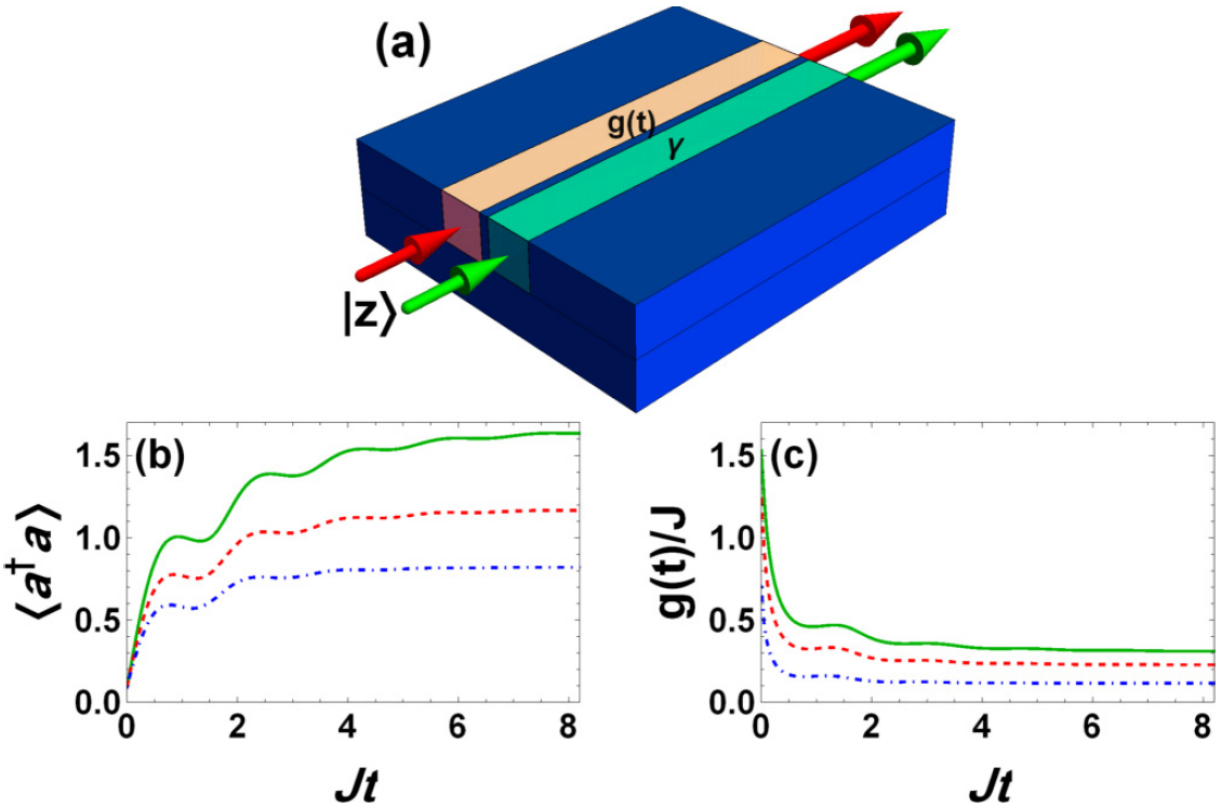

Figure 3.1: The light intensity I_a and I_b (proportional to the respective photon numbers) out of the gain and loss waveguide, represented by red and blue curves, respectively, as compared with the corresponding quantities $I_{a,h}$, and $I_{b,h}$ calculated without the noise drives (the dashed red and blue curves). Here the dimensionless time gt is used to indicate how long the light fields evolve in the waveguides. We set the parameters as $\theta = 0$, $J = 1.9g$, and $g = -\gamma$. The squeezing parameter: (a) $r = 0$, (b) $r = 0.5g$, (c) $r = g$, and (d) $r = 1.5g$. The input coherent states are given as $\alpha = \beta = 0.6$.

picture, examining the gain saturation effect in the coupled gain-loss waveguide system discussed in the previous chapter, and considering the inevitable quantum noise effect (see Figure 3.1). We suppose that the gain medium is saturable, but the loss medium is with a constant damping rate. Moreover, this time there is no squeezing element inside the waveguides, but the input light fields can be in squeezed states. As examples, we show that the gain saturation effect alters the time evolution pattern of the Wigner function and the entanglement of the output fields. In contrast to

a constant gain coefficient that often leads to a non-steady state situation, gain saturation generally prompts a "quasi-steady" state of the Wigner function and the entanglement of the light fields. Notably, in some circumstances, an ideal constant gain rate leads to "entanglement sudden death", but the gain saturation introduces a steady entangled state of the light field by reducing the detrimental quantum noise effect.

3.2 Theoretical Model

The non-Hermitian system of coupled, single-mode waveguides is depicted in Figure 3.1. Waveguide A carries a saturable gain medium with a gain coefficient $g(t)$, and waveguide B is a non-saturable loss medium with a coefficient γ. Like the previous chapter, we denote the light field operator propagating in waveguide $A(B)$ by $\hat{a}(\hat{b})$, which shares the same frequency ω_0. The waveguides are coupled via evanescent waves so that the coupling strength J can be adjusted by the gap between them.

The non-Hermitian "effective Hamiltonian" ($\hbar = 1$) for this system reads:

$$\hat{H}_{\text{eff}} = ig(t)\hat{a}^\dagger\hat{a} - i\gamma\hat{b}^\dagger\hat{b} + J(\hat{a}\hat{b}^\dagger + \hat{a}^\dagger\hat{b}), \tag{3.1}$$

which is similar to equation (2.20), except that here $g(t)$ is a function of time. The first two terms describe the amplification and dissipation of light in waveguides A and B, and the third term characterizes the coupling between the waveguides. Since equation (3.1) does not explicitly include the quantum noise effect, the quantum correlation functions obtained by this mean-field approach deviate from the real correlation functions.

As our purpose is to examine the dynamical behavior of quantum features of light, again we adopt the stochastic Schrödinger equation that takes the noise terms into account [47]. The

total Hamiltonian includes the system, the reservoir, and the system-reservoir interaction. Similar to chapter 2, using the rotating-wave approximation with smooth system-reservoir coupling and after applying the Markovian approximation, the total Hamiltonian in the interaction picture is

$$\hat{H} = J\left(\hat{a}^\dagger \hat{b} + \hat{a}\hat{b}^\dagger\right) + i\sqrt{2g(t)}\left[\hat{f}_a^\dagger(t)\hat{a}^\dagger - \hat{f}_a(t)\hat{a}\right] + i\sqrt{2\gamma}\left[\hat{f}_b(t)\hat{b}^\dagger - \hat{f}_b^\dagger(t)\hat{b}\right]. \tag{3.2}$$

Note that the relevant terms to the amplification and dissipation noises are defined such that $[\hat{f}_c(t), \hat{f}_c{}^\dagger(t')] = \delta(t-t')$. The corresponding equations of motion are

$$\begin{aligned} \frac{\mathrm{d}\hat{a}}{\mathrm{d}t} &= g(t)\hat{a} - iJ\hat{b} + \sqrt{2g}\,\hat{f}_a^\dagger(t), \\ \frac{\mathrm{d}\hat{b}}{\mathrm{d}t} &= -iJ\hat{a} - \gamma\hat{b} + \sqrt{2\gamma}\,\hat{f}_b(t), \end{aligned} \tag{3.3}$$

where $g(t)$ depends on the intensity of the light field propagating in waveguide A.

An example of the gain medium is an erbium-doped amplifier [120], as an ensemble of two-level atoms. If a pump laser excites the erbium ions into the higher level so that the population difference between the upper and lower level is positive, an optical signal propagating in this medium will be amplified exponentially. The amplification is due to the stimulated emission of photons from dopant ions. The excited ions can also decay via spontaneous emission or nonradiative processes that reduce the efficiency of light amplification [133].

If the length of the medium is long enough or the doping level is high enough, the light eventually reaches an intensity at a certain specific length such that the energy stored in the upper level is not sufficient to satisfy the exponential growth condition. In other words, when the signal intensity increases to a certain value I_{sat}, the population difference between the upper and lower levels and hence the gain coefficient decreases. This phenomenon is called gain saturation, with I_{sat} being the saturation intensity at the center frequency of the optical beam. The gain coefficient

as a function of time (or, as a function of saturation intensity) is

$$g(t) = g_0/(1 + I_a(t)/I_{\text{sat}}), \tag{3.4}$$

where g_0 and $I_a(t)$ are the small-signal gain and the intensity of light in waveguide A at time t, respectively. In equation (3.4), the saturation intensity is defined such that the stimulated rate downward equals the normal radiative decay of the upper level. For simplicity, we will use the dimensionless saturation intensity as defined in [25]. Physically, the energy difference between the upper and lower levels, the stimulated cross-section, and the lifetime of the upper level determine the saturation intensity [133].

We will study the effect of such gain saturation on quantum properties of light fields through the examples of the Wigner function of light fields in the gain-loss coupler and the time evolution of the entanglement of the fields. In both cases, we assume that the input to the waveguides is a single-mode squeezed vacuum state, $|z\rangle = S(z)|0\rangle$, where $S(z) = \exp\left(\frac{1}{2}z(\hat{c}^\dagger)^2 - \frac{1}{2}z^*\hat{c}^2\right)$ for $\hat{c} = \hat{a}, \hat{b}$. The squeezing parameter is defined as $z = r\exp(i\theta)$.

To obtain the results, in all subsequent sections we normalize the equation (3.3). Let define the new dimensionless variables $g/J \equiv G$, $\gamma/J \equiv \Gamma$, and $Jt \equiv \tau$. Also,

$$G = \frac{G_0}{1 + I_a/I_{sat}}. \tag{3.5}$$

Thus,

$$\frac{\mathrm{d}}{\mathrm{d}\tau}\begin{pmatrix}\hat{a}\\ \hat{b}\end{pmatrix} = \begin{pmatrix}G & -i\\ -i & -\Gamma\end{pmatrix}\begin{pmatrix}\hat{a}\\ \hat{b}\end{pmatrix} + \frac{1}{\sqrt{J}}\begin{pmatrix}\sqrt{2G}\,\hat{f}_a^\dagger(t)\\ \sqrt{2\Gamma}\,\hat{f}_b(t)\end{pmatrix}. \tag{3.6}$$

The noise operators are still a function of t. We know that

$$\langle \hat{f}_a(\tau/J)\hat{f}_a^\dagger(\tau'/J)\rangle = J\delta(\tau - \tau'). \tag{3.7}$$

So, we can change the second part as

$$\frac{1}{\sqrt{J}}\hat{\xi}_a^\dagger(\tau/J) \to \hat{\xi}_a^\dagger(\tau),$$

and finally obtain

$$\frac{\mathrm{d}}{\mathrm{d}\tau}\begin{pmatrix}\hat{a}\\ \\ \hat{b}\end{pmatrix} = \begin{pmatrix}G & -i\\ \\ -i & -\Gamma\end{pmatrix}\begin{pmatrix}\hat{a}\\ \\ \hat{b}\end{pmatrix} + \begin{pmatrix}\sqrt{2G}\,\hat{\xi}_a^\dagger(\tau)\\ \\ \sqrt{2\Gamma}\,\hat{\xi}_b(\tau)\end{pmatrix}. \tag{3.8}$$

Now everything is expressed versus normalized variables. If we define

$$\mathbf{M} = \begin{pmatrix}G & -i\\ \\ -i & -\Gamma\end{pmatrix}, \tag{3.9}$$

$$\hat{\mathbf{c}}(\tau) = \big(\hat{a}(\tau), \hat{b}(\tau)\big)^T, \tag{3.10}$$

and

$$\hat{\mathbf{n}}(\tau) = \big(\sqrt{2G}\,\hat{\xi}_a^\dagger(\tau), \sqrt{2\Gamma}\,\hat{\xi}_b(\tau)\big)^T, \tag{3.11}$$

then the solution is

$$\hat{\mathbf{c}}(\tau) = \hat{T}\exp\Big[\int_0^\tau \mathbf{M}(s)\,\mathrm{d}s\Big]\hat{\mathbf{c}}(0) + \int_0^\tau \mathrm{d}s\,\hat{T}\exp\Big[\int_s^\tau \mathbf{M}(s')\,\mathrm{d}s'\Big]\hat{\mathbf{n}}(s) = \hat{\mathbf{c}}_{\mathrm{h}}(\tau) + \hat{\mathbf{c}}_{\mathrm{in}}(\tau). \tag{3.12}$$

where $\hat{\mathbf{c}}_{\mathrm{h}}(\tau)$ and $\hat{\mathbf{c}}_{\mathrm{in}}(\tau)$ are the homogeneous and inhomogeneous solutions, respectively. One can

write the solution as

$$\begin{pmatrix} \hat{a}(\tau) \\ \hat{b}(\tau) \end{pmatrix} = \begin{pmatrix} r_{11}(\tau) & r_{12}(\tau) \\ r_{21}(\tau) & r_{22}(\tau) \end{pmatrix} \begin{pmatrix} \hat{a}(0) \\ \hat{b}(0) \end{pmatrix} + \int_0^\tau \mathrm{d}s \begin{pmatrix} r_{11}(\tau,s) & r_{12}(\tau,s) \\ r_{21}(\tau,s) & r_{22}(\tau,s) \end{pmatrix} \begin{pmatrix} \sqrt{2G}\,\hat{f}_a^\dagger(\tau) \\ \sqrt{2\Gamma}\,\hat{f}_b(\tau) \end{pmatrix}, \quad (3.13)$$

where

$$\hat{T}\exp\Big[\int_0^\tau \mathbf{M}(s)\,\mathrm{d}s\Big] \equiv \begin{pmatrix} r_{11}(\tau) & r_{12}(\tau) \\ r_{21}(\tau) & r_{22}(\tau) \end{pmatrix} \quad (3.14)$$

and

$$\hat{T}\exp\Big[\int_s^\tau \mathbf{M}(s')\,\mathrm{d}s'\Big] \equiv \begin{pmatrix} r_{11}(\tau,s) & r_{12}(\tau,s) \\ r_{21}(\tau,s) & r_{22}(\tau,s) \end{pmatrix}. \quad (3.15)$$

Since G varies with time, we cannot simply convert the matrix exponential in equation (3.12) as we did in chapter 2. We need to find the intensity in order to solve the equation numerically. Noting that only $\langle \hat{f}_i(s)\hat{f}_i^\dagger(s')\rangle = \delta(s-s')$ and the other commutation relations are zero, and that $|\Psi(\tau)\rangle = |z,z\rangle\otimes|0,0\rangle$ and $|z\rangle = \hat{S}(z)|0\rangle$, the intensity in the amplifying channel is

$$\begin{aligned} I_a(\tau) &= \langle \hat{a}^\dagger(\tau)\hat{a}(\tau)\rangle \\ &= r_{11}^*(\tau)r_{11}(\tau)\langle \hat{a}^\dagger(0)\hat{a}(0)\rangle + r_{11}^*(\tau)r_{12}(\tau)\langle \hat{a}^\dagger(0)\hat{b}(0)\rangle \\ &+ r_{12}^*(\tau)r_{11}(\tau)\langle \hat{b}^\dagger(0)\hat{a}(0)\rangle + r_{12}^*(\tau)r_{12}(\tau)\langle \hat{b}^\dagger(0)\hat{b}(0)\rangle \\ &+ 2G\int_0^\tau \mathrm{d}s \int_0^\tau \mathrm{d}s'\, r_{11}^*(\tau,s)r_{11}(\tau,s')\langle \hat{f}_a(s)\hat{f}_a^\dagger(s')\rangle \\ &= \big(r_{11}(\tau)r_{11}^*(\tau) + r_{12}^*(\tau)r_{12}(\tau)\big)\sinh^2 r \\ &+ 2G\int_0^\tau \mathrm{d}s\, r_{11}^*(\tau,s)r_{11}(\tau,s). \end{aligned} \quad (3.16)$$

At $t = 0$, we have $I_a(0) = \sinh^2 r$, and hence

$$G = \frac{G_0}{1 + (\sinh^2 r)/I_{\text{sat}}}. \tag{3.17}$$

Our algorithm to solve equation (3.12) is as follows: at $\tau = 0$ we substitute equation (3.17) into equation (3.9). Then we solve the system of equations assuming that the gain is constant, and thereby find $r_{i,j}(\tau, s)$. Afterward, we substitute these coefficients into equation (3.16) and find the new intensity. Substitute the new I_a in the dynamic matrix and repeat the same procedure until $I_a = I_{sat}$, for which $G = G_0/2$. Having $r_{ij}(\tau_i)$, where $i = 0 : 0.00001 :$ final time, in hand, we can find all favorite quantities such as the entanglement of the output fields or the Wigner function (see the next sections).

3.3 The time evolution of Wigner function

In quantum mechanics, a pure (mixed) microscopic system is described by a state vector (density matrix). In addition to these abstract objects, there are some representations in phase space, called distribution functions, that directly introduce the properties of a quantum state. These distribution functions are of interest because the extension of the quantum theory of radiation involves the non-quantum stochastic effects such as thermal fluctuations. Moreover, using the methods of classical statistical physics, one can calculate such distributions elucidate the interface between classical and quantum physics such that quantities of interest in a quantum-mechanical problem [134]. This quantum-classical correspondence is particularly appealing for partial differential equations like the master equation. Furthermore, in quantum optics, often the radiation fields are nearly classical but still have important quantum features [135]. The essentially quantum mechanical nature of the problem is present in terms of the interpretation of apparently classical variables [47].

One should note that the commutation relation between the position and momentum operators, $[\hat{x},\hat{p}] = i$, imposes some limitations on the phase space description. For example, while in classical mechanics it is possible to show a point in phase space with a well-defined position and momentum, the commutation relation does not allow to define a genuine phase-space distribution. Nonetheless, we can define an object like the Wigner function that depends on the eigenvalues of the position as well as the momentum operator [136]. One can use the Wigner function to calculate a class of quantum mechanical averages in the same manner as the classical phase-space distribution function is used to calculate classical averages provided the operator is Weyl, or symmetrically, ordered in terms of creation and annihilation operators [136].

The Wigner function facilitates the visualization and tomographic reconstruction of quantum states. It has a lot of applications in optics and signal processing [137, 138] as well as quantum computing [139, 140, 141]. The Wigner function of a quantum state described by a density operator $\hat{\rho}$ is defined as [136]:

$$W(x,p) \equiv \frac{1}{2\pi}\int_{-\infty}^{\infty} d\xi \exp(-ip\xi)\Big\langle x+\frac{1}{2}\xi|\hat{\rho}|x-\frac{1}{2}\xi\Big\rangle, \tag{3.18}$$

where $|x-\frac{1}{2}\xi\rangle$ is the eigenket of position operator. Moreover, $\int_{-\infty}^{\infty} d\xi \int_{-\infty}^{\infty} dp W(x,p) = 1$. In contrast to classical distribution functions that only accept positive values, the Wigner function can also take negative values, which is a signature of nonclassical states (because of possible negative values, the Wigner function is called "quasi-distribution"). However, the positivity of the Wigner function does not necessarily imply that the state is classical. For example, the squeezed states have a positive Wigner function, though they are nonclassical [86].

Since the Wigner function provides information about the system, it is interesting to know how it evolves with time. In open systems like that depicted in Figure 3.1, the time evolution is

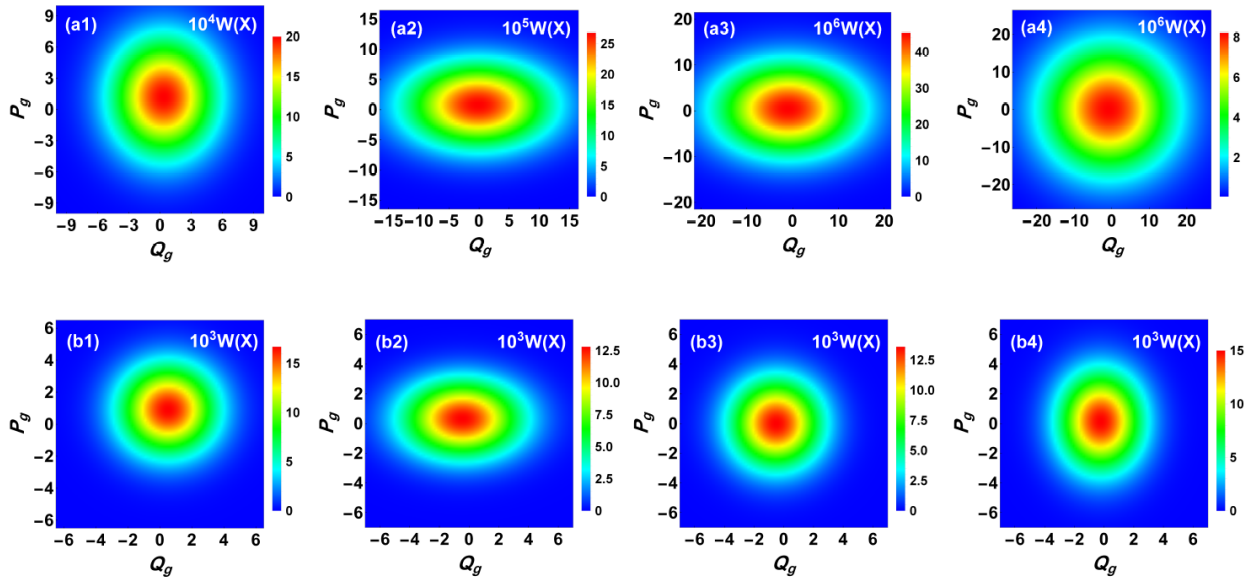

Figure 3.2: The projection of the scaled Wigner function of the coupled gain-loss waveguides on (Q_B, P_B) plane. The top row (a1 to a4) shows the time evolution of the Wigner function in the unsaturated case at times $Jt = 2, 4, 6$, and 8, respectively. We have assumed the squeezing parameters of both input signals to be equal: $r_1 = r_2 = 0.8$ and $\theta_1 = \theta_2 = 0$. Also, $\tilde{g}/J = 0.5$ and $\gamma/J = 0.3$. The bottom row (b1 to b4) demonstrates the time evolution in the saturated case at the same time intervals. All parameters, except the gain, are equal to those in the unsaturated case. Here, in the normalized version of equation (3.4), $g_0/J = 4.5$, $I_{\text{sat}} = 0.1$, and $I_a(Jt) = \langle \hat{a}^\dagger(Jt)\hat{a}(Jt)\rangle$.

affected by the quantum noise and the amplification (dissipation) process. In particular, one may ask how the gain saturation affects the dynamical behavior of the Wigner function. We address this question by comparing the time evolution of the Wigner function in the unsaturated and saturated cases. We will also show the interplay between the quantum noise and the amplification results in a quasi-steady state of the Wigner function.

The Wigner functions of fields in the coupled gain-loss waveguides have some special features. If the gain rate is fixed, the quantum states of the fields inside the system keep to be Gaussian, which takes the form [142]

$$W(X) = \frac{\exp\left[-\frac{1}{2}XVX^T\right]}{\pi\sqrt{\det[V]}}, \tag{3.19}$$

because the inputs to waveguides A and B are squeezed vacuum states. In this equation, $X \equiv (Q_A, P_A; Q_B, P_B)$, and the parameters inside the parenthesis are quadratures of the fields defined as

$$\hat{Q}_m = \frac{1}{\sqrt{2}}\left(\hat{c} + \hat{c}^\dagger\right),\ \hat{P}_m = -\frac{i}{\sqrt{2}}\left(\hat{c} - \hat{c}^\dagger\right), \tag{3.20}$$

where m stands for A and B and $c = a, b$. The 4×4 matrix V in equation (3.19) is the covariance matrix (CM) [83] we defined in equation (2.15):

$$V = \begin{pmatrix} A & C \\ C^T & B \end{pmatrix}, \tag{3.21}$$

whose entries are

$$V_{ij} = \frac{1}{2}\langle \hat{X}_i \hat{X}_j + \hat{X}_j \hat{X}_i \rangle - \langle \hat{X}_i \rangle \langle \hat{X}_j \rangle. \tag{3.22}$$

Here we assume that the input to the waveguides is a single-mode squeezed vacuum state, $|z\rangle = S(z)|0\rangle$. One should note that the quadratures involved in equation (3.19) include two parts: contribution of the input that is going to be amplified or dissipated (the homogeneous part of equation (3.3)) and the contribution of the quantum noises (the non-homogeneous part of equation (3.3)). Therefore, the gain saturation can directly affect both parts. Particularly, it alters the time evolution due to the noise terms, which is proportional to the square root of the gain coefficient.

The first and second rows of Figure 3.2 show two examples of time evolutions of the Wigner function in the unsaturated and saturated cases, respectively. We assume that, in the top row, the gain coefficient is larger than the loss coefficient. In the unsaturated case, the gain coefficient is constant but, in the saturated case, an effectively time-dependent factor $g(t)$ gives a different evolution pattern. Under the gain saturation, the gain coefficient becomes lower than the loss coefficient, regardless of whether it is initially higher than the loss coefficient. As Figures 3.2(a1)-(a4) show, the non-zero domain of the Wigner function expands with time, but its peak value substantially decreases. On the other hand, neither the domain nor the peak value of the Wigner function changes

remarkably with time in the saturated case (Figures 3.2(b1)-(b4)). In other words, the Wigner function evolves into a quasi-steady state. Since the gain coefficient decreases considerably upon the saturation, the quantum noise effect also diminishes on the way to evolve into the quasi-steady state. One should note that the magnitudes and shapes of the Wigner functions are different due to the absence or the presence of the gain saturation. For example, the Wigner function profile in Figure 3.2(a4) is circular, but in Figure 3.2(b4) it becomes elliptical. Moreover, in the unsaturated case, the Wigner function profile keeps switching between circular and elliptical profiles (Gaussian and non-Gaussian functions) for long times, whereas in the saturated case the profile becomes almost circular after a short time and remains circular.

3.4 The effect of gain saturation of entanglement

3.4.1 Time evolution of entanglement

In the previous chapter, we showed that the coupled gain-loss waveguide system can be a platform for generating continuous-variable entangled output fields [143]. However, amplifiers add quantum noises to the optical fields, and the noise is especially significant in the amplification of fields with low photon numbers. Even if the input is shot-noise-limited, the output remains noisy [86]. Meanwhile, one should understand that the quantum noise associated with amplification is more detrimental to entanglement because in the amplification process more photons are added to the optical field, while in the dissipation process, a portion of the photons disappears via absorption. Mathematically, one can confirm the dominant role of the amplification noise by the fact that in the calculation of $\langle \hat{a}^{\dagger}\hat{a} \rangle$ the noise terms associated with the dissipation vanish because of the commutation relations.

Moreover, the eigenvalues of such a non-Hermitian system are in general complex, and

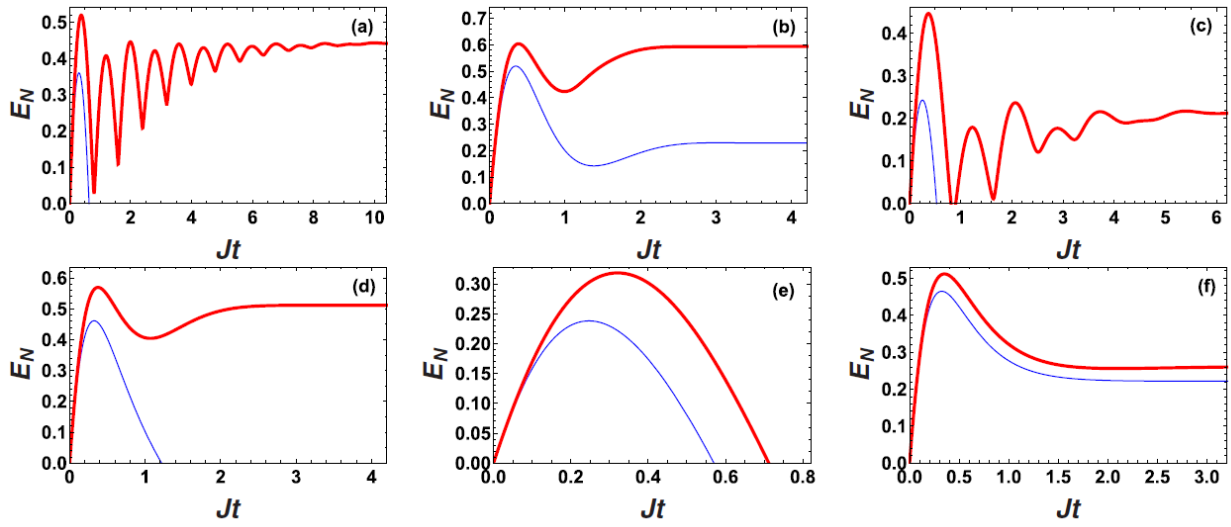

Figure 3.3: The time evolutions of the logarithmic negativity, E_N, in the unsaturated (thin, blue curves) and saturated (thick, red curves) cases. In all figures we assume that $r_1 = r_2 = 0.3$ and $\theta_1 = \theta_2 = \pi/4$. Moreover, we assume that the constant gain coefficient, $\tilde{g}$, in each case is equal to the initial value of $g(t) = g_0/(1 + I_a(t)/I_{\rm sat}$. The other parameters are (a) $g(0)/J = 0.3$, $g_0/J = 0.8$, $\gamma/J = 0.3$; (b) $g(0)/J = 0.3$, $g_0/J = 0.8$, $\gamma/J = 1.3$; (c) $g(0)/J = 0.7$, $g_0/J = 2$, $\gamma/J = 0.5$; (d) $g(0)/J = 0.7$, $g_0/J = 2$, $\gamma/J = 1.5$; (e) $g(0)/J = 1.25$, $g_0/J = 1.5$, $\gamma/J = 0.8$; (f) $g(0)/J = 1.25$, $g_0/J = 1.5$, $\gamma/J = 1.8$. The saturation intensity, $I_{\rm sat}$, in panels (a-d) is 0.05. In panels (e-f), $I_{\rm sat} = 0.5$.

the eigenvectors are nonorthogonal [144]. The main consequence of non-orthogonality of the eigenvectors is that, when random forces due to coupling to the reservoir drive the system, then the noise introduced to the system can be stronger than that in the systems with orthogonal eigenvectors [145]. If the quantum noise is intense, it degenerates a nonclassical light field into a classical one. Therefore, one may expect that noise-sensitive quantities such as entanglement deteriorate significantly in non-Hermitian systems. Knowing that the saturation of gain reduces the quantum noise strength, one may ask how the gain saturation impacts the nonclassical features of light fields such as entanglement. In particular, one could ask if the saturation effect can reduce the quantum noise to a level that the entanglement sudden death is avoided.

Regarding the above points, we show below that the saturation effect can thoroughly al-

ter the time evolution of entanglement. Under some special circumstances, the saturation of gain significantly reduces the quantum noise so that the entanglement of output fields can be well preserved. Like the previous chapter, to quantify the degree of entanglement of a field in Gaussian state, we use the logarithmic negativity (2.19):

$$E_N = \max[0, -\ln 2\eta],$$

In Figure 3.3, we present the numerically calculated time evolutions for some examples of field entanglement, comparing the evolved E_N in the unsaturated case (denoted by a thin, blue curve) to that of the saturated case (shown by a thick, red curve). The gain coefficient in the unsaturated case, $\tilde{g}$, keeps being equal to $g(0)$. Since the input fields are in squeezed vacuum states, in all cases we have chosen small saturation intensities to demonstrate the difference between the unsaturated and saturated cases better. If we assume other inputs like squeezed coherent states, larger saturation intensities yield the same time evolution patterns. In Figure 3.3(a) we impose the conditions $\tilde{g} \approx \gamma$ and $\tilde{g} + \gamma < 2J$. One should note that the eigenvalues of equation (3.3) in the unsaturated case are $1/2[\tilde{g} + \gamma \pm \sqrt{(\tilde{g} + \gamma)^2 - 4J^2}]$, so that the exponential factors involved in the solution are pure imaginary. In the saturated case, the exponentials are complex because of $g(t) < \gamma$. Moreover, in both cases, we expect to observe oscillations in E_N due to the imaginary parts of the exponentials. Figure 3.3(a) shows that the output field remains entangled within a finite time range in the unsaturated case. It reaches a maximum value, which depends on the coupling of the waveguides and the squeezing parameters of the input fields. In the beginning, the two fields are independent, but as they propagate, the optical field of waveguide A (B) penetrates the other waveguide, and thus they become entangled. However, due to the domination of quantum noise, E_N vanishes then. This phenomenon is entanglement sudden death as discussed in the previous chapter. In the saturated

case, however, E_N reaches a quasi-steady state after a short time. Also, the oscillatory behavior of E_N is consistent with the expectation. Nevertheless, the oscillations are tiny at long times because the intensity of the field propagating in waveguide A has approached its steady state, and it reaches a constant value since the gain coefficient depends on the intensity. Consequently, the strength of quantum noise substantially decreases so that E_N comes to a quasi-steady state.

Without changing $\tilde{g}$, we increase γ in Figure 3.3(b) such that $\tilde{g} < \gamma$, but still keep the relation $\tilde{g} + \gamma < 2J$. In contrast to Figure 3.3(a) where $g(t)/\gamma < 1$ after a short time, this ratio is always less than one in Figure 3.3(b). Since the gain is substantially smaller than loss (in this case, roughly four times), the quantum noise associated with the amplification is not strong enough to erase the entanglement. Therefore, after a long time, a steady state of entanglement is achieved. Here the saturation effect does not change the evolution pattern substantially. The only difference between the unsaturated and saturated cases is that, in the saturated case, E_N in the steady state is higher than that of the unsaturated case because the gain saturation reduces the quantum noise effect.

In Figure 3.3(c), there is the relation $\tilde{g} > \gamma$ but one still keeps $\tilde{g} + \gamma < 2J$. Since the gain is higher than the loss in the unsaturated case, we expect that the entanglement vanishes after a finite time. On the other hand, the saturation effect decreases the gain to a value much smaller than the loss, and hence the associated quantum noise is not dominant. Therefore, the entanglement measure E_N again approaches a steady state.

Without changing the gain, we increase the loss coefficient in Figure 3.3(d) so that $\tilde{g} < \gamma$ and $\tilde{g} + \gamma > 2J$. Although the gain is lower than the loss, it is not low enough to avoid the entanglement sudden death. However, the saturation effect reduces the quantum noise and results in a steady state. One should note that $g(t) + \gamma < 2J$ due to the saturation, although $g(0) + \gamma > 2J$.

In Figure 3.3(e), the system parameters keep the relations $\tilde{g} > \gamma$ and $\tilde{g} + \gamma \approx 2J$. Moreover,

we use a higher saturation intensity for Figures 3.3(e) and 3.3(f) (10 times higher than that of the previous figures). In this case, there is no considerable difference between the unsaturated and saturated cases because in both cases the gain factor is large enough, so the associated quantum noise cancels the entanglement. The saturation effect only modifies the maximum value of E_N. In Figure 3.3(f), one has the relations $\tilde{g} < \gamma$ and $\tilde{g} + \gamma > 2J$. Interestingly, in both unsaturated and saturated cases, E_N approaches a steady state. Moreover, the difference between these cases is small. In contrast to the previous situations, the relation $g(t) + \gamma > 2J$ is held forever for the saturated cases, the saturation effect only leads to a small modification.

To sum up, one notices that a non-zero E_N is possible when $g(t) \ll \gamma$, provided the initial gain is not too high so that the associated quantum noise quickly erases the entanglement. The numerical calculations are based on parameters achievable in laboratory. For example, they are close to those in a recent experiment [25] of two high-Q silica-microtoroid resonators with balanced, effective gain, in which $\gamma =$ 227-2210 MHz, $g =$ 2835 MHz, and $J =$ 8-544 MHz. Therefore, by choosing large coupling coefficients, it is possible to obtain $g/J < 10$ or $\gamma < 10$. One can engineer the gain and saturation intensity by changing the dopant density of the gain medium. We assumed low saturation intensity to better demonstrate the difference between the situation of unsaturated gain and that with saturated gain. If the saturation intensity is very high, then $g(t) \approx g_0$ and hence no difference exists in the two situations. Due to the difference between the coupling between micro-resonators and waveguides, more exact simulation of possible experiments with waveguides should be based on the actual couplings between waveguides, which can be realized.

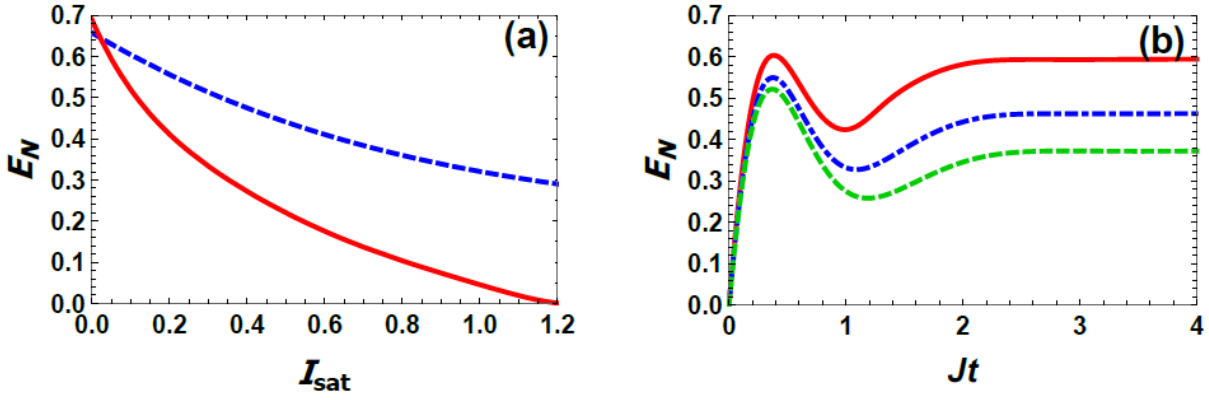

Figure 3.4: Panel (a) shows the variation of the degree of entanglement with the saturation intensity. We assume that $r_1 = r_2 = 0.3$, $\theta_1 = \theta_2 = 0$, $Jt = 4$, and $\gamma/J = 1.3$. The red curve corresponds to $g_0/J = 0.8$, and the dashed, blue curve matches $g_0/J = 0.4$. The figure shows that the degree of entanglement decays in a quasi-exponential manner to zero as the saturation intensity increases. Panel (b) exhibits how the time evolution of E_N varies with changing the saturation intensity. In this case, $g_0/J = 0.8$, and the saturation intensities are 0.05 (red curve), 0.15 (dotted-dashed, blue curve), and 0.25 (dashed, green curve).

3.4.2 Entanglement variation with the saturation intensity

After one sees the time evolution change of entanglement due to gain saturation, it is interesting to know how the degree of entanglement varies with the saturation intensity. For this purpose, we consider a particular time when E_N approaches a steady state. As an example, we adopt the parameters of Figure 3.3(b) and select $Jt = 4$ in Figure 3.4(a), but the saturation intensity remains a variable. The solid (red) and dashed (blue) curves in the figure correspond to $g_0/J = 0.8$ and $g_0/J = 0.4$, respectively. Figure 3.4(a) shows that E_N quasi-exponentially decays to zero as the saturation intensity increases. Since higher saturation intensity leads to a higher gain coefficient that intensifies the quantum noise, such quasi-exponential decay occurs. Also, by comparing the results, one notes that a lower gain demands a higher saturation intensity so that the quantity E_N vanishes. Figure 3.4(b) shows that the time evolution changes as the saturation intensity increases.

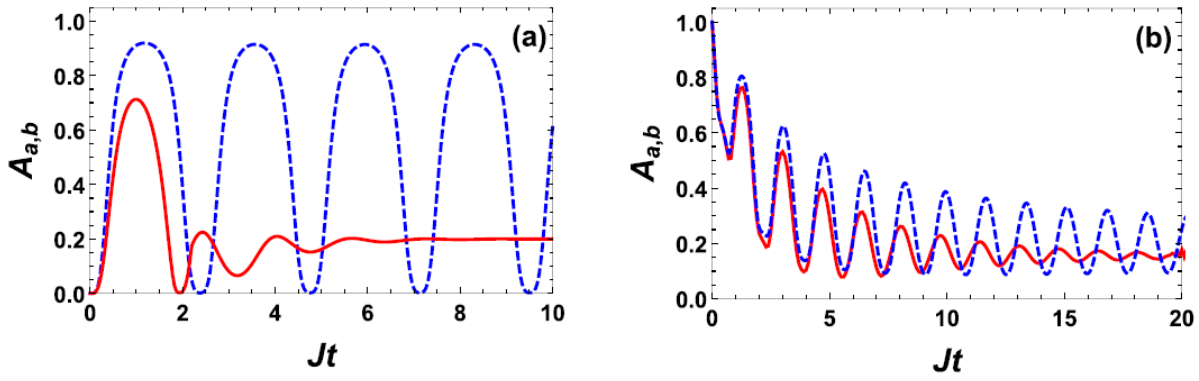

Figure 3.5: Panel (a) shows the cross-correlation function for the input fields to the waveguides in the Fock state, $|n,m\rangle$. The dashed and solid curves demonstrate the unsaturated and saturated cases, respectively. Here we assume $n = m = 10$. The other parameters are: $\gamma/J = 0.5$, $g_0/J = 2$, $g(0) = 1$, and $I_{sat} = 10$. In panel (b) the input to the waveguides is in the coherent state $|\alpha,\beta\rangle$. We assume $\alpha = 1$ and $\beta = 2$. The other parameters are $\gamma/J = 0.4$, $g_0/J = 0.5$, $g(0) = 0.42$, and $I_{sat} = 5$.

For higher saturation intensities, the steady-state value of $g(t)$ and hence the quantum noise increases and the steady-state value of E_N decreases.

3.5 Influence of gain saturation on cross-correlation function

Finally, we examine the Hanbury-Brown-Twiss (HBT) cross-correlation [86] between the two modes $\hat{a}$ and $\hat{b}$:

$$A_{a,b} = \frac{\langle \hat{a}^\dagger(t)\hat{b}^\dagger(t)\hat{a}(t)\hat{b}(t)\rangle}{\langle \hat{a}^\dagger(t)\hat{a}(t)\rangle\langle \hat{b}^\dagger(t)\hat{b}(t)\rangle}, \tag{3.23}$$

where $\langle \hat{a}^\dagger(t)\hat{b}^\dagger(t)\hat{a}(t)\hat{b}(t)\rangle$ is proportional to the probability of simultaneously detecting one photon each in the output of both waveguides. $\langle \hat{a}^\dagger(t)\hat{a}(t)\rangle$ and $\langle \hat{b}^\dagger(t)\hat{b}(t)\rangle$ are the photon numbers in waveguides A and B, respectively (individual detections in the outputs). One can use the quantum regression theorem [86] for Gaussian states to simplify equation (3.23):

$$\langle \hat{a}^\dagger(t)\hat{b}^\dagger(t)\hat{a}(t)\hat{b}(t)\rangle = \langle \hat{a}^\dagger(t)\hat{a}(t)\rangle\langle \hat{b}^\dagger(t)\hat{b}(t)\rangle + \langle \hat{a}^\dagger(t)\hat{b}(t)\rangle\langle \hat{b}^\dagger(t)\hat{a}(t)\rangle. \tag{3.24}$$

We classify the outputs according to their cross-correlation functions (for a single mode, the second order correlation function). If $A_{a,b} > 1$, then the photon statistics is sub-Poissonian. In this case the photons are not equally spaced, but rather appear in bunches. If $A_{a,b} = 1$, the photon statistics is Poissonian, which is the characteristic of a coherent light filed. Then the photons are randomly spaced. If $A_{a,b} < 1$, the photon statistics is super-Poissonian, and the photons are anti-bunched (equally spaced) [80]. The latter is the feature of non-classical light. One may ask how the gain saturation affects the cross-correlation function. To address this question, we consider two different cases in Figure 3.5. In Figure 3.5(a), we assume that the input to the waveguides is in the Fock state $|n,m\rangle$ (tensor product of two independent Fock states). Moreover, we suppose that the gain coefficient is larger than the loss coefficient. A dashed (solid) curve denotes the unsaturated (saturated) case. Initially, the state is purely quantum mechanical and accordingly $A_{a,b} = 0$, but because of the coupling between the waveguides, the photons can tunnel from one waveguide to the other one. Therefore, the cross-correlation function oscillates in time. In the saturated case, however, the oscillations disappear after a short time, and the cross-correlation function approaches a constant value. Also, the average value of $A_{a,b}$ in the saturated case is less than that of the unsaturated case. This shows that the non-classical behavior of the fields is preserved better in the saturated case because the quantum noise is damped due to the gain saturation.

In Figure 3.5(b) we consider the input to the waveguides to be in coherent state $|\alpha,\beta\rangle$, which is a quantum state showing classical features. Because of this reason, one expects that the differences between the saturated and unsaturated cases is not significant. As Figure 3.5(b) shows, the difference between the two cases is indeed less important. An interesting feature of the coherent input fields is that the cross-correlation function becomes not to remain to one throughout the non-Hermitian process. This behavior is in contrast to the case of an unprocessed coherent

state whose cross-correlation function remains equal to one forever.

3.6 Summary and conclusion

We have demonstrated how the gain saturation affects the quantum noise in a non-Hermitian system when the quantum properties of light are concerned. As the quantum noise alters the nonclassical properties of light, one sees that the gain saturation substantially changes the nonclassical features of light. As examples, we first considered the Wigner function, which is an alternative to the state vector and density matrix for the system. We find that the Wigner function evolves into a quasi-steady state due to gain saturation, whereas in the unsaturated case, the distribution of Wigner function in phase space expands, and its peak value drastically decreases. Moreover, the profile of the evolved Wigner function is different for the saturated and unsaturated cases. The gain saturation reduces the gain coefficient with time, and therefore the quantum noise effect is reduced. Also, we investigated the time evolution of entanglement, which is a pure quantum feature with no classical counterpart. We consider different cases in which the gain, loss, and coupling coefficients are comparable or very different from each other. Generally, as long as the quantum noise level is high, a steady-state of entanglement is not achievable. However, the gain saturation reduces the quantum noise strength, and hence in most cases, one can attain a final steady state. A non-zero entanglement of the output fields is possible only for the cases with $g(t) \ll \gamma$. Then, we show that the gain saturation is especially meaningful when the saturation intensity is low. On the other hand, if the saturation intensity is sufficiently high, the degree of entanglement vanishes, or the difference between the saturated and unsaturated cases is negligible. Finally, we examined the cross-correlation function between the output modes for the inputs in quantum states. All these results indicate that gain saturation does exert considerable impact on the quantum properties of

light fields processed by our concerned non-Hermitian setup.

4 Dyanmical phonon laser operating in a magnomechanical system

4.1 Phonon laser basics

As the same wave equation governs the oscillations of atoms, ions, and molecules in a sound wave and the oscillation of electric and magnetic fields in an optical wave, electromagnetic waves and sound waves are similar. Therefore, one can apply the concepts and techniques used in optics in acoustic. For example, one can refer to the analogy between the acoustic and optical microscopes, radar and sonar, and electrical and acoustic impedances. According to quantum physics, the quanta of light (photons) and sound (phonons) obey the same commutation relations describing the bosons [146].

The quantum nature of light allows us to plan a device that emits coherent photons of identical frequencies and phases. In 1917, Albert Einstein predicted the so-called stimulated emission, but it took four decades to bring this concept to practice. Laser, the device emitting coherent light through a process of optical amplification based on the stimulated emission of electromagnetic radiation, was built in 1960. Regarding the similarities between the optical and sound waves, one may ask if it is possible to make a device emitting coherent "phonons" of the same frequency and phase via a stimulated process. Since sound waves propagate five orders of magnitude slower than the speed of light, the wavelength of sound waves is much shorter than that of light waves of the same frequency. Therefore, one can perform highly precise nondestructive measurements and achieve a high concentration of energy using focused sound waves. Conventional sources of sound waves, such as piezoelectric transducers, do not operate efficiently above a few tens of gigahertz. Hence, a phonon laser would be of great interest. Despite the similarities between photons

and phonons, it is hard to develop a phonon laser because the short wavelength of sound causes spontaneous emission processes to dominate over the stimulated emission unless one modifies the density of phonon states [146].

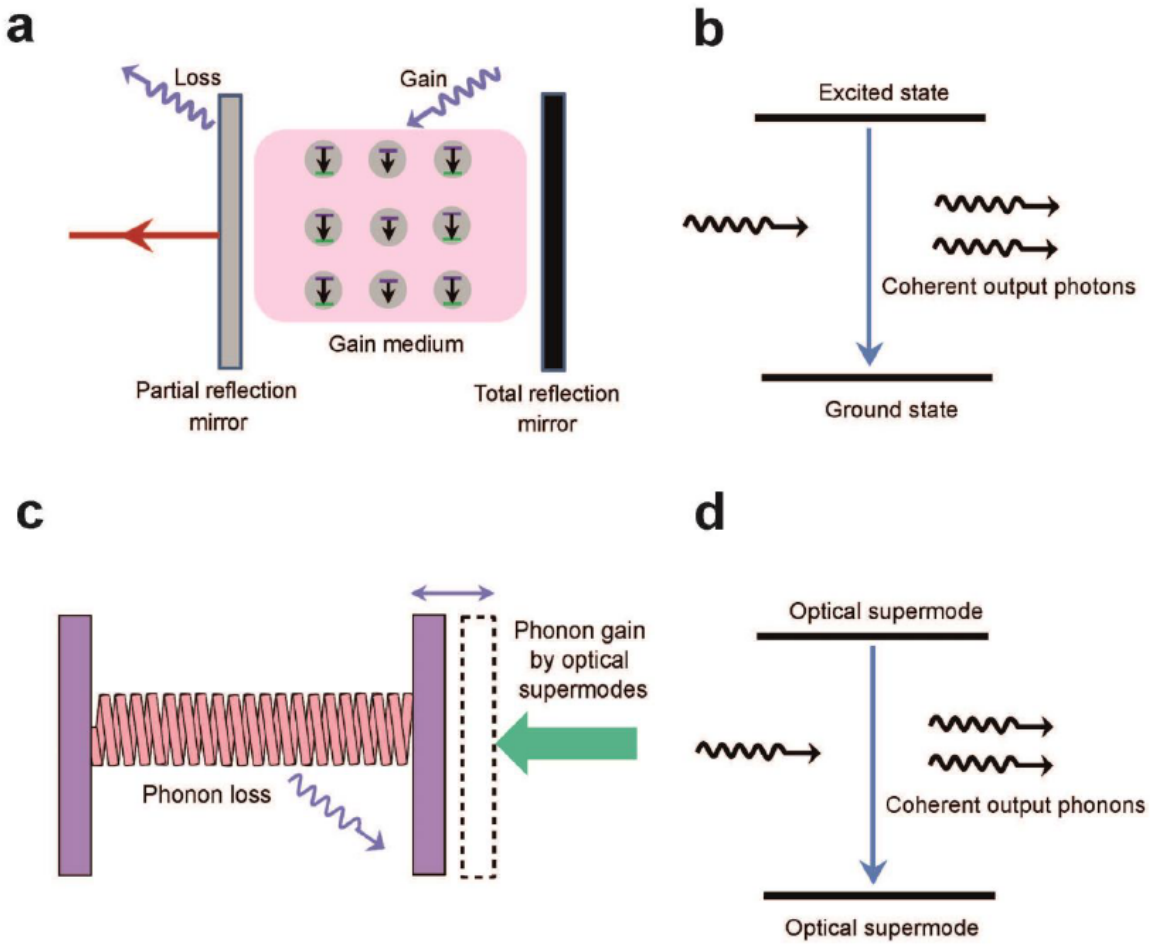

Figure 4.1: (a) The scheme of a one-dimensional optical laser with a gain medium in an optical cavity having one fully-reflecting mirror at one end and a partially-reflecting mirror at the other end. (b) Mechanism of an optical laser, in which an optical mode interacts with the gain medium and coherent output photons are generated via the stimulated emission process. (c) Equivalent one-dimensional phonon laser with gain provided by the optical supermodes acting as a "two-level system". (d) The mechanism of a phonon laser in which the mechanical mode interacts with the optical supermodes that play the role of a two-level system, such that coherent output phonons are generated [147].

In 2010, a research group at Caltech demonstrated the first experimental work on an optically pumped phonon laser in an optomechanical [51] system of coupled whispering-gallery-mode (WGM) passive optical resonators, one of which supports mechanical mode [148]. In conventional lasers, stimulated emission occurs from upper to lower states of the atoms and ions. But in the Caltech setup, the supermodes of the WGM resonators play the role of upper and lower levels (in the next sections, we will define supermode). The transitions between these levels are induced by a phonon field due to the mechanical mode. However, there is a subtle difference between the two-level atom and the supermodes of the WGM resonators. In the phonon laser, the traditional roles of the material (laser medium) and cavity modes (lasing field) are reversed. Here the medium is purely optical, while the laser field is provided by the material as a phonon mode (see Figure 4.1) [148].

One attains the best operation of the phonon laser if the frequency separation between the upper and lower supermodes equals that of the mechanical mode. Under this resonance condition, the upper state is populated with a sufficient number of photons coming from the pump laser via the optical fiber. Then, these photons are split into the lower frequency photons of the lower state and the "coherent phonons". These vibrations are picked up optically and their power depends on the pump power. This dependence demonstrates evidence of the onset of stimulated emission, also known as the lasing threshold. Since phonons, as well as photons, are bosons, one can interpret this process as a three-wave parametric process in which two waves (the "pump" and the "idler") are optical, and the third one (the "signal") is acoustic. Also, one can view it as a stimulated Brillouin scattering, i.e., an inelastic collision in which a photon is converted to a downshifted photon and a phonon with energy equal to the difference is emitted. But one must achieve the threshold when the phonon gain surpasses the phonon loss, whereas in Brillouin or Raman lasers the threshold is

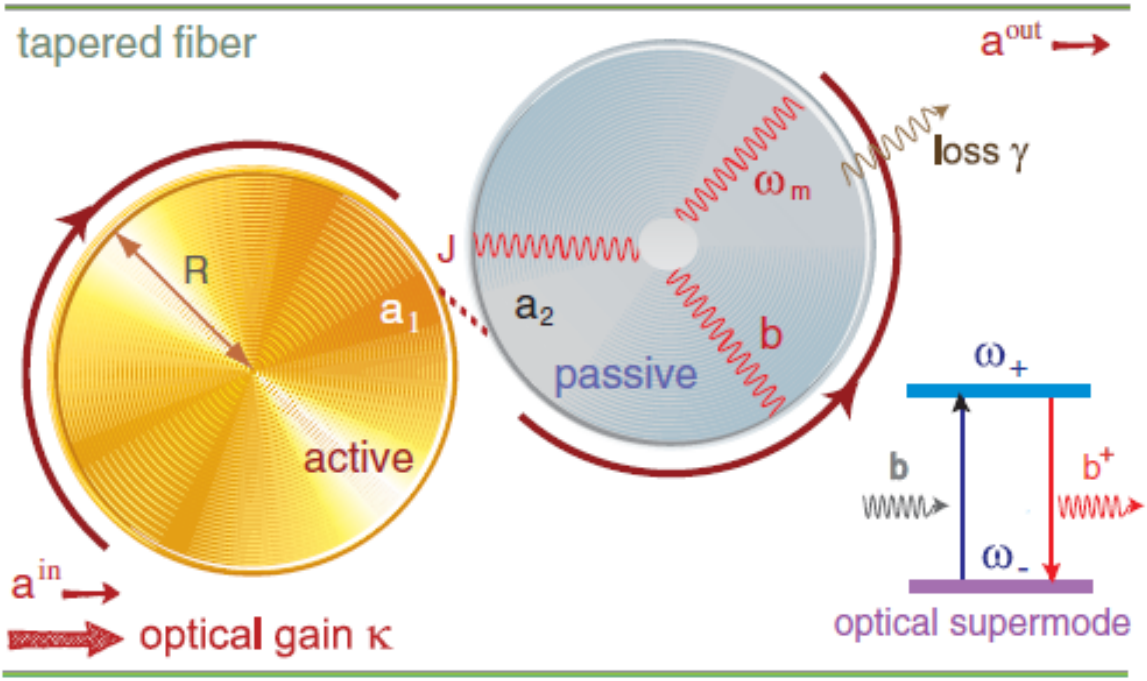

Figure 4.2: Coupled whispering- gallery-mode resonators. The optical tunneling rate J is tuned by changing the distance between the rsonators. The corresponding optical supermodes with frequencies ω_+ and ω_- coupled by phonons are also plotted [3].

achieved when the photon gain supersedes photon loss, and the coherent phonons are no more than a byproduct [146].

The Caltech setup with two "passive microresonators" suceeded by a $\mathscr{P}\mathscr{T}$-symmetric scheme. This later device has one active and one passive WGM resonator. The active resonator is doped with Erbium ions that provide a gain medium. This resonator is coupled to a taper fiber that conveys the optical pump. Also, there is a passive WGM resonator, supporting a mechanical mode, coupled to another tapered fiber that is used for the output field. The resonators are coupled via the evanescent wave, and the coupling can be adjusted by the gap between the resonators (see Figure 4.2). In contrast to passive COM, the $\mathscr{P}\mathscr{T}$-symmetric COM features a transition from linear to nonlinear regimes for intracavity-photon intensity. One can observe this transition by controlling

the gain-loss ratio. In the nonlinear regime, the optical pressure and hence the mechanical gain is enhanced. The enhanced nonlinearity leads to the ultralow threshold of the phonon laser [3]. The $\mathscr{P}\mathscr{T}$-symmetric phonon laser analysis modified by investigating it in the dynamical regime (beyond the steady state) [4] and under the gain saturation effect [132].

In addition to the phonon laser schemes mentioned above, we should refer to other setups like nonreciprocal phonon laser [149], a phonon laser operating near the exceptional point [147], phonon lasing in an electromechanical resonator [150], and semiconductor superlattices [151].

4.2 Magnomechanical phonon laser

Until today, most theoretical and experimental works on phonon laser are restricted to optomechanical systems. The traditional optomechanical systems operate based on the radiation force [51, 62, 152, 153, 154, 155], electrostatic force [156, 157], and piezoelectric force [158] for the interaction between phonons and cavity photons, but these mechanisms are not well adjustable.

Recently, a phonon laser in a cavity magnomechanical system is proposed [2]. This system includes a microwave cavity, a sphere of magnetic material, and a uniform external bias magnetic field (see Figure 4.3). In this system, the magnetostrictive interaction realizes the phonon-magnon coupling and magnetic dipole interaction leads to the cavity photon-magnon coupling. The magnons are simultaneously driven directly by a strong microwave field. In this scheme, the adjustable external magnetic field is a desirable control method for the phonon laser. Compared with optomechanical phonon laser, this scheme provides a new degree of freedom of manipulation [2].

This magnomechanical phonon laser is investigated in a steady state. However, as we know from optomechanical phonon lasers, the results in the dynamical case radically differ from

those in the steady-state. For example, for the $\mathscr{PT}$-symmetric phonon laser, the results show that only in the $\mathscr{PT}$-symmetric domain the phonon lasing is possible [3, 147], but dynamical investigation shows three fundamental differences: (1) phonon laser should operate under a blue-detuned pump rather than resonant and red-detuned pumps. Under blue-detuned drives, the phonon laser has a better performance with increased optical gain instead of reaching the optimum at the balanced gain and loss; (2) the phonon laser can operate even better in the $\mathscr{PT}$-symmetry broken in contrast to the steady-state case; (3) the quantum noise can significantly contribute to the supermode population inversion for magnifying the stimulated phonon field [4].

Regarding the mathematical isomorph between the optomechanical and magnomechanical Hamiltonians, one may ask if the dynamic magnomechanical phonon laser demonstrates a significant difference. Also, we are interested to know if/how the quantum noise changes the analysis. Since the magnomechanical systems have a better tunability, if one can achieve a strong phonon number, the magnomechanical phonon laser would be a good alternative to optomechanical phonon lasers.

Before we start analyzing the dynamical magnomechanical phonon laser, we disclose our motivation for choosing this kind of system. The magnetostrictive force is one of the main ingredients of magnomechanical systems. About two centuries ago, J. P. Joule discovered the magnetostrictive effect, which describes the deformation of magnetic material in response to an external magnetic field [52]. This phenomenon reveals itself as a change in volume in a strong magnetic field or as changes in linear dimensions in relatively low fields. The latter not only depends on the intensity of magnetization in the material but also varies with the direction in the crystal [159]. The deformation of the magnetic material also changes the magnetization. One can attribute the magnetostrictive effect to three types of interactions depending on the distance between ions: exchange

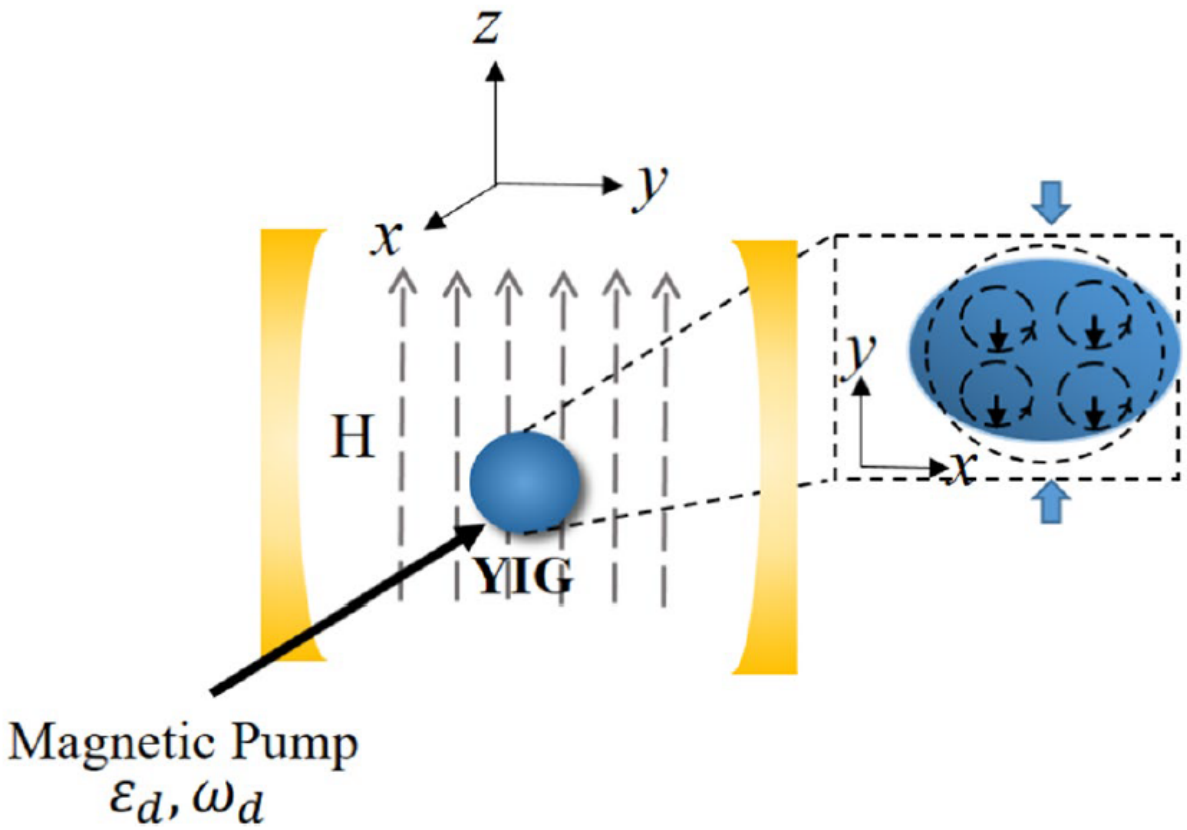

Figure 4.3: Schematic diagram of the magnomechanical phonon laser. The YIG sphere is inserted in the maximum magnetic field of the microwave cavity mode. Applying an external magnetic field H along the z-direction provides a uniform magnon mode for the YIG sphere. The enlarged YIG sphere on the right shows the magnetization of magnon (black down arrows), which leads to deformations on the surface of spheres (y-direction). Also, the deformation leads to changes in the magnetization of magnetons. [2].

interaction, dipole-dipole interaction, and spin-orbital interaction [52]. The magnetostrictive force provides an alternative mechanism allowing magnon —a different information carrier— to couple with phonon. Magnon is a collective excitation of magnetization, whose frequency is tuned by adjusting the bias magnetic field [59, 160, 161]. The magnetostrictive interaction is negligibly weak in dielectric or metallic materials, but in magnetic materials becomes dominant, which provides a great opportunity to establish a highly tunable hybrid system for coherent information processing.

Also, the magnetic field dependence of magnon provides our system with unprecedented tunability compared with optomechanical or electromechanical systems. Furthermore, the great flexibility allows us to achieve triple resonance among magnon, phonon, and photon [52].

The collective spins in a yttrium-iron-garnet (YIG) ferromagnetic material can be strongly [162, 163] or even ultrastrongly [164] coupled to a microwave cavity. The YIG material is ferromagnetic at both cryogenic [162] and room temperatures [163] because its Curie temperature is as high as 559 K. In contrast to spin ensembles in dilute paramagnetic impurities, these spins are strongly exchange-coupled and have a much higher density ($\approx 4.2 \times 10^{21}\mathrm{cm}^{-3}$) [165]. Because of high spin density, spin excitations can strongly couple to the cavity using a YIG sample as small as sub-millimeter in size. Also, one can achieve the ultrastrong coupling regime by increasing the size of the YIG sample or by using a specially designed microwave cavity [164]. Furthermore, the strong exchange coupling between the ferromagnetic electrons suppresses the contribution of magnetic dipole interactions to the linewidth of spin excitations, which can have a dominant role among paramagnetic impurities. Thus, for the same spin density, the spin excitations in YIG exhibits a much better quantum coherence than those of the paramagnetic impurities [165]. The YIG sphere is also an excellent mechanical resonator due to its superior material and geometrical properties. The changing magnetization induced by the magnon excitation inside the YIG sphere leads to deformation of its spherical geometry (and vice versa), introducing the coupling between magnon and phonon modes [52].

In summary, our main motivation of using magnomechanical systems are [166]: (1) Due to the high spin density and the strong spin-spin exchange interactions, the Kittel mode in the YIG sample has a long coherence time and a low damping rate, providing the condition of strong-coupling and even the ultrastrong-coupling regime; (2) Owing to the high tunability and good

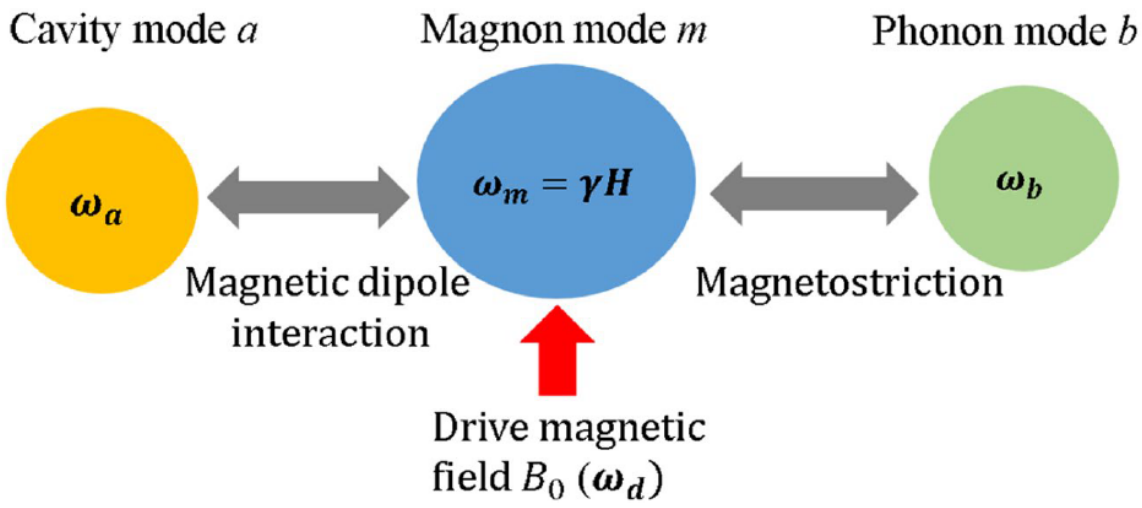

Figure 4.4: The equivalent coupling model. An external magnetic field **H** controls the frequency of magnon mode, and the phonon mode $\hat{b}$ regulates the intensity of the drive magnetic field. The frequency of drive magnetic field is ω_d. The drive magnetic field B_0 is the magnetic part of the microwave drive [2].

coherence, the cavity magnomechanical systems have become a promising platform to implement various novel phenomena; (3) The magnons in the small YIG sample can couple to the optical photons [167, 69, 168, 169], phonons [52], and superconducting qubits [70, 170]. This makes it possible to produce the magnon-photon- phonon entanglement [171] and squeezed states of magnons and phonons in cavity magnomechanics [172]. Moreover, owing to the superior material and geometrical features of the YIG, it acts as a perfect mechanical resonator, which introduces the phonon-magnon interaction. This property allows one to achieve magnetomechanically induced transparency (MMIT), which arises from the quantum interference between different excitation paths [52, 173]. MMIT is a coherent phenomenon similar to the electromagnetically induced transparency (EIT) [174] and optomechanically induced transparency (OMIT) [175].

4.3 Dynamics of the system

4.3.1 The Hamiltonian of the system

Figure 4.3 shows the phonon laser setup of reference [2] and Figure 4.4 demonstrates the a coupling model for the interactions involved in the process. In this section, we investigate the phonon laser system beyond the steady-state. In the Figure 4.3, we place a highly polished YIG sphere of 1 mm in a microwave cavity. Simultaneously, we apply a uniform external bias magnetic field **H** in the vertical direction. The range of the field **H** is between 0 and 1 T. This field establishes magnon-photon coupling. One can tune the rate of coupling by changing the position of the sphere. There are three modes in this system: cavity photon mode (with angular frequency ω_a), magnon mode (ω_m), and phonon mode (ω_b).

As indicated before, the magnetostrictive interaction leads to the coupling between magnons and phonons. The magnon excitation changes the magnetization, which leads to the deformation of the YIG sphere, converting it to a mechanical resonator with the phonon mode. We use a microwave source to drive the magnon mode. The directions of **H**, the drive magnetic field, and the magnetic field of the cavity mode are perpendicular to each other. Thus, we can adjust each one independently. Furthermore, we assume that the size of the YIG sphere is much smaller than the wavelength of the cavity so that the photon-photon coupling is negligible.

We consider the YIG sphere as an ensemble of N spins with a quantum number $1/2$ and of operator $\hat{S}_i$ with nearest-neighbor ferromagnetic exchange interaction $J > 0$ in an external magnetic field **H**. Then, the Hamiltonian of such a spin ensemble is [60]

$$\hat{H}_{\text{mag}} = g^* \mu_B \sum_{i=1}^{N} \hat{\mathbf{H}} \cdot \hat{S}_i - 2J \sum_{i,j} \hat{S}_i \cdot \hat{S}_j, \tag{4.1}$$

where g^* and μ_B are the g-factor and Bohr magneton, respectively. The first term is a magnetic

dipole interaction describing the Zeeman effect and the second term demonstrates the ferromagnetic exchange interaction between neighboring spins. Using a dispersion relation, we can unify these two terms and write

$$\hat{H}_{\text{mag}} = \sum_{\mathbf{k}} \omega_m(\mathbf{k})\, \hat{m}^\dagger \hat{m}, \tag{4.2}$$

where $\mathbf{k}$ is the wavevector of the spin-wave mode, and $\omega_m(\mathbf{k})$ includes two terms for the magnetic dipole and exchange interaction. In the static magnetic filed limit, the long-range dipole-dipole interaction between spins is dominant over the short-range exchange interactions. In the simplest case where the static magnetic field is uniform (Kittle mode), $\omega_m(\mathbf{k}) \rightarrow \omega_m = g^* \mu_B H$, and hence $\hat{H}_{\text{magnon}} = \omega_m \hat{m}^\dagger \hat{m}$.

The Hamiltonian of a microwave cavity mode is given by $\hat{H}_{\text{photon}} = \omega_a \hat{a}^\dagger \hat{a}$, where $\hat{a}^\dagger$ and $\hat{a}$ are the creation and annihilation operators of a microwave photon in the mode. Both magnetostatic modes and microwave cavity modes are linear systems described as quantum harmonic oscillators.

The Hamiltonian describing the magnetic dipole interaction of the Kittle mode with the microwave frequency cavity mode is

$$\hat{H}_{\text{coupling}} = g^* \mu_B (\hat{a} + \hat{a}^\dagger) \sum_{i=1}^{N} \delta\mathbf{B}(\mathbf{r}_i) \cdot \hat{S}_i. \tag{4.3}$$

If the microwave magnetic field $\delta\mathbf{B}(\mathbf{r}_i)$ is uniform throughout the YIG crystal, magnetic dipole coupling vanishes except for the uniform magnetostatic mode, i.e., the Kittel mode. Considering only the Kittel mode, the Hamiltonian takes a simple form (after cancelling nonconservative terms)

$$\hat{H}_{\text{coupling}} = J(\hat{a}\hat{m}^\dagger + \hat{a}^\dagger \hat{m}), \tag{4.4}$$

where J is the coupling strength between the Kittel mode and the microwave cavity mode. The coupling strength J between the Kittel mode and the microwave cavity mode must be compared

with the decay of the Kittel mode, γ_m, and the decay of the cavity mode, γ_a. If $J \gg \gamma_m, \gamma_a$, the hybrid system enters the strong coupling regime [60].

The Hamiltonian of the magnomechanical interaction is given by

$$\hat{H}_{\mathrm{M}} = -g\hat{m}^{\dagger}\hat{m}\left(\hat{b}+\hat{b}^{\dagger}\right), \tag{4.5}$$

whose full proof is presented in reference [52]. After including the microwave drive Hamiltonian, the total Hamiltonian can be written as the sum of the linear, nonlinear, and system-reservoir parts that the latter demonstrates the quantum noise:

$$\hat{H} = \hat{H}_L + \hat{H}_{NL} + \hat{H}_{SR}, \tag{4.6}$$

where

$$\hat{H}_L = \omega_a \hat{a}^{\dagger}\hat{a} + \omega_m \hat{m}^{\dagger}\hat{m} + \omega_b \hat{b}^{\dagger}\hat{b} + J\left(\hat{a}^{\dagger}\hat{m} + \hat{m}^{\dagger}\hat{a}\right) + iE\left(\hat{m}^{\dagger}e^{-i\omega_d t} - \hat{m}\,e^{i\omega_d t}\right), \tag{4.7}$$

$$\hat{H}_{NL} = -g\hat{m}^{\dagger}\hat{m}\left(\hat{b}+\hat{b}^{\dagger}\right), \tag{4.8}$$

and

$$\hat{H}_{SR} = i\left[\sqrt{2\gamma_a}\left(\hat{a}^{\dagger}\hat{f}_a - \hat{a}\hat{f}_a^{\dagger}\right) + \sqrt{2\gamma_m}\left(\hat{m}^{\dagger}\hat{f}_m - \hat{m}\hat{f}_m^{\dagger}\right) + \sqrt{2\gamma_b}\left(\hat{b}^{\dagger}\hat{f}_b - \hat{b}\hat{f}_b^{\dagger}\right)\right]. \tag{4.9}$$

Using equation (1.19), we obtain the system of differential equations describing the time evolution of the system operators:

$$\begin{aligned}
\dot{\hat{a}} &= -(\gamma_a - ig\hat{x})\hat{a} - iJ\hat{m} + Ee^{-i\delta t} + \sqrt{2\gamma_a}\,\hat{f}_a, \\
\dot{\hat{m}} &= \gamma_m \hat{m} - iJ\hat{a} + \sqrt{2\gamma_m}\,\hat{f}_m, \\
\dot{\hat{b}} &= -\gamma_b \hat{b} - i\omega_b \hat{b} + ig\hat{a}^{\dagger}\hat{a} + \sqrt{2\gamma_b}\,\hat{f}_b,
\end{aligned} \tag{4.10}$$

where $\hat{x} = (\hat{a} + \hat{a}^{\dagger})$ and $\delta = \omega_a - \omega_d$. The common method to solve this system of nonlinear equations is converting each operator to a classical average value plus a quantum fluctuation, i.e.,

$\hat{a} \to \alpha_s + \delta\hat{a}$. But this approximation requires a steady-state exists, whereas it is shown in reference [4] that there is no steady-state for the $\mathscr{P}\mathscr{T}$-symmetric optomechanical phonon laser. Intuitively, there should not be a steady-state for the magnomechanical phonon laser as well. Therefore, we use an alternative method for linearizing the equation (4.10), called the time evolution decomposition method. In section 1.3, we introduced the basics of this method, but here we fully explain it.

4.3.2 Decomposing the total evolution operator and the linearized equations of motion

Using equation (1.31), we can decompose the total time evolution operator as follows:

$$\begin{aligned}
\hat{U}(t) &= \hat{T}\exp\left[-i\int_0^t ds\left[\hat{H}_L(s)+\hat{H}_{NL}(s)+\hat{H}_{SR}(s)\right]\right] \\
&= \hat{U}_0(t)\hat{T}\exp\left[-i\int_0^t ds\,\hat{U}_0^\dagger(s)\left[\hat{H}_{NL}(s)+\hat{H}_{SR}(s)\right]\hat{U}_0(s)\right] \\
&= \hat{U}_0(t)\hat{T}\exp\left[-i\int_0^t ds\,\left[\hat{H}_1(s)+\hat{H}_2(s)\right]\right] \\
&= \hat{U}_0(t)\hat{T}\exp\left[-i\int_0^t ds\,\hat{U}_2(t,s)\hat{H}_1(s)\hat{U}_2^\dagger(t,s)\right]\hat{U}_2(t) \\
&\equiv \hat{U}_0(t)\hat{U}_1(t)\hat{U}_2(t),
\end{aligned} \tag{4.11}$$

where $\hat{U}_i(t) = \exp\big(-i\int_0^t ds\,\hat{H}_i(s)\big)$. First, we find $\hat{U}_0(t)$:

$$\begin{aligned}
\hat{U}_0(t) &= \hat{T}\exp\Big[-i\int_0^t \hat{H}_L(s)\,ds\Big] = \exp\Big[(-i\omega_a t)\hat{a}^\dagger\hat{a} + (-i\omega_m t)\hat{m}^\dagger\hat{m} \\
&\quad + (-i\omega_b t)\hat{b}^\dagger\hat{b} + (-iJt)\big(\hat{a}^\dagger\hat{m}+\hat{m}^\dagger\hat{a}\big) + E\hat{m}^\dagger\int_0^t e^{-i\omega_d s}ds - E\hat{m}\int_0^t e^{i\omega_d s}ds\big)\Big] \\
&= \exp\Big[(-i\omega_a t)\hat{a}^\dagger\hat{a} + (-i\omega_m t)\hat{m}^\dagger\hat{m} + (-i\omega_b t)\hat{b}^\dagger\hat{b} \\
&\quad + (-iJt)\left(\hat{a}^\dagger\hat{m}+\hat{m}^\dagger\hat{a}\right) + i\frac{E}{\omega_d}\hat{m}^\dagger\big(e^{-i\omega_d t}-1\big) + i\frac{E}{\omega_d}\hat{m}\big(e^{i\omega_d t}-1\big)\Big].
\end{aligned} \tag{4.12}$$

We simplify the second integral in equation (4.11) as $\hat{U}_0^\dagger(\tau)\big(\hat{H}_{NL}(\tau)+\hat{H}_{SR}(\tau)\big)\hat{U}_0(\tau) \equiv \hat{H}_1(\tau) + \hat{H}_2(\tau)$. To find the explicit form, we need to find $\hat{U}_0^\dagger(\tau)\hat{c}\hat{U}_0(\tau)$, where $\hat{c} = \hat{a}, \hat{m}, \hat{b}$. We can also sandwich $\hat{U}_0\hat{U}_0^\dagger$ between operators if necessary. Let define $\hat{U}_0 \equiv e^{-\hat{G}}$ and $\hat{A}(t) = e^{\hat{G}}\hat{a}e^{-\hat{G}}$, where

$\hat{G}^\dagger = -\hat{G}$. Then,

$$\frac{d\hat{A}}{dt} = e^{\hat{G}}\left[\frac{d\hat{G}}{dt}, \hat{a}\right]e^{-\hat{G}} = \left[\frac{d\hat{G}}{dt}, \hat{A}\right]. \tag{4.13}$$

And similarly we can find the eqautions related to $\hat{b}$ and $\hat{m}$ in this rotating frame. After simplifying equation (4.13), we obtain

$$\frac{d}{dt}\begin{pmatrix}\hat{A}\\ \hat{M}\end{pmatrix} = \begin{pmatrix}-i\omega_a & -iJ\\ -iJ & -i\omega_m\end{pmatrix}\begin{pmatrix}\hat{A}\\ \hat{M}\end{pmatrix} + \begin{pmatrix}0\\ Ee^{-i\omega_d t}\end{pmatrix}. \tag{4.14}$$

We define $\sqrt{4J^2 + (\omega_a - \omega_m)^2} = 2\Omega$, $\omega_a - \omega_m = \Delta$, and $\omega_a + \omega_m = 2\eta$. Then,

$$\begin{pmatrix}\hat{A}(t)\\ \hat{M}(t)\end{pmatrix} = \begin{pmatrix}\frac{2\Omega\cos(\Omega t) - i\Delta\sin(\Omega t)}{2\Omega} & e^{-i\eta t}\frac{iJ\sin(\Omega t)}{\Omega}\\ -e^{-i\eta t}\frac{iJ\sin(\Omega t)}{\Omega} & \frac{2\Omega\cos(\Omega t) + i\Delta\sin(\Omega t)}{2\Omega}\end{pmatrix}\begin{pmatrix}\hat{A}(0)\\ \hat{M}(0)\end{pmatrix} + \begin{pmatrix}\frac{iE\left(4\Omega^2 - \Delta^2\right)}{8J\Omega}\left(\frac{e^{-i(\Omega+\eta)t} - e^{-i\omega_d t}}{\eta + \Omega - \omega_d} + \frac{e^{i(\Omega-\eta)t} - e^{-i\omega_d t}}{\eta + \Omega - \omega_d}\right)\\ \frac{iE}{4\Omega}\left(\frac{(2\Omega - \Delta)\left(e^{-i(\Omega+\eta)t} - e^{-i\omega_d t}\right)}{\eta + \Omega - \omega_d} + \frac{(2\Omega + \Delta)\left(e^{i(\Omega-\eta)t} - e^{i\omega_d t}\right)}{\Omega - \eta + \omega_d}\right)\end{pmatrix}. \tag{4.15}$$

Noting that $\hat{A}(0) = \hat{a}$ and $\hat{M}(0) = \hat{m}$, we define "superoperators" as

$$\hat{o}_1 = \frac{\hat{a} + \hat{m}}{\sqrt{2}}, \qquad \hat{o}_2 = \frac{\hat{a} - \hat{m}}{\sqrt{2}}, \tag{4.16}$$

so that

$$\hat{a} = \frac{\hat{o}_1 + \hat{o}_2}{\sqrt{2}}, \qquad \hat{m} = \frac{\hat{o}_1 - \hat{o}_2}{\sqrt{2}}.$$

In fact, the superoperators are the orthogonal eigenstates of the Hermitian Hamiltonian $\omega_a\hat{a}^\dagger\hat{a} + \omega_m\hat{m}^\dagger\hat{m} + J\left(\hat{a}^\dagger\hat{m} + \hat{m}^\dagger\hat{a}\right)$. We can rewrite equation (4.15) versus new supermode operators:

$$\begin{pmatrix}\hat{A}(t)\\ \hat{M}(t)\end{pmatrix} = \frac{1}{\sqrt{2}}\begin{pmatrix}\cos(\Omega t) - i\frac{\Delta}{2\Omega}\sin(\Omega t) - i\frac{J}{\Omega}\sin(\Omega t)e^{-i\eta t} & \cos(\Omega t) - i\frac{\Delta}{2\Omega}\sin(\Omega t) + i\frac{J}{\Omega}\sin(\Omega t)e^{-i\eta t}\\ \cos(\Omega t) + i\frac{\Delta}{2\Omega}\sin(\Omega t) - i\frac{J}{\Omega}\sin(\Omega t)e^{-i\eta t} & -\cos(\Omega t) - i\frac{\Delta}{2\Omega}\sin(\Omega t) - i\frac{J}{\Omega}\sin(\Omega t)e^{-i\eta t}\end{pmatrix}\begin{pmatrix}\hat{o}_1\\ \hat{o}_2\end{pmatrix} \tag{4.17}$$

$$+\begin{pmatrix} \frac{iE\left(4\Omega^2-\Delta^2\right)}{8J\Omega}\left(\frac{e^{-i(\Omega+\eta)t}-e^{-i\omega_d t}}{\eta+\Omega-\omega_d}+\frac{e^{i(\Omega-\eta)t}-e^{-i\omega_d t}}{\eta+\Omega-\omega_d}\right) \\ \frac{iE}{4\Omega}\left(\frac{(2\Omega-\Delta)\left(e^{-i(\Omega+\eta)t}-e^{-i\omega_d t}\right)}{\eta+\Omega-\omega_d}+\frac{(2\Omega+\Delta)\left(e^{i(\Omega-\eta)t}-e^{i\omega_d t}\right)}{\Omega-\eta+\omega_d}\right) \end{pmatrix}$$

The equation for $\hat{B}$ is simple:

$$\hat{B}(t)=\hat{b}e^{-i\omega_b t}. \tag{4.18}$$

Thereby, we define a brief notation for equation (4.17) together with $\hat{B}(t)$:

$$\begin{pmatrix} \hat{A}(t) \\ \hat{M}(t) \\ \hat{B}(t) \end{pmatrix}=\begin{pmatrix} \alpha_{11} & \alpha_{12} & 0 \\ \alpha_{21} & \alpha_{22} & 0 \\ 0 & 0 & e^{-i\omega_b t} \end{pmatrix}\begin{pmatrix} \hat{o}_1 \\ \hat{o}_2 \\ \hat{b} \end{pmatrix}+\begin{pmatrix} E_1 \\ E_2 \\ 0 \end{pmatrix} \tag{4.19}$$

Then,

$$\begin{aligned} \hat{U}_0^\dagger(t)\left[\hat{H}_{NL}+\hat{H}_{SR}\right]\hat{U}_0(t) &= -g\hat{M}^\dagger\hat{M}\left(\hat{B}+\hat{B}^\dagger\right) \\ &+ i\left[\sqrt{2\gamma_a}\left(\hat{A}^\dagger\hat{f}_a-\hat{A}\hat{f}_a^\dagger\right)+\sqrt{2\gamma_m}\left(\hat{M}^\dagger\hat{f}_m-\hat{M}\hat{f}_m^\dagger\right)+\sqrt{2\gamma_b}\left(\hat{B}^\dagger\hat{f}_b-\hat{B}\hat{f}_b^\dagger\right)\right], \end{aligned} \tag{4.20}$$

$$\begin{aligned} \hat{H}_1 &= -g\left(\alpha_{21}E_2^*\hat{o}_1+\alpha_{22}E_2\hat{o}_2+\alpha_{21}^*E_2\hat{o}_1^\dagger+\alpha_{22}^*E_2\hat{o}_2^\dagger+|E_2|^2\right)\left(\hat{B}+\hat{B}^\dagger\right) \\ &+ i\sqrt{2\gamma_a}\left[\left(\alpha_{11}^*\hat{o}_1^\dagger+\alpha_{12}^*\hat{o}_2^\dagger+E_1^*\right)\hat{f}_a-\left(\alpha_{11}\hat{o}_1+\alpha_{12}\hat{o}_2+E_1\right)\hat{f}_a^\dagger\right] \\ &+ i\sqrt{2\gamma_m}\left[\left(\alpha_{21}^*\hat{o}_1^\dagger+\alpha_{22}^*\hat{o}_2^\dagger+E_2^*\right)\hat{f}_m-\left(\alpha_{21}\hat{o}_1+\alpha_{22}\hat{o}_2+E_2\right)\hat{f}_a^\dagger\right] \\ &+ i\sqrt{2\gamma_b}\left[\hat{B}^\dagger\hat{f}_b-\hat{B}\hat{f}_b^\dagger\right] \end{aligned} \tag{4.21}$$

and

$$\begin{aligned} \hat{H}_2 = -g\Big(&\alpha_{21}\alpha_{21}^*\hat{o}_1^\dagger\hat{o}_1+\alpha_{21}\alpha_{22}^*\hat{o}_2^\dagger\hat{o}_1+\alpha_{22}\alpha_{21}^*\hat{o}_1^\dagger\hat{o}_2+\alpha_{22}\alpha_{22}^*\hat{o}_2^\dagger\hat{o}_2\Big) \\ &\times\left(\hat{B}+\hat{B}^\dagger\right). \end{aligned} \tag{4.22}$$

Now we should calculate $\hat{U}_2(t,s)\hat{H}_1(s)\hat{U}_2^\dagger(t,s)$ appeared in equation (4.11). For example, we find an operator of $\hat{H}_1(s)$, say, $\hat{o}_1$ as follows:

$$\begin{aligned}\hat{U}_2(t,s)\hat{o}_1\hat{U}_2^\dagger(t,s) = \hat{o}_1 - i\mu_1\hat{o}_1\hat{b} - i\mu_2\hat{o}_1\hat{b}^\dagger - i\mu_3\hat{o}_2\hat{b} - i\mu_4\hat{o}_2\hat{b}^\dagger \\ + \text{ higher order terms},\end{aligned} \tag{4.23}$$

where, for example,

$$\mu_1 = g\int_s^t \alpha_{21}\alpha_{21}^* e^{-i\omega_b s}\, ds. \tag{4.24}$$

After finding all operators of $\hat{H}_1(s)$ in this rotating frame, noting that

$$g \ll \Omega, J, \eta, \omega_a, \omega_m, \gamma_a, \gamma_m,$$

we conclude that the corrections of this order are negligible, because we have terms like $g/2\Omega$ in the products. This is the only approximation we use. One should note that the effect of nonlinear magnomechanical term is included in $\hat{H}_1$ as well because of factor g in it. This approximation, which is independent of the drive E, linearizes the equations of motion.

Under this approximation, we can write the supermode populations as

$$\begin{aligned}\langle\hat{o}_i^\dagger\hat{o}_i(t)\rangle &= \mathrm{Tr}_{S,R}\big(\hat{U}_2^\dagger(t)\hat{U}_1^\dagger(t)\hat{U}_0^\dagger(t)\hat{o}_i^\dagger\hat{o}_i\hat{U}_0(t)\hat{U}_1(t)\hat{U}_2(t)\rho_S(0)\otimes\rho_R\big) \\ &= \mathrm{Tr}_{S,R}\big(\hat{U}_1^\dagger(t)\hat{U}_0^\dagger(t)\hat{o}_i^\dagger\hat{o}_i\hat{U}_0(t)\hat{U}_1(t)\hat{U}_2(t)\rho_S(0)\otimes\rho_R\hat{U}_2^\dagger(t)\big) \\ &= \mathrm{Tr}_{S,R}\big(\hat{U}_1^\dagger(t)\hat{U}_0^\dagger(t)\hat{o}_i^\dagger\hat{o}_i\hat{U}_0(t)\hat{U}_1(t)\rho_S(0)\otimes\rho_R\big),\end{aligned} \tag{4.25}$$

where the action $U_2(t)$ does not change the quantum state $\rho_S(0)\otimes\rho_R$ because the initial state $\rho_S(0)$ is the product of a cavity vacuum state and the mechanical thermal state $|\Psi\rangle = |0\rangle\langle 0|\otimes \sum_{n=0}^{\infty}\frac{n_{th}^n}{(1+n_{th})^{n+1}}|n\rangle\langle n|$, where n_{th} is the thermal reservoir mean occupation number. Thus, $H_2(t)|0\rangle_c = 0$ for the cavity vacuum state $|0\rangle_c$. The supermode populations $\langle\hat{o}_i^\dagger\hat{o}_i(t)\rangle$ only evolve due to the successive actions of $\hat{U}_0(t)$ and $\hat{U}_1(t)$. The unitary operation $\hat{U}_0(t)$ only displaces the supermode

operators in equation (4.17), but using (1.27) we find that the action $\hat{U}_1(t)$ of the Hamiltonian $\hat{H}_1$ leads to a system of dynamical equations:

$$\frac{d\hat{c}}{dt} = M\hat{c} + \lambda(t) + \hat{n}(t) \tag{4.26}$$

where

$$\hat{c} = \left(\hat{o}_1, \hat{o}_1^\dagger, \hat{o}_2, \hat{o}_2^\dagger, \hat{b}, \hat{b}^\dagger\right)^T. \tag{4.27}$$

The matrix M includes entries $m_{i,j}$ where i, j vary between 1 and 6. Also,

$$\begin{aligned}
\hat{n}_1 &= -\sqrt{2\gamma_a}\alpha_{11}^* \hat{f}_a - \sqrt{2\gamma_m}\alpha_{21}^* \hat{f}_m, \\
\hat{n}_2 &= -\sqrt{2\gamma_a}\alpha_{12}^* \hat{f}_a - \sqrt{2\gamma_m}\alpha_{22}^* \hat{f}_m, \\
\hat{n}_3 &= -\sqrt{2\gamma_b} e^{i\omega_b t} \hat{f}_b,
\end{aligned} \tag{4.28}$$

and

$$\begin{aligned}
\lambda_1 &= -\left(\gamma_a \alpha_{11}^* E_1 + \gamma_m \alpha_{21}^* E_2\right), \\
\lambda_2 &= -\left(\gamma_a \alpha_{12}^* E_1 + \gamma_m \alpha_{22}^* E_2\right), \\
\lambda_3 &= ig|E_2|^2 e^{i\omega_b t}.
\end{aligned} \tag{4.29}$$

Since M cannot be shown due to its big size, we write only a few of its elements:

$$\begin{aligned}
m_{11} &= -\left(\gamma_a \alpha_{11}^* \alpha_{11} + \gamma_m \alpha_{21}^* \alpha_{21}\right), \\
m_{12} &= 0, \\
m_{13} &= -\left(\gamma_a \alpha_{11}^* \alpha_{12} + \gamma_m \alpha_{21}^* \alpha_{22}\right), \\
m_{14} &= 0, \\
m_{15} &= ig\alpha_{21}^* E_2 e^{-i\omega_b t}, \\
m_{16} &= ig\alpha_{21}^* E_2 e^{i\omega_b t}.
\end{aligned} \tag{4.30}$$

The formal solution is

$$\begin{aligned}\hat{c}(t) &= \hat{T}\exp\left[\int_0^t d\tau\, M(\tau)\right]\hat{c}(0)\\ &+ \int_0^t d\tau\, \hat{T}\exp\left[\int_\tau^t ds\, M(s)\right]\Big(\lambda(\tau)+\hat{n}(\tau)\Big)\\ &= \hat{c}_s(t)+\hat{c}_{ds}(t)+\hat{c}_n(t).\end{aligned} \tag{4.31}$$

We can formally write

$$\hat{T}\exp\left[\int_\tau^t ds\, M(s)\right] = \begin{pmatrix} d_{11}(t,\tau) & d_{12}(t,\tau) & \dots & d_{16}(t,\tau)\\ d_{21}(t,\tau) & d_{22}(t,\tau) & \dots & d_{26}(t,\tau)\\ \vdots & \ddots & & \\ d_{61}(t,\tau) & & & d_{66}(t,\tau)\end{pmatrix}. \tag{4.32}$$

Since it is difficult to find the matrix exponential, we use the following approximation

$$\hat{T}\exp\left[\int_0^t ds\, M(s)\right] \approx \prod_{i=N-1}^{0}\Big(1+M(s_i)\,h\Big), \tag{4.33}$$

in which the step size h is chosen so small to assure $M(s_i)M(s_{i+1}) = M(s_{i+1})M(s_i)$. Similar to the previous chapter, we cannot solve the equations of motion using the traditional methods, because we cannot assign an initial value to the quantum operators. What has a physical meaning is their expectation values like $\langle\hat{c}^\dagger(0)\hat{c}(0)\rangle$. Therefore, we use the algorithm developed in [132] which is suitable for such cases dealing with quantum mechanical operators.

There are three terms in the solution (4.31). The supermode populations from the first term are obtained by taking the average of $\hat{o}^\dagger_{i,s}\hat{o}_{i,s}(t)$ with respect to the system's initial state $|0\rangle_c\langle 0|\otimes \sum_n \frac{n_{th}^n}{(1+n_{th})^{n+1}}|n\rangle_m\langle n|$. Noting that $\langle 0|\hat{o}^\dagger_1(0)\hat{o}_1(0)|0\rangle = 0$ and $\langle 0|\hat{o}_1\hat{o}^\dagger_1(0)|0\rangle = 1$, this part of the contribution is found as

$$\begin{aligned}\langle \hat{o}_{1,s}^{\dagger} \hat{o}_{1,s} \rangle &= d_{21}(t,0)\, d_{12}(t,0) + d_{23}(t,0)\, d_{14}(t,0) \\ &\quad + d_{25}(t,0)\, d_{16}(t,0)\left(n_{th}+1\right) + d_{26}(t,0)\, d_{15}(t,0)\, n_{th},\end{aligned} \tag{4.34}$$

$$\begin{aligned}\langle \hat{o}_{2,s}^{\dagger} \hat{o}_{2,s} \rangle &= d_{41}(t,0)\, d_{32}(t,0) + d_{43}(t,0)\, d_{34}(t,0) \\ &\quad + d_{45}(t,0)\, d_{36}(t,0)\left(n_{th}+1\right) + d_{46}(t,0)\, d_{35}(t,0)\, n_{th}.\end{aligned} \tag{4.35}$$

Considering the displacement terms due to the action of $\hat{U}_0(t)$, the second pure drive term $\lambda(t)$ yields to the following contribution:

$$\begin{aligned}\left\langle \hat{o}_{1,ds}^{\dagger} \hat{o}_{1,ds} \right\rangle &= |E_1 + E_2 + \hat{o}_{1,ds}(t)|^2, \\ \left\langle \hat{o}_{2,ds}^{\dagger} \hat{o}_{2,ds} \right\rangle &= |E_1 - E_2 + \hat{o}_{2,ds}(t)|^2.\end{aligned} \tag{4.36}$$

where

$$\begin{aligned}\hat{o}_{1,ds} = \int_0^t d\tau \Big[& d_{11}(t,\tau)\,\lambda_1 + d_{12}(t,\tau)\,\lambda_1^* + d_{13}(t,\tau)\,\lambda_2 \\ & + d_{14}(t,\tau)\,\lambda_2^* + d_{15}(t,\tau)\,\lambda_3 + d_{16}(t,\tau)\,\lambda_3^* \Big]\end{aligned} \tag{4.37}$$

and

$$\begin{aligned}\hat{o}_{2,ds} = \int_0^t d\tau \Big[& d_{31}(t,\tau)\,\lambda_1 + d_{32}(t,\tau)\,\lambda_1^* + d_{33}(t,\tau)\,\lambda_2 \\ & + d_{34}(t,\tau)\,\lambda_2^* + d_{35}(t,\tau)\,\lambda_3 + d_{36}(t,\tau)\,\lambda_3^* \Big].\end{aligned} \tag{4.38}$$

Finally, having the following commutation relations for the noise terms,

$$\begin{aligned}
\left\langle \hat{n}_1(t)\,\hat{n}_1^\dagger(t')\right\rangle &= \left(2\gamma_a\alpha_{11}^*\alpha_{11} + 2\gamma_m\alpha_{21}^*\alpha_{21}\right)\delta(t-t'),\\
\left\langle \hat{n}_1(t)\,\hat{n}_2^\dagger(t')\right\rangle &= \left(2\gamma_a\alpha_{11}^*\alpha_{12} + 2\gamma_m\alpha_{21}^*\alpha_{22}\right)\delta(t-t'),\\
\left\langle \hat{n}_2(t)\,\hat{n}_2^\dagger(t')\right\rangle &= \left(2\gamma_a\alpha_{12}^*\alpha_{12} + 2\gamma_m\alpha_{22}^*\alpha_{22}\right)\delta(t-t'),\\
\left\langle \hat{n}_2(t)\,\hat{n}_1^\dagger(t')\right\rangle &= \left(2\gamma_a\alpha_{12}^*\alpha_{11} + 2\gamma_m\alpha_{22}^*\alpha_{21}\right)\delta(t-t'),\\
\left\langle \hat{n}_3(t)\,\hat{n}_3^\dagger(t')\right\rangle &= \left(2\gamma_b(n_{th}+1)\right)\delta(t-t'),\\
\left\langle \hat{n}_3^\dagger(t)\,\hat{n}_3(t')\right\rangle &= \left(2\gamma_b n_{th}\right)\delta(t-t'),
\end{aligned} \tag{4.39}$$

the contribution from the noise drive terms $\hat{n}(t)$ is

$$\begin{aligned}
\hat{o}_{1,n} = \int_0^t d\tau \Big[& d_{11}(t,\tau)\,\hat{n}_1 + d_{12}(t,\tau)\,\hat{n}_1^\dagger + d_{13}(t,\tau)\,\hat{n}_2 + d_{14}(t,\tau)\,\hat{n}_2^\dagger \\
& + d_{15}(t,\tau)\,\hat{n}_3 + d_{16}(t,\tau)\,\hat{n}_3^\dagger\Big]
\end{aligned} \tag{4.40}$$

Therefore,

$$\begin{aligned}
\left\langle \hat{o}_{1,n}^\dagger \hat{o}_{1,n}\right\rangle = \int_0^t d\tau \Big[& d_{12}(t,\tau)\,d_{21}(t,\tau)\left(2\gamma_a\alpha_{11}^*\alpha_{11} + 2\gamma_m\alpha_{21}^*\alpha_{21}\right) \\
& + d_{14}(t,\tau)\,d_{23}(t,\tau)\left(2\gamma_a\alpha_{12}^*\alpha_{12} + 2\gamma_m\alpha_{22}^*\alpha_{22}\right) \\
& + d_{14}(t,\tau)\,d_{21}(t,\tau)\left(2\gamma_a\alpha_{11}^*\alpha_{12} + 2\gamma_m\alpha_{21}^*\alpha_{22}\right) \\
& + d_{12}(t,\tau)\,d_{23}(t,\tau)\left(2\gamma_a\alpha_{12}^*\alpha_{11} + 2\gamma_m\alpha_{22}^*\alpha_{21}\right) \\
& + d_{16}(t,\tau)\,d_{25}(t,\tau)\left(2\gamma_b(n_{th}+1)\right) \\
& + d_{15}(t,\tau)\,d_{26}(t,\tau)\left(2\gamma_b n_{th}\right)\Big]
\end{aligned} \tag{4.41}$$

and, similarly,

$$\begin{aligned}\left\langle \hat{o}_{2,n}^{\dagger}\hat{o}_{2,n}\right\rangle = \int_0^t d\tau \Big[& d_{41}(t,\tau)\, d_{32}(t,\tau)\Big(2\gamma_a\alpha_{11}^{*}\alpha_{11} + 2\gamma_m\alpha_{21}^{*}\alpha_{21}\Big) \\ & + d_{43}(t,\tau)\, d_{34}(t,\tau)\Big(2\gamma_a\alpha_{12}^{*}\alpha_{12} + 2\gamma_m\alpha_{22}^{*}\alpha_{22}\Big) \\ & + d_{41}(t,\tau)\, d_{34}(t,\tau)\Big(2\gamma_a\alpha_{11}^{*}\alpha_{12} + 2\gamma_m\alpha_{21}^{*}\alpha_{22}\Big) \\ & + d_{43}(t,\tau)\, d_{32}(t,\tau)\Big(2\gamma_a\alpha_{12}^{*}\alpha_{11} + 2\gamma_m\alpha_{22}^{*}\alpha_{21}\Big) \\ & + d_{45}(t,\tau)\, d_{36}(t,\tau)\Big(2\gamma_b(n_{th}+1)\Big) \\ & + d_{46}(t,\tau)\, d_{35}(t,\tau)\Big(2\gamma_b n_{th}\Big)\Big].\end{aligned} \tag{4.42}$$

Adding the three parts of contributions, the total supermode populations becomes

$$\left\langle \hat{o}_i^{\dagger}\hat{o}_i\right\rangle = \left\langle \hat{o}_{i,s}^{\dagger}\hat{o}_{i,s}\right\rangle + \left\langle \hat{o}_{i,ds}^{\dagger}\hat{o}_{i,ds}\right\rangle + \left\langle \hat{o}_{i,n}^{\dagger}\hat{o}_{i,n}\right\rangle \tag{4.43}$$

Then, the population inversion is

$$\Delta N = \left\langle \hat{o}_1^{\dagger}\hat{o}_1\right\rangle - \left\langle \hat{o}_2^{\dagger}\hat{o}_2\right\rangle. \tag{4.44}$$

4.4 Results and discussion

To achieve a reasonably strong phonon field, one should provide a high population inversion condition between the optical supermodes. As discussed in the previous section, the population inversion is a dynamical quantity varying with time, whereas in other references (i.e., [148, 3, 149, 2]) it is treated as a constant value. The equation (4.26) not only yields the superoperators equations of motion but also describes the "thermal" phonon evolution with time. But we need the "stimulated" phonon evolution as well. In analogy to an optical laser [134], the phonon laser dynamical equations are similar to those in [148, 3, 4, 132]:

$$\begin{aligned}\frac{db_s}{dt} &= \big(-\gamma_b - i\omega_b\big)b_s - i\frac{g}{2}p, \\ \frac{dp}{dt} &= i\frac{g}{2}\Delta N(t)b_s + \big(-\gamma_a - \gamma_m - 2iJ\big)p.\end{aligned} \tag{4.45}$$

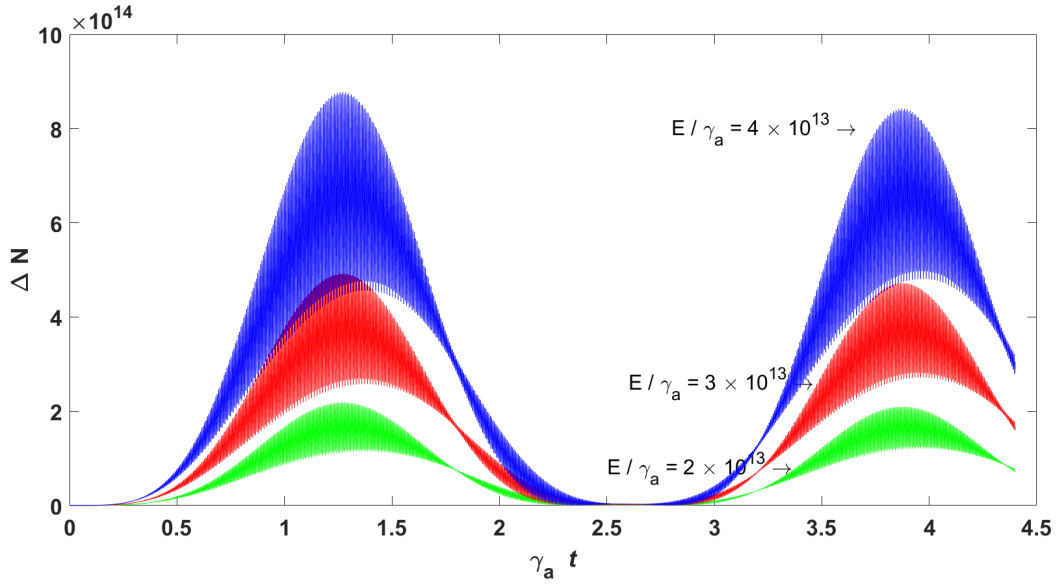

Figure 4.5: The population inversion between superoperators for different values of the drive field. Here we have set $\gamma_a = 2.6$ MHz, $\gamma_m = 1.6$ MHz, $\gamma_b = 628$ Hz, $\omega_a = \omega_m = \omega_d = 20\pi$ GHz (the resonant condition), $\omega_b = 24\pi$ MHz, $J = 2\pi$ MHz, $g = 0.2\pi$, $n_{th} = 2.4 \times 10^5$. A higher population inversion is obtained for a stronger drive filed.

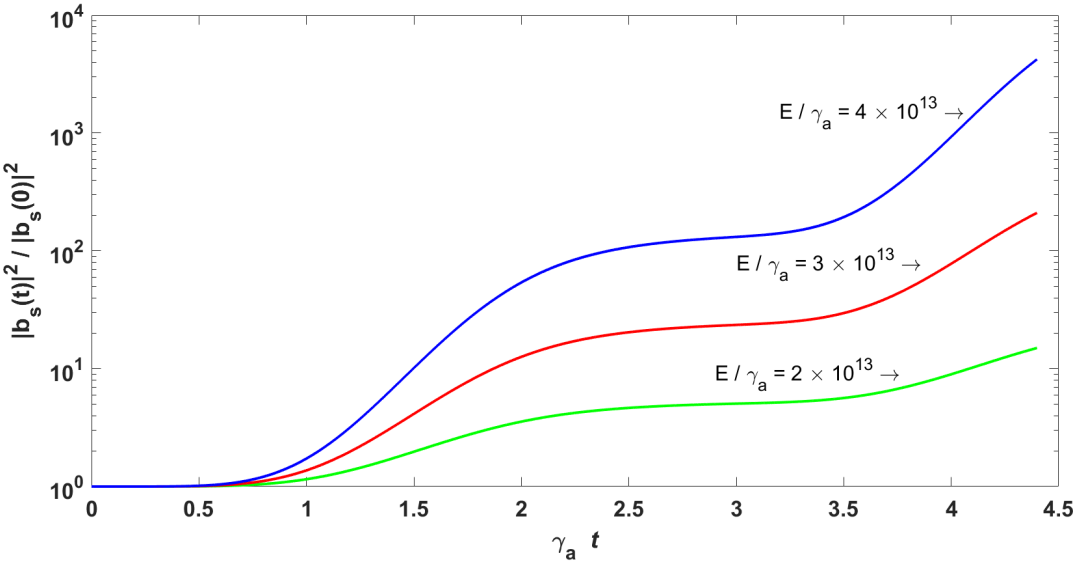

Figure 4.6: The normalized amplified phonon filed using the parameter of Figure 4.5. Here if we double the drive power, the difference between the amplified stimulated phonon fields is several orders of magnitude in large time scales.

In this equation, we have used a subscript "s" indicating it is the stimulated phonon (one can draw an analogy between the spontaneous and stimulated emission of a photon in an optical laser and thermal and stimulated phonons in a phonon laser). Also, $p = \langle \hat{o}_2^\dagger \hat{o}_1 \rangle$. The variables in equation (4.45) are not quantum operators, but mean-field values. However, we insert the population inversion $\Delta N(t)$ in it determined quantum mechanically in the previous section. This analogy also comes from the similarity between the semiclassical treatment of atomic level transitions, in which the atomic levels are described quantum mechanically while the radiations are regarded as classical. Because of the mean-field treatment, there are no noise terms in equation (4.45). After we solve the system of differential equations in equation (4.45), we numerically obtain $b_s(t)$. In the following, we demonstrate the plots of population inversion ΔN and the normalized stimulated phonon number $|b_s(t)/b_s(0)|^2$. Here we use parameters close to the experimental values used in other setups [52].

In the first case, we choose these parameters: $\gamma_a = 2.6$ MHz, $\gamma_m = 1.6$ MHz, $\gamma_b = 628$ Hz, $\omega_a = \omega_m = \omega_d = 20\pi$ GHz (the resonant condition), $\omega_b = 24\pi$ MHz, $J = 2\pi$ MHz, $g = 0.2\pi$, and $n_{th} = 2.4 \times 10^5$. E remains a variable in this case, but its order of magnitude is 10^{13}. Figure 4.5 shows that the population inversion demonstrates fast oscillations modulated on slow oscillations. As we increase the drive power, on average we obtain a higher population inversion, but the maxima and minima of the slow oscillation do not displace. We observe the same behavior for the amplified phonon filed in Figure 4.6. Here also a stronger phonon field is achieved for higher drive power. However, notice in the case of population inversion, if we double the drive filed, on average the population inversion is roughly four folded, but for the amplified phonon field, at large times, we observe a significant difference for the amplified phonon for drive powers $E = 2 \times 10^{13}\gamma_a$ and $E = 4 \times 10^{13}\gamma_a$. Physically, a strong drive field generates a higher magnon number and a more

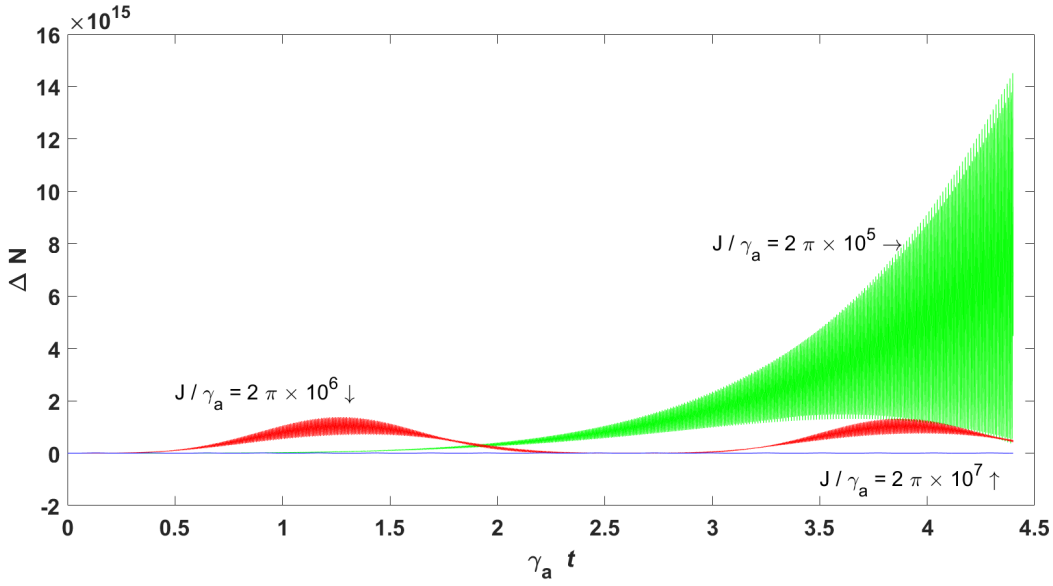

Figure 4.7: The population inversion for the same parameters used in Figure 4.6, except that here we have fixed the value of the drive power to $E = 5 \times 10^{13}\gamma_a$, but J remains a variable. We observe that a lower coupling power yields a higher population inversion at larger times, because in this case the relative strengths of J and g determine the output.

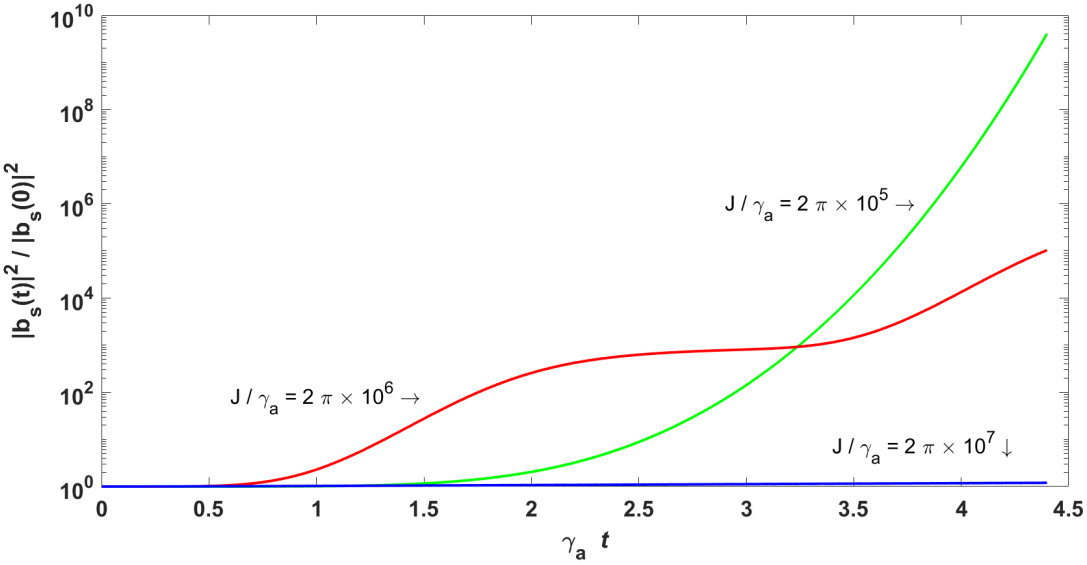

Figure 4.8: The amplified stimulated phonon field for the same parameters used in Figure (4.7). Here also a lower coupling leads to a stronger phonon field as illustrated in the text.

powerful mechanical oscillation due to the magnetostriction interaction. Therefore, it is normal to achieve a stronger phonon field for higher power drives.

In Figure 4.7, we are interested to know how the coupling strength changes the population inversion and the stimulated phonon field. Therefore, we have fixed the value of the drive power to $E = 5 \times 10^{13}\gamma_a$ in Figure 4.7, but we allow J to vary. The other parameters are the same as in Figures 4.5 and 4.6. The figure shows a lower coupling power yields a higher population inversion. However, this time the maxia and minima of ΔN are displaced as we change the coupling power. Figure 4.8 exhibits the amplified phonon field for different values of the coupling power. Here also we observe at large times a lower coupling power leads to a stronger phonon field. We can explain this phenomenon by comparing the coupling Hamiltonian $J(\hat{a}^\dagger \hat{m} + \hat{a}\hat{m}^\dagger)$ and the magnomechanical Hamiltonian $g\hat{m}^\dagger \hat{m}(\hat{b} + \hat{b}^\dagger)$ that describes the magnon-phonon coupling. Normally, $J \gg g$, and hence the magnomechanical interaction is much smaller than the coupling interaction. Therefore, a larger value of J indicates that magnomechanical interaction is less determining and vice versa. Accordingly, we expect to have a stronger phonon field for lower coupling powers.

One should notice that initially, a higher coupling power may lead to a stronger phonon field. For example, the red curve in Figure 4.8 corresponds to a coupling power ten times bigger than that of the green curve, but initially, it is above the green curve. However, this is a transient behavior that disappears at large times. We can illustrate this by noting that initially, when we drive the system, first the magnon-phonon coupling occurs which deforms the YIG sphere and hence vibrates the sphere, and thereby phonons are generated. Therefore, a time interval is needed for the magnetostriction interaction. If the coupling power is larger, we expect a faster magnon-phonon coupling, but finally, the amplified phonon field is decided by the relative strength of the coupling power J and the magnomechanical coefficient g.

In addition to the drive power and the coupling strength, we are interested to know what happens if the system is not in the resonance condition. Therefore, in Figures 4.9 and 4.10 we fix

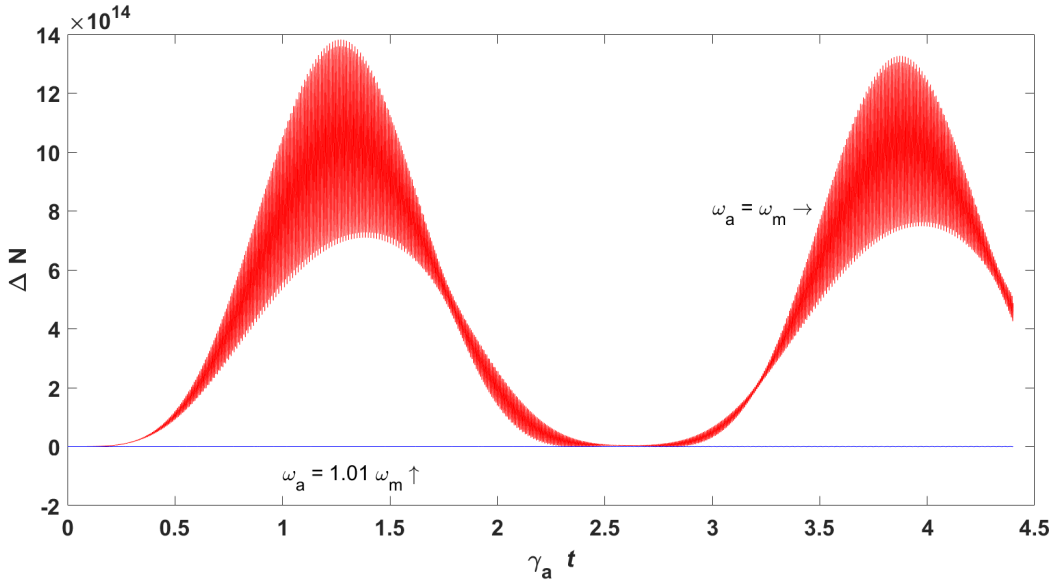

Figure 4.9: The population inversion for the same parameters used in Figure 4.8, but here we allow a nonzero detuning between the frequencies of the cavity photons and the magnons. The figure shows the population inversion is very sensitive to the detuning, so it either drops to very low values for $\Delta = 0.01$ (blue curve)or disappears totally for $\Delta = -0.01$. To have a reasonably large population inversion, the detuning should be as small as a few Hz.

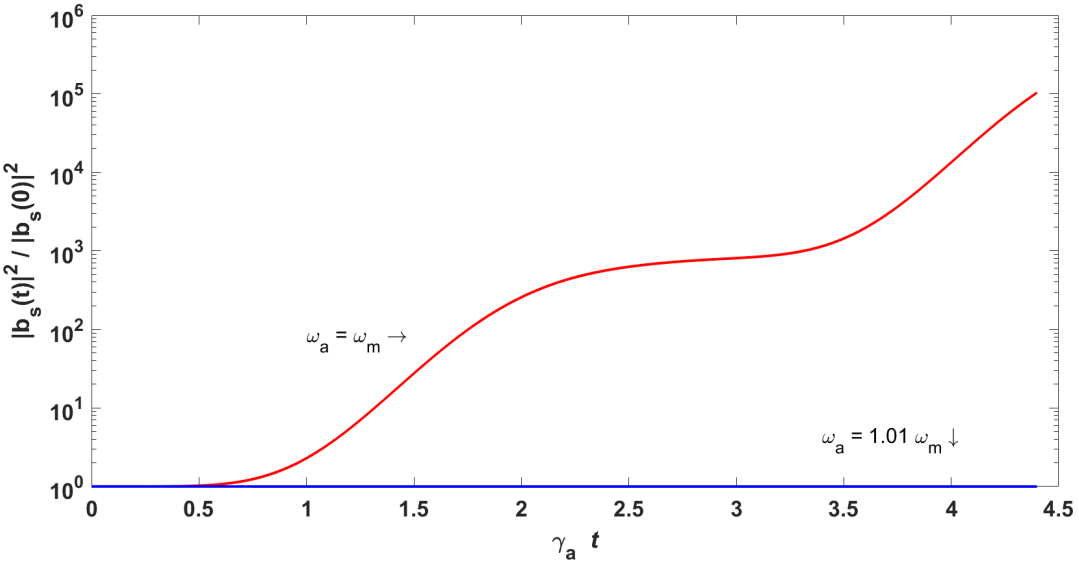

Figure 4.10: The amplified phonon field for the same parameters used in Figure 4.9. The same conclusion applied to Figure 4.9 is also valid for this case. To have a strong phonon field, the detuning must be as small as a few Hz.

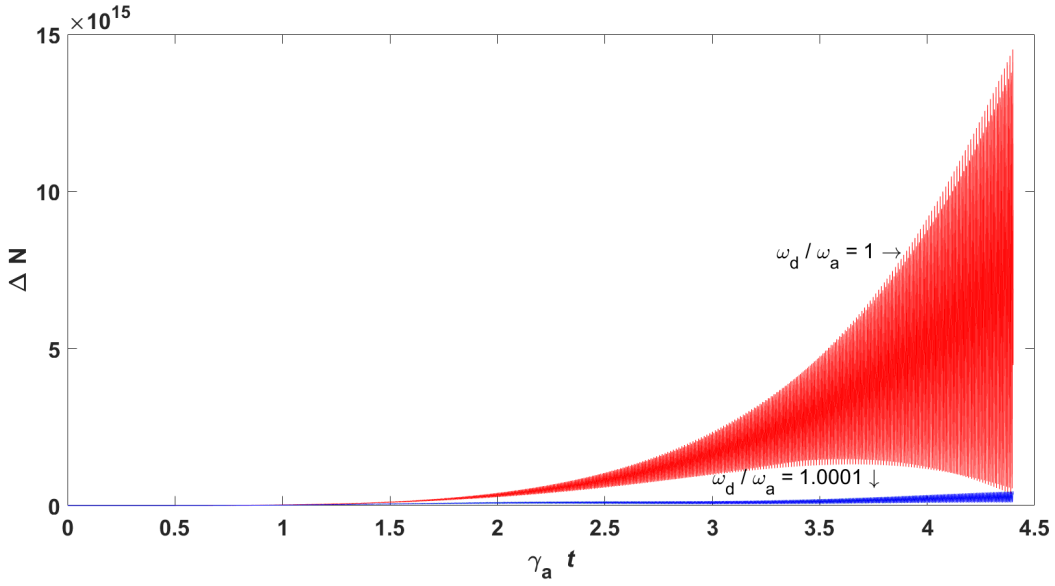

Figure 4.11: The population inversion for the same parameters used in Figure 4.10, but here we allow a nonzero detuning between the frequencies of the cavity photons and the magnons and that of the drive field. The figure shows the population inversion is very sensitive to the detuning, so it either drops to very low values for $\omega_d - \omega_a = 0.1$ MHz (blue curve) or disappears totally for $\omega_d - \omega_a = -0.1$. To have a reasonably large population inversion, the detuning should be as small as a few Hz.

the values of the drive power and the coupling strength to $E = 5 \times 10^{13}\gamma_a$ and $J = 2\pi \times 10^6 \gamma_a$, but we allow a nonzero detuning $\Delta = \pm 0.01$. As we observe in both Figures 4.9 and 4.10, there is no significant population inversion and amplified the phonon field for this value of detuning. This result is because the magnetic field of the drive must be matched to the Kittel frequency of the YIG sphere (which is adjusted by the fixed magnetic field **H**) to have a considerable magnon-phonon coupling. Our detuning is relatively large (10^8 Hz), and it is normal not to have phonon lasing. Thus, the detuning must be as small as possible, roughly a few Hz, so as not to affect the population inversion and the phonon field substantially.

Finally, we terminate our discussion by investigating a frequency mismatch between the drive field ω_d and the cavity photon ω_a and magnon ω_m frequencies ($\omega_a = \omega_m$). As we expect,

the results of Figures 4.9 and 4.10 are repeated for the population inversion and the phonon field in Figures 4.11 and 4.12 respectively. In these figures, use the same parameter of Figures 4.9 and 4.10, but we fix $\omega_a = \omega_m = 20\pi$ GHz and allow ω_d to vary a bit. Here also we observe even a tiny frequency mismatch between the drive field and that of the cavity photon and magnon leads to a visible difference. As both Figures, 4.11 and 4.12 show, a positive frequency mismatch $\omega_d - \omega_a = 0.1$ MHz significantly drops the population inversion and the amplified phonon field (the blue curve in both figures), and for a negative mismatch, there is no population inversion and hence no phonon lasing at all. This phenomenon is consistent with our expectation as one compares this case to an optical laser. If we pump a two-level atom at a frequency different from the transition frequency, no transition is induced. The same argument applies to the phonon laser. If the drive or the pump frequency mismatches that of the cavity photon and magnon, there would not be an efficient mechanical oscillation and hence no phonon lasing in the system.

Also, we emphasize in contrast to the reference [2] that has defined a "mechanical gain" and a "threshold" for the drive field, here we cannot present an analyitcal expression for these two. In [2], it is assumed there is a steady state for the population inversion. Then, one can obtain an analytical expression for the "constant" population inversion (by constant, we mean it does not vary with time, however it can change by changing the drive field). Given the constant population inversion, after substituting it in equation (4.45) and some mathematical work, one can obtain an expression like $\dot{b}_s = \Delta_b b_s + \text{cte.}$, where Δ_b contains the mechanical gain coefficient and some other parameters. Having the mechanical gain and the losses of the system in hand, one can obtain a threshold for the phonon laser. However, our analysis it totally different, showing the population inversion in all cases is oscillatory, and therefor one cannot obtain an analytical expression for the threshold, although below some particular drive filed no phonon lasing is possible.

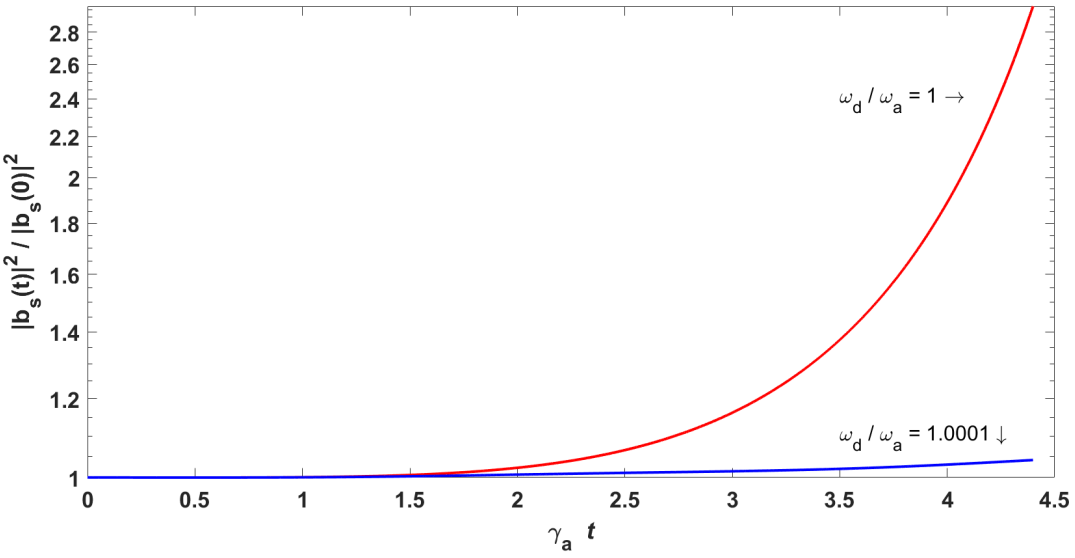

Figure 4.12: The amplified phonon field for the same parameters used in Figure 4.11. The same conclusion applied to Figure 4.10 is also valid for this case. To have a strong phonon field, the detuning must be as small as a few Hz.

Besides, we noticed the quantum noise does not play a significant role in the magnomechanical phonon laser. The effect is so negligible that cannot be represented on the plots because the corresponding curves almost coincide with those obtained without considering the noise. This is in contrast to the results of chapters 2 and 3 in which the quantum noise was an important factor for the degree of the entanglement of the light fields. Here we deal with "coherent" emission of phonons (similar to the coherent emission of photons in an optical laser). And, as we know, the coherent states are similar to the classical states [134]. Therefore, it seems natural that the noise does not have a determining effect because we do not deal with the pure quantum features of the bosonic fields.

In summary, we studied a magnomechanical phonon laser beyond the steady-state approximation. Our results show that the population inversion between the upper and lower supemodes of the system demonstrates an oscillatory behavior with time. This oscillation is in contrast to the

previous studies that assume a constant population inversion with time. Despite the oscillations of the population inversion, one can achieve relatively large stimulated phonon numbers if the power of the drive field is beyond a threshold and the frequency of the drive field is matched to the frequencies of the cavity photons and magnons. Any detuning significantly drops the phonon number. Since the magnomechanical system we considered is highly tunable with low loss and also it has an extra degree of freedom provided by the constant magnetic field, it can be an alternative to the traditional optomechanical systems.

5 Conclusion

5.1 Summary

Quantum dynamics determines the time evolution of the quantum operators. In this thesis, we studied the three cases quantum dynamically along with the quantum noise effect.

The first case was a hybrid $\mathscr{P}\mathscr{T}$-symmetric system of a gain-loss coupler with an added squeezing element. We studied how quantum noises influence the continuous-variable entanglement generated with that setup. According to the prediction of the non-Hermitian Hamiltonian formalism, one can create highly entangled, high-intensity light fields by such a setup, especially when the system is operating in the broken symmetry regime where the light fields can simultaneously be amplified and entangled. However, the quantum noise can completely erase the entanglement. The results obtained by the full dynamics indicate one can achieve certain amounts of the entanglement, though they are weaker than those predicted without considering the quantum noises. In particular, placing the squeezing element inside the waveguide amplifying the propagating light field enables one to realize light fields with considerable CV entanglement. The importance of studying this model setup was to clarify that quantum noises must be considered in $\mathscr{P}\mathscr{T}$-symmetric optical systems for engineering the quantum properties of light fields.

We extended the study of the gain-loss coupler in chapter 3 by including the gain saturation effect. We demonstrated how gain saturation affects quantum noise when the quantum properties of light are concerned. As quantum noise alters the nonclassical properties of light, the gain saturation substantially changes the nonclassical features of light. As examples, we first considered the Wigner function, which is an alternative to the state vector and density matrix for the system. We

found that the Wigner function evolves into a quasisteady state due to gain saturation, whereas in the unsaturated case, the distribution of the Wigner function in phase space expands, and its peak value drastically decreases. Furthermore, the profile of the evolved Wigner function was different for the saturated and unsaturated cases. The gain saturation reduces the gain coefficient with time, and therefore the quantum noise effect is reduced. Second, we investigated the time evolution of entanglement by considering different cases in which the gain, loss, and coupling coefficients are comparable or very different from each other. Generally, as long as the quantum noise level is high, a steady state of entanglement is not achievable. However, gain saturation reduces the quantum noise level, and hence in most cases, one can attain a final steady state. Then, we showed that gain saturation is especially meaningful when the saturation intensity is low. On the other hand, if the saturation intensity is sufficiently high, the degree of entanglement vanishes, or the difference between the saturated and unsaturated cases is negligible. All these results indicate that gain saturation does exert considerable impact on the quantum properties of light fields processed by our non-Hermitian setup.

In the last chapter, we studied a magnomechanical phonon laser beyond the steady state. This system includes a microwave cavity and a YIG sphere in it. The system is driven by two fields: the first is a microwave whose intensity (or, power) should be beyond its threshold. The second is a constant magnetic field that is perpendicular to the first drive field. The magnetic field provides the collective excitation of the YIG sphere. As the magnomechanical systems are highly tunable with low loss and having an extra degree of freedom due to the constant magnetic field, they seem to be a good alternative to the optomechanical systems. Using the decomposition of the time evolution operator, we linearzied the nonlinear set of differential equations describing the dynamics of the system. After the numerical solving of the equations, we concluded it is possible to

generate stimulated emitted phonons at relatively large numbers. Another feature of the dynamical magnomechanical laser was the oscillatory behavior of the population inversion between optical supermodes. Our results show one should finely tune the drive field frequency to the frequencies of the cavity photon and magnon. Also, the drive field power must be larger than the threshold power which can only be calculated numerically.

5.2 Outlook

As the future work, we have a couple of ideas that are related to the the topics investigated in this thesis:

- Is that possible to have the magnetostriction cooling similar to the radiation pressure cooling in optomechanics? If so, we are going to study it as a quantum dynamical process using the the method of decomposing the time evolution operator.

- It is shown one can achieve entanglement using the magnomechanical systems [171] and also it is possible to have a $\mathscr{PT}$-symmetric magnomechanical system [176, 177, 58]. Thus, one can think about macroscopic, intense entanglement generation using a magnomechanical $\mathscr{PT}$-symmetric system. Notably, the magnomechanical $\mathscr{PT}$-symmetric system is passive, having no material gain. Therefore, the quantum noise associated with the amplification is absent, and one may expect a high degree of entanglement.

Bibliography

[1] C. M. Bender and S. Boettcher, "Real spectra in non-hermitian hamiltonians having $\mathscr{P}\mathscr{T}$-symmetry," *Physical Review Letters*, vol. 80, no. 24, p. 5243, 1998.

[2] M.-S. Ding, L. Zheng, and C. Li, "Phonon laser in a cavity magnomechanical system," *Scientific reports*, vol. 9, no. 1, pp. 1–8, 2019.

[3] H. Jing, S. Özdemir, X.-Y. Lü, J. Zhang, L. Yang, and F. Nori, "Pt-symmetric phonon laser," *Physical review letters*, vol. 113, no. 5, p. 053604, 2014.

[4] B. He, L. Yang, and M. Xiao, "Dynamical phonon laser in coupled active-passive microresonators," *Physical Review A*, vol. 94, no. 3, p. 031802, 2016.

[5] D. J. Griffiths and D. F. Schroeter, *Introduction to quantum mechanics*. Cambridge University Press, 2018.

[6] R. El-Ganainy, K. G. Makris, M. Khajavikhan, Z. H. Musslimani, S. Rotter, and D. N. Christodoulides, "Non-hermitian physics and pt symmetry," *Nature Physics*, vol. 14, no. 1, pp. 11–19, 2018.

[7] G. Gamow, "Zur quantentheorie des atomkernes," *Zeitschrift für Physik*, vol. 51, no. 3-4, pp. 204–212, 1928.

[8] G. Lindblad, "On the generators of quantum dynamical semigroups," *Communications in Mathematical Physics*, vol. 48, no. 2, pp. 119–130, 1976.

[9] H. Carmichael, *An open systems approach to quantum optics: lectures presented at the Université Libre de Bruxelles, October 28 to November 4, 1991*. Springer Science & Business Media, 2009, vol. 18.

[10] L. Feng, R. El-Ganainy, and L. Ge, "Non-hermitian photonics based on parity–time symmetry," *Nature Photonics*, vol. 11, no. 12, pp. 752–762, 2017.

[11] R. El-Ganainy, K. Makris, D. Christodoulides, and Z. H. Musslimani, "Theory of coupled optical pt-symmetric structures," *Optics letters*, vol. 32, no. 17, pp. 2632–2634, 2007.

[12] C. M. Bender, D. C. Brody, and H. F. Jones, "Complex extension of quantum mechanics," *Physical Review Letters*, vol. 89, no. 27, p. 270401, 2002.

[13] A. Zyablovsky, A. P. Vinogradov, A. A. Pukhov, A. V. Dorofeenko, and A. A. Lisyansky, "Pt-symmetry in optics," *Physics-Uspekhi*, vol. 57, no. 11, p. 1063, 2014.

[14] C. E. Rüter, K. G. Makris, R. El-Ganainy, D. N. Christodoulides, M. Segev, and D. Kip, "Observation of parity–time symmetry in optics," *Nature physics*, vol. 6, no. 3, pp. 192–195, 2010.

[15] H. Zhao and L. Feng, "Parity–time symmetric photonics," *National Science Review*, vol. 5, no. 2, pp. 183–199, 2018.

[16] M.-A. Miri and A. Alu, "Exceptional points in optics and photonics," *Science*, vol. 363, no. 6422, 2019.

[17] C. M. Bender, R. Tateo, P. E. Dorey, T. C. Dunning, G. Levai, S. Kuzhel, H. F. Jones, A. Fring, and D. W. Hook, *PT symmetry: In quantum and classical physics*. World Scientific Publishing, 2018.

[18] K. G. Makris, R. El-Ganainy, D. Christodoulides, and Z. H. Musslimani, "Beam dynamics in p t symmetric optical lattices," *Physical Review Letters*, vol. 100, no. 10, p. 103904, 2008.

[19] A. Mostafazadeh, "Spectral singularities of complex scattering potentials and infinite reflection and transmission coefficients at real energies," *Physical Review Letters*, vol. 102, no. 22, p. 220402, 2009.

[20] S. Klaiman, U. Günther, and N. Moiseyev, "Visualization of branch points in p t-symmetric waveguides," *Physical review letters*, vol. 101, no. 8, p. 080402, 2008.

[21] E.-M. Graefe and H. Jones, "Pt-symmetric sinusoidal optical lattices at the symmetry-breaking threshold," *Physical Review A*, vol. 84, no. 1, p. 013818, 2011.

[22] A. Guo, G. Salamo, D. Duchesne, R. Morandotti, M. Volatier-Ravat, V. Aimez, G. Siviloglou, and D. Christodoulides, "Observation of p t-symmetry breaking in complex optical potentials," *Physical Review Letters*, vol. 103, no. 9, p. 093902, 2009.

[23] Y. N. Joglekar and A. K. Harter, "Passive parity-time-symmetry-breaking transitions without exceptional points in dissipative photonic systems," *Photonics Research*, vol. 6, no. 8, pp. A51–A57, 2018.

[24] B. Peng, Ş. K. Özdemir, F. Lei, F. Monifi, M. Gianfreda, G. L. Long, S. Fan, F. Nori, C. M. Bender, and L. Yang, "Parity–time-symmetric whispering-gallery microcavities," *Nature Physics*, vol. 10, no. 5, pp. 394–398, 2014.

[25] L. Chang, X. Jiang, S. Hua, C. Yang, J. Wen, L. Jiang, G. Li, G. Wang, and M. Xiao, "Parity–time symmetry and variable optical isolation in active–passive-coupled microresonators," *Nature photonics*, vol. 8, no. 7, pp. 524–529, 2014.

[26] B. Peng, Ş. Özdemir, S. Rotter, H. Yilmaz, M. Liertzer, F. Monifi, C. Bender, F. Nori, and L. Yang, "Loss-induced suppression and revival of lasing," *Science*, vol. 346, no. 6207, pp. 328–332, 2014.

[27] V. V. Konotop and B. I. Mantsyzov, "Light propagation through a pt-symmetric photonic-crystal," *Optics express*, vol. 24, no. 23, pp. 26 146–26 151, 2016.

[28] Z. Liu, Q. Zhang, F. Qin, Y. Chen, and J. J. Xiao, "Mode coupling in pt-symmetric photonic crystals with a flat band," *Physical Review A*, vol. 98, no. 4, p. 043844, 2018.

[29] M. Kremer, T. Biesenthal, L. J. Maczewsky, M. Heinrich, R. Thomale, and A. Szameit, "Demonstration of a two-dimensional $\mathscr{P}\mathscr{T}$-symmetric crystal," *Nature communications*, vol. 10, no. 1, pp. 1–7, 2019.

[30] Z. Lin, H. Ramezani, T. Eichelkraut, T. Kottos, H. Cao, and D. N. Christodoulides, "Unidirectional invisibility induced by p t-symmetric periodic structures," *Physical Review Letters*, vol. 106, no. 21, p. 213901, 2011.

[31] A. Regensburger, C. Bersch, M.-A. Miri, G. Onishchukov, D. N. Christodoulides, and U. Peschel, "Parity–time synthetic photonic lattices," *Nature*, vol. 488, no. 7410, pp. 167–171, 2012.

[32] L. Feng, Y.-L. Xu, W. S. Fegadolli, M.-H. Lu, J. E. Oliveira, V. R. Almeida, Y.-F. Chen, and A. Scherer, "Experimental demonstration of a unidirectional reflectionless parity-time metamaterial at optical frequencies," *Nature materials*, vol. 12, no. 2, pp. 108–113, 2013.

[33] H. Hodaei, M.-A. Miri, M. Heinrich, D. N. Christodoulides, and M. Khajavikhan, "Parity-time–symmetric microring lasers," *Science*, vol. 346, no. 6212, pp. 975–978, 2014.

[34] J. Schindler, A. Li, M. C. Zheng, F. M. Ellis, and T. Kottos, "Experimental study of active lrc circuits with pt symmetries," *Physical Review A*, vol. 84, no. 4, p. 040101, 2011.

[35] S. Bittner, B. Dietz, U. Günther, H. Harney, M. Miski-Oglu, A. Richter, and F. Schäfer, "P t symmetry and spontaneous symmetry breaking in a microwave billiard," *Physical review letters*, vol. 108, no. 2, p. 024101, 2012.

[36] C. M. Bender, B. K. Berntson, D. Parker, and E. Samuel, "Observation of pt phase transition in a simple mechanical system," *American Journal of Physics*, vol. 81, no. 3, pp. 173–179, 2013.

[37] R. Fleury, D. Sounas, and A. Alu, "An invisible acoustic sensor based on parity-time symmetry," *Nature communications*, vol. 6, no. 1, pp. 1–7, 2015.

[38] C. Hang, G. Huang, and V. V. Konotop, "P t symmetry with a system of three-level atoms," *Physical review letters*, vol. 110, no. 8, p. 083604, 2013.

[39] Z. Zhang, Y. Zhang, J. Sheng, L. Yang, M.-A. Miri, D. N. Christodoulides, B. He, Y. Zhang, and M. Xiao, "Observation of parity-time symmetry in optically induced atomic lattices," *Physical review letters*, vol. 117, no. 12, p. 123601, 2016.

[40] P. Peng, W. Cao, C. Shen, W. Qu, J. Wen, L. Jiang, and Y. Xiao, "Anti-parity–time symmetry with flying atoms," *Nature Physics*, vol. 12, no. 12, pp. 1139–1145, 2016.

[41] Z. Zhang, D. Ma, J. Sheng, Y. Zhang, Y. Zhang, and M. Xiao, "Non-hermitian optics in atomic systems," *Journal of Physics B: Atomic, Molecular and Optical Physics*, vol. 51, no. 7, p. 072001, 2018.

[42] G. Agarwal and K. Qu, "Spontaneous generation of photons in transmission of quantum fields in p t-symmetric optical systems," *Physical Review A*, vol. 85, no. 3, p. 031802, 2012.

[43] A. Rivas and S. F. Huelga, *Open quantum systems*. Springer, 2012, vol. 13.

[44] D. Suter and G. A. Álvarez, "Colloquium: Protecting quantum information against environmental noise," *Reviews of Modern Physics*, vol. 88, no. 4, p. 041001, 2016.

[45] C. H. Henry and R. F. Kazarinov, "Quantum noise in photonics," *Reviews of Modern Physics*, vol. 68, no. 3, p. 801, 1996.

[46] C. Gardiner and P. Zoller, *The Quantum World of Ultra-Cold Atoms and Light Book I: Foundations of Quantum Optics*. World Scientific Publishing Company, 2014, vol. 2.

[47] C. Gardiner, P. Zoller, and P. Zoller, *Quantum noise: a handbook of Markovian and non-Markovian quantum stochastic methods with applications to quantum optics*. Springer Science & Business Media, 2004.

[48] P. Zoller and C. W. Gardiner, "Quantum noise in quantum optics: the stochastic schr\" odinger equation," *arXiv preprint quant-ph/9702030*, 1997.

[49] C. W. Gardiner and M. J. Collett, "Input and output in damped quantum systems: Quantum stochastic differential equations and the master equation," *Physical Review A*, vol. 31, no. 6, p. 3761, 1985.

[50] B. He, S.-B. Yan, J. Wang, and M. Xiao, "Quantum noise effects with kerr-nonlinearity enhancement in coupled gain-loss waveguides," *Physical Review A*, vol. 91, no. 5, p. 053832, 2015.

[51] M. Aspelmeyer, T. J. Kippenberg, and F. Marquardt, "Cavity optomechanics," *Reviews of Modern Physics*, vol. 86, no. 4, p. 1391, 2014.

[52] X. Zhang, C.-L. Zou, L. Jiang, and H. X. Tang, "Cavity magnomechanics," *Science advances*, vol. 2, no. 3, p. e1501286, 2016.

[53] D. Vitali, S. Gigan, A. Ferreira, H. Böhm, P. Tombesi, A. Guerreiro, V. Vedral, A. Zeilinger, and M. Aspelmeyer, "Optomechanical entanglement between a movable mirror and a cavity field," *Physical review letters*, vol. 98, no. 3, p. 030405, 2007.

[54] B. He, "Quantum optomechanics beyond linearization," *Physical Review A*, vol. 85, no. 6, p. 063820, 2012.

[55] Q. Lin, B. He, R. Ghobadi, and C. Simon, "Fully quantum approach to optomechanical entanglement," *Physical Review A*, vol. 90, no. 2, p. 022309, 2014.

[56] Q. Lin, B. He, and M. Xiao, "Entangling two macroscopic mechanical resonators at high temperature," *Physical Review Applied*, vol. 13, no. 3, p. 034030, 2020.

[57] B. He, L. Yang, Q. Lin, and M. Xiao, "Radiation pressure cooling as a quantum dynamical process," *Physical Review Letters*, vol. 118, no. 23, p. 233604, 2017.

[58] S.-N. Huai, Y.-L. Liu, J. Zhang, L. Yang, and Y.-x. Liu, "Enhanced sideband responses in a pt-symmetric-like cavity magnomechanical system," *Physical Review A*, vol. 99, no. 4, p. 043803, 2019.

[59] A. Serga, A. Chumak, and B. Hillebrands, "Yig magnonics," *Journal of Physics D: Applied Physics*, vol. 43, no. 26, p. 264002, 2010.

[60] D. Lachance-Quirion, Y. Tabuchi, A. Gloppe, K. Usami, and Y. Nakamura, "Hybrid quantum systems based on magnonics," *Applied Physics Express*, vol. 12, no. 7, p. 070101, 2019.

[61] B. D. Cullity and C. D. Graham, *Introduction to magnetic materials*. John Wiley & Sons, 2011.

[62] M. Li, W. Pernice, C. Xiong, T. Baehr-Jones, M. Hochberg, and H. Tang, "Harnessing optical forces in integrated photonic circuits," *Nature*, vol. 456, no. 7221, pp. 480–484, 2008.

[63] J. D. Teufel, D. Li, M. Allman, K. Cicak, A. Sirois, J. Whittaker, and R. Simmonds, "Circuit cavity electromechanics in the strong-coupling regime," *Nature*, vol. 471, no. 7337, pp. 204–208, 2011.

[64] J. Bochmann, A. Vainsencher, D. D. Awschalom, and A. N. Cleland, "Nanomechanical coupling between microwave and optical photons," *Nature Physics*, vol. 9, no. 11, pp. 712–716, 2013.

[65] Y.-P. Wang, G.-Q. Zhang, D. Zhang, T.-F. Li, C.-M. Hu, and J. You, "Bistability of cavity magnon polaritons," *Physical review letters*, vol. 120, no. 5, p. 057202, 2018.

[66] X. Zhang, C.-L. Zou, N. Zhu, F. Marquardt, L. Jiang, and H. X. Tang, "Magnon dark modes and gradient memory," *Nature communications*, vol. 6, no. 1, pp. 1–7, 2015.

[67] L. Bai, M. Harder, P. Hyde, Z. Zhang, C.-M. Hu, Y. Chen, and J. Q. Xiao, "Cavity mediated manipulation of distant spin currents using a cavity-magnon-polariton," *Physical Review Letters*, vol. 118, no. 21, p. 217201, 2017.

[68] B. Yao, Y. Gui, J. Rao, S. Kaur, X. Chen, W. Lu, Y. Xiao, H. Guo, K.-P. Marzlin, and C.-M. Hu, "Cooperative polariton dynamics in feedback-coupled cavities," *Nature communications*, vol. 8, no. 1, pp. 1–6, 2017.

[69] A. Osada, R. Hisatomi, A. Noguchi, Y. Tabuchi, R. Yamazaki, K. Usami, M. Sadgrove, R. Yalla, M. Nomura, and Y. Nakamura, "Cavity optomagnonics with spin-orbit coupled photons," *Physical review letters*, vol. 116, no. 22, p. 223601, 2016.

[70] Y. Tabuchi, S. Ishino, A. Noguchi, T. Ishikawa, R. Yamazaki, K. Usami, and Y. Nakamura, "Coherent coupling between a ferromagnetic magnon and a superconducting qubit," *Science*, vol. 349, no. 6246, pp. 405–408, 2015.

[71] M. A. Nielsen and I. L. Chuang, "Quantum computation and quantum information," *Phys. Today*, vol. 54, no. 2, p. 60, 2001.

[72] C. Fabre and N. Treps, "Modes and states in quantum optics," *Reviews of Modern Physics*, vol. 92, no. 3, p. 035005, 2020.

[73] R. Blatt and D. Wineland, "Entangled states of trapped atomic ions," *Nature*, vol. 453, no. 7198, pp. 1008–1015, 2008.

[74] P. Kok, W. J. Munro, K. Nemoto, T. C. Ralph, J. P. Dowling, and G. J. Milburn, "Linear optical quantum computing with photonic qubits," *Reviews of Modern Physics*, vol. 79, no. 1, p. 135, 2007.

[75] J. Clarke and F. K. Wilhelm, "Superconducting quantum bits," *Nature*, vol. 453, no. 7198, pp. 1031–1042, 2008.

[76] L. DiCarlo, J. M. Chow, J. M. Gambetta, L. S. Bishop, B. R. Johnson, D. Schuster, J. Majer, A. Blais, L. Frunzio, S. Girvin *et al.*, "Demonstration of two-qubit algorithms with a superconducting quantum processor," *Nature*, vol. 460, no. 7252, pp. 240–244, 2009.

[77] X. Li, Y. Wu, D. Steel, D. Gammon, T. Stievater, D. Katzer, D. Park, C. Piermarocchi, and L. Sham, "An all-optical quantum gate in a semiconductor quantum dot," *Science*, vol. 301, no. 5634, pp. 809–811, 2003.

[78] J. R. Petta, A. C. Johnson, J. M. Taylor, E. A. Laird, A. Yacoby, M. D. Lukin, C. M. Marcus, M. P. Hanson, and A. C. Gossard, "Coherent manipulation of coupled electron spins in semiconductor quantum dots," *Science*, vol. 309, no. 5744, pp. 2180–2184, 2005.

[79] C. Barthel, D. Reilly, C. M. Marcus, M. Hanson, and A. Gossard, "Rapid single-shot measurement of a singlet-triplet qubit," *Physical Review Letters*, vol. 103, no. 16, p. 160503, 2009.

[80] M. Fox, *Quantum optics: an introduction*. OUP Oxford, 2006, vol. 15.

[81] C. Cohen-Tannoudji, P. C. Davies, B. Diu, F. Laloe, B. Dui *et al.*, *Quantum mechanics*. John Wiley & Sons, 2019, vol. 3.

[82] R. Horodecki, P. Horodecki, M. Horodecki, and K. Horodecki, "Quantum entanglement," *Reviews of modern physics*, vol. 81, no. 2, p. 865, 2009.

[83] C. Weedbrook, S. Pirandola, R. García-Patrón, N. J. Cerf, T. C. Ralph, J. H. Shapiro, and S. Lloyd, "Gaussian quantum information," *Reviews of Modern Physics*, vol. 84, no. 2, p. 621, 2012.

[84] S. L. Braunstein and P. Van Loock, "Quantum information with continuous variables," *Reviews of modern physics*, vol. 77, no. 2, p. 513, 2005.

[85] G. Adesso, S. Ragy, and A. R. Lee, "Continuous variable quantum information: Gaussian states and beyond," *Open Systems & Information Dynamics*, vol. 21, no. 01n02, p. 1440001, 2014.

[86] G. S. Agarwal, *Quantum optics*. Cambridge University Press, 2012.

[87] R. Simon, "Peres-horodecki separability criterion for continuous variable systems," *Physical Review Letters*, vol. 84, no. 12, p. 2726, 2000.

[88] M. Horodecki, "Entanglement measures." *Quantum Inf. Comput.*, vol. 1, no. 1, pp. 3–26, 2001.

[89] P. Horodecki and R. Horodecki, "Distillation and bound entanglement." *Quantum Inf. Comput.*, vol. 1, no. 1, pp. 45–75, 2001.

[90] L.-M. Duan, G. Giedke, J. I. Cirac, and P. Zoller, "Inseparability criterion for continuous variable systems," *Physical Review Letters*, vol. 84, no. 12, p. 2722, 2000.

[91] M. B. Plenio, "Logarithmic negativity: a full entanglement monotone that is not convex," *Physical review letters*, vol. 95, no. 9, p. 090503, 2005.

[92] G. Adesso, A. Serafini, and F. Illuminati, "Extremal entanglement and mixedness in continuous variable systems," *Physical Review A*, vol. 70, no. 2, p. 022318, 2004.

[93] A. Lvovsky, R. Ghobadi, A. Chandra, A. Prasad, and C. Simon, "Observation of micro–macro entanglement of light," *Nature Physics*, vol. 9, no. 9, pp. 541–544, 2013.

[94] H. Jeong, A. Zavatta, M. Kang, S.-W. Lee, L. S. Costanzo, S. Grandi, T. C. Ralph, and M. Bellini, "Generation of hybrid entanglement of light," *Nature Photonics*, vol. 8, no. 7, pp. 564–569, 2014.

[95] B. He, M. Nadeem, and J. A. Bergou, "Scheme for generating coherent-state superpositions with realistic cross-kerr nonlinearity," *Physical Review A*, vol. 79, no. 3, p. 035802, 2009.

[96] S. Raeisi, P. Sekatski, and C. Simon, "Coarse graining makes it hard to see micro-macro entanglement," *Physical review letters*, vol. 107, no. 25, p. 250401, 2011.

[97] A. V. Sharypov and B. He, "Generation of arbitrary symmetric entangled states with conditional linear optical coupling," *Physical Review A*, vol. 87, no. 3, p. 032323, 2013.

[98] M. Chekhova, G. Leuchs, and M. Żukowski, "Bright squeezed vacuum: Entanglement of macroscopic light beams," *Optics Communications*, vol. 337, pp. 27–43, 2015.

[99] T. Eichelkraut, R. Heilmann, S. Weimann, S. Stützer, F. Dreisow, D. N. Christodoulides, S. Nolte, and A. Szameit, "Mobility transition from ballistic to diffusive transport in non-hermitian lattices," *Nature communications*, vol. 4, no. 1, pp. 1–7, 2013.

[100] H. Schomerus, "Quantum noise and self-sustained radiation of p t-symmetric systems," *Physical review letters*, vol. 104, no. 23, p. 233601, 2010.

[101] Y. Chong, L. Ge, H. Cao, and A. D. Stone, "Coherent perfect absorbers: time-reversed lasers," *Physical review letters*, vol. 105, no. 5, p. 053901, 2010.

[102] C. M. Bender, M. Gianfreda, Ş. K. Özdemir, B. Peng, and L. Yang, "Twofold transition in pt-symmetric coupled oscillators," *Physical Review A*, vol. 88, no. 6, p. 062111, 2013.

[103] X. Luo, J. Huang, H. Zhong, X. Qin, Q. Xie, Y. S. Kivshar, C. Lee *et al.*, "Pseudo-parity-time symmetry in optical systems," *Physical review letters*, vol. 110, no. 24, p. 243902, 2013.

[104] R. El-Ganainy, M. Khajavikhan, and L. Ge, "Exceptional points and lasing self-termination in photonic molecules," *Physical Review A*, vol. 90, no. 1, p. 013802, 2014.

[105] M. Teimourpour, R. El-Ganainy, A. Eisfeld, A. Szameit, and D. N. Christodoulides, "Light transport in pt-invariant photonic structures with hidden symmetries," *Physical Review A*, vol. 90, no. 5, p. 053817, 2014.

[106] S. Longhi, "Half-spectral unidirectional invisibility in non-hermitian periodic optical structures," *Optics letters*, vol. 40, no. 23, pp. 5694–5697, 2015.

[107] T. Goldzak, A. A. Mailybaev, and N. Moiseyev, "Light stops at exceptional points," *Physical review letters*, vol. 120, no. 1, p. 013901, 2018.

[108] W. Langbein, "No exceptional precision of exceptional-point sensors," *Physical Review A*, vol. 98, no. 2, p. 023805, 2018.

[109] M. Zhang, W. Sweeney, C. W. Hsu, L. Yang, A. Stone, and L. Jiang, "Quantum noise theory of exceptional point amplifying sensors," *Physical review letters*, vol. 123, no. 18, p. 180501, 2019.

[110] Z. Zhang, Y.-P. Wang, and X. Wang, "Pt-symmetry-breaking-enhanced cavity optomechanical magnetometry," *Physical Review A*, vol. 102, no. 2, p. 023512, 2020.

[111] S. Longhi, "Quantum statistical signature of pt-symmetry breaking," *Optics Letters*, vol. 45, no. 6, pp. 1591–1594, 2020.

[112] T. E. Lee, F. Reiter, and N. Moiseyev, "Entanglement and spin squeezing in non-hermitian phase transitions," *Physical review letters*, vol. 113, no. 25, p. 250401, 2014.

[113] B. He, L. Yang, Z. Zhang, and M. Xiao, "Cyclic permutation-time symmetric structure with coupled gain-loss microcavities," *Physical Review A*, vol. 91, no. 3, p. 033830, 2015.

[114] K. V. Kepesidis, T. J. Milburn, J. Huber, K. G. Makris, S. Rotter, and P. Rabl, "-symmetry breaking in the steady state of microscopic gain–loss systems," *New Journal of Physics*, vol. 18, no. 9, p. 095003, 2016.

[115] Y.-L. Liu, R. Wu, J. Zhang, Ş. K. Özdemir, L. Yang, F. Nori, and Y.-x. Liu, "Controllable optical response by modifying the gain and loss of a mechanical resonator and cavity mode in an optomechanical system," *Physical Review A*, vol. 95, no. 1, p. 013843, 2017.

[116] T. Yu and J. Eberly, "Finite-time disentanglement via spontaneous emission," *Physical Review Letters*, vol. 93, no. 14, p. 140404, 2004.

[117] ——, "Sudden death of entanglement," *Science*, vol. 323, no. 5914, pp. 598–601, 2009.

[118] A. Stahlhofen and G. Nimtz, "Evanescent modes are virtual photons," *EPL (Europhysics Letters)*, vol. 76, no. 2, p. 189, 2006.

[119] Z.-Y. Wang, C.-D. Xiong, and B. He, "Alternative perspective on photonic tunneling," *Physical Review A*, vol. 75, no. 1, p. 013813, 2007.

[120] P. M. Becker, A. A. Olsson, and J. R. Simpson, *Erbium-doped fiber amplifiers: fundamentals and technology*. Elsevier, 1999.

[121] H. J. Carmichael, *Statistical methods in quantum optics 2: Non-classical fields*. Springer Science & Business Media, 2009.

[122] G. Agarwal and S. Huang, "Strong mechanical squeezing and its detection," *Physical Review A*, vol. 93, no. 4, p. 043844, 2016.

[123] G. B. Arfken and H.-J. Weber, *Mathematical methods for physicists*. Academic Press, San Diego, 2006.

[124] V. D'Auria, S. Fornaro, A. Porzio, S. Solimeno, S. Olivares, and M. Paris, "Full characterization of gaussian bipartite entangled states by a single homodyne detector," *Physical review letters*, vol. 102, no. 2, p. 020502, 2009.

[125] C. Henkel, "Laser theory in manifest lindblad form," *Journal of Physics B: Atomic, Molecular and Optical Physics*, vol. 40, no. 12, p. 2359, 2007.

[126] J. Wen, X. Jiang, M. Zhang, L. Jiang, S. Hua, H. Wu, C. Yang, and M. Xiao, "Modeling of on-chip optical nonreciprocity with an active microcavity," in *Photonics*, vol. 2, no. 2. Multidisciplinary Digital Publishing Institute, 2015, pp. 498–508.

[127] X. Jiang, C. Yang, H. Wu, S. Hua, L. Chang, Y. Ding, Q. Hua, and M. Xiao, "On-chip optical nonreciprocity using an active microcavity," *Scientific reports*, vol. 6, p. 38972, 2016.

[128] B. He, L. Yang, X. Jiang, and M. Xiao, "Transmission nonreciprocity in a mutually coupled circulating structure," *Physical review letters*, vol. 120, no. 20, p. 203904, 2018.

[129] D. R. Barton III, H. Alaeian, M. Lawrence, and J. Dionne, "Broadband and wide-angle nonreciprocity with a non-hermitian metamaterial," *Physical Review B*, vol. 97, no. 4, p. 045432, 2018.

[130] S. Sunada, "Enhanced response of non-hermitian photonic systems near exceptional points," *Physical Review A*, vol. 97, no. 4, p. 043804, 2018.

[131] M. Teimourpour, A. Rahman, K. Srinivasan, and R. El-Ganainy, "Non-hermitian engineering of synthetic saturable absorbers for applications in photonics," *Physical review applied*, vol. 7, no. 1, p. 014015, 2017.

[132] Y. F. Xie, Z. Cao, B. He, and Q. Lin, "Pt-symmetric phonon laser under gain saturation effect," *Optics Express*, vol. 28, no. 15, pp. 22 580–22 593, 2020.

[133] W. T. Silfvast, *Laser fundamentals*. Cambridge university press, 2004.

[134] M. O. Scully and M. S. Zubairy, *Quantum optics*. Cambridge University Press, 1999.

[135] H. J. Carmichael, *Statistical methods in quantum optics 1: master equations and Fokker-Planck equations*. Springer Science & Business Media, 2013.

[136] W. P. Schleich, *Quantum optics in phase space*. John Wiley & Sons, 2011.

[137] L. Cohen, "Time-frequency distributions-a review," *Proceedings of the IEEE*, vol. 77, no. 7, pp. 941–981, 1989.

[138] D. Dragoman, "Applications of the wigner distribution function in signal processing," *EURASIP Journal on Advances in Signal Processing*, vol. 2005, no. 10, p. 264967, 2005.

[139] V. Veitch, C. Ferrie, D. Gross, and J. Emerson, "Negative quasi-probability as a resource for quantum computation," *New Journal of Physics*, vol. 14, no. 11, p. 113011, 2012.

[140] V. Veitch, N. Wiebe, C. Ferrie, and J. Emerson, "Efficient simulation scheme for a class of quantum optics experiments with non-negative wigner representation," *New Journal of Physics*, vol. 15, no. 1, p. 013037, 2013.

[141] A. Mari and J. Eisert, "Positive wigner functions render classical simulation of quantum computation efficient," *Physical review letters*, vol. 109, no. 23, p. 230503, 2012.

[142] M. G. Paris, F. Illuminati, A. Serafini, and S. De Siena, "Purity of gaussian states: Measurement schemes and time evolution in noisy channels," *Physical Review A*, vol. 68, no. 1, p. 012314, 2003.

[143] S. Vashahri-Ghamsari, B. He, and M. Xiao, "Continuous-variable entanglement generation using a hybrid pt-symmetric system," *Physical Review A*, vol. 96, no. 3, p. 033806, 2017.

[144] A. Mostafazadeh, "Pseudo-hermiticity versus pt symmetry: the necessary condition for the reality of the spectrum of a non-hermitian hamiltonian," *Journal of Mathematical Physics*, vol. 43, no. 1, pp. 205–214, 2002.

[145] S. Sunada, "Enhanced response of non-hermitian photonic systems near exceptional points," *Physical Review A*, vol. 97, no. 4, p. 043804, 2018.

[146] J. B. Khurgin, "Phonon lasers gain a sound foundation," *Physics*, vol. 3, p. 16, 2010.

[147] J. Zhang, B. Peng, Ş. K. Özdemir, K. Pichler, D. O. Krimer, G. Zhao, F. Nori, Y.-x. Liu, S. Rotter, and L. Yang, "A phonon laser operating at an exceptional point," *Nature Photonics*, vol. 12, no. 8, pp. 479–484, 2018.

[148] I. S. Grudinin, H. Lee, O. Painter, and K. J. Vahala, "Phonon laser action in a tunable two-level system," *Physical review letters*, vol. 104, no. 8, p. 083901, 2010.

[149] Y. Jiang, S. Maayani, T. Carmon, F. Nori, and H. Jing, "Nonreciprocal phonon laser," *Physical Review Applied*, vol. 10, no. 6, p. 064037, 2018.

[150] I. Mahboob, K. Nishiguchi, A. Fujiwara, and H. Yamaguchi, "Phonon lasing in an electromechanical resonator," *Physical review letters*, vol. 110, no. 12, p. 127202, 2013.

[151] A. Kent, R. Kini, N. Stanton, M. Henini, B. Glavin, V. Kochelap, and T. Linnik, "Acoustic phonon emission from a weakly coupled superlattice under vertical electron transport: observation of phonon resonance," *Physical review letters*, vol. 96, no. 21, p. 215504, 2006.

[152] A. H. Safavi-Naeini, T. M. Alegre, J. Chan, M. Eichenfield, M. Winger, Q. Lin, J. T. Hill, D. E. Chang, and O. Painter, "Electromagnetically induced transparency and slow light with optomechanics," *Nature*, vol. 472, no. 7341, pp. 69–73, 2011.

[153] J. Huang, Y. Li, L. K. Chin, H. Cai, Y. Gu, M. F. Karim, J. Wu, T. Chen, Z. Yang, Y. Hao *et al.*, "A dissipative self-sustained optomechanical resonator on a silicon chip," *Applied Physics Letters*, vol. 112, no. 5, p. 051104, 2018.

[154] P. Rabl, "Photon blockade effect in optomechanical systems," *Physical review letters*, vol. 107, no. 6, p. 063601, 2011.

[155] T. P. Purdy, P.-L. Yu, R. Peterson, N. Kampel, and C. Regal, "Strong optomechanical squeezing of light," *Physical Review X*, vol. 3, no. 3, p. 031012, 2013.

[156] R. W. Andrews, R. W. Peterson, T. P. Purdy, K. Cicak, R. W. Simmonds, C. A. Regal, and K. W. Lehnert, "Bidirectional and efficient conversion between microwave and optical light," *Nature Physics*, vol. 10, no. 4, pp. 321–326, 2014.

[157] T. Bagci, A. Simonsen, S. Schmid, L. G. Villanueva, E. Zeuthen, J. Appel, J. M. Taylor, A. Sørensen, K. Usami, A. Schliesser *et al.*, "Optical detection of radio waves through a nanomechanical transducer," *Nature*, vol. 507, no. 7490, pp. 81–85, 2014.

[158] L. Fan, K. Y. Fong, M. Poot, and H. X. Tang, "Cascaded optical transparency in multimode-cavity optomechanical systems," *Nature communications*, vol. 6, no. 1, pp. 1–6, 2015.

[159] K. M. Krishnan, *Fundamentals and applications of magnetic materials*. Oxford University Press, 2016.

[160] B. Lenk, H. Ulrichs, F. Garbs, and M. Münzenberg, "The building blocks of magnonics," *Physics Reports*, vol. 507, no. 4-5, pp. 107–136, 2011.

[161] A. V. Chumak, V. I. Vasyuchka, A. A. Serga, and B. Hillebrands, "Magnon spintronics," *Nature Physics*, vol. 11, no. 6, pp. 453–461, 2015.

[162] H. Huebl, C. W. Zollitsch, J. Lotze, F. Hocke, M. Greifenstein, A. Marx, R. Gross, and S. T. Goennenwein, "High cooperativity in coupled microwave resonator ferrimagnetic insulator hybrids," *Physical Review Letters*, vol. 111, no. 12, p. 127003, 2013.

[163] X. Zhang, C.-L. Zou, L. Jiang, and H. X. Tang, "Strongly coupled magnons and cavity microwave photons," *Physical review letters*, vol. 113, no. 15, p. 156401, 2014.

[164] M. Goryachev, W. G. Farr, D. L. Creedon, Y. Fan, M. Kostylev, and M. E. Tobar, "High-cooperativity cavity qed with magnons at microwave frequencies," *Physical Review Applied*, vol. 2, no. 5, p. 054002, 2014.

[165] D. Zhang, X.-M. Wang, T.-F. Li, X.-Q. Luo, W. Wu, F. Nori, and J. You, "Cavity quantum electrodynamics with ferromagnetic magnons in a small yttrium-iron-garnet sphere," *npj Quantum Information*, vol. 1, no. 1, pp. 1–6, 2015.

[166] G.-Q. Zhang and J. You, "Higher-order exceptional point in a cavity magnonics system," *Physical Review B*, vol. 99, no. 5, p. 054404, 2019.

[167] J. Haigh, S. Langenfeld, N. Lambert, J. Baumberg, A. Ramsay, A. Nunnenkamp, and A. Ferguson, "Magneto-optical coupling in whispering-gallery-mode resonators," *Physical Review A*, vol. 92, no. 6, p. 063845, 2015.

[168] X. Zhang, N. Zhu, C.-L. Zou, and H. X. Tang, "Optomagnonic whispering gallery microresonators," *Physical review letters*, vol. 117, no. 12, p. 123605, 2016.

[169] J. Haigh, A. Nunnenkamp, A. Ramsay, and A. Ferguson, "Triple-resonant brillouin light scattering in magneto-optical cavities," *Physical Review Letters*, vol. 117, no. 13, p. 133602, 2016.

[170] D. Lachance-Quirion, Y. Tabuchi, S. Ishino, A. Noguchi, T. Ishikawa, R. Yamazaki, and Y. Nakamura, "Resolving quanta of collective spin excitations in a millimeter-sized ferromagnet," *Science advances*, vol. 3, no. 7, p. e1603150, 2017.

[171] J. Li, S.-Y. Zhu, and G. Agarwal, "Magnon-photon-phonon entanglement in cavity magnomechanics," *Physical Review Letters*, vol. 121, no. 20, p. 203601, 2018.

[172] ——, "Squeezed states of magnons and phonons in cavity magnomechanics," *Physical Review A*, vol. 99, no. 2, p. 021801, 2019.

[173] C. Kong, B. Wang, Z.-X. Liu, H. Xiong, and Y. Wu, "Magnetically controllable slow light based on magnetostrictive forces," *Optics express*, vol. 27, no. 4, pp. 5544–5556, 2019.

[174] K.-J. Boller, A. Imamoğlu, and S. E. Harris, "Observation of electromagnetically induced transparency," *Physical Review Letters*, vol. 66, no. 20, p. 2593, 1991.

[175] S. Weis, R. Rivière, S. Deléglise, E. Gavartin, O. Arcizet, A. Schliesser, and T. J. Kippenberg, "Optomechanically induced transparency," *Science*, vol. 330, no. 6010, pp. 1520–1523, 2010.

[176] M. Wang, D. Zhang, X.-H. Li, Y.-Y. Wu, and Z.-Y. Sun, "Magnon chaos in *pt*-symmetric cavity magnomechanics," *IEEE Photonics Journal*, vol. 11, no. 3, pp. 1–8, 2019.

[177] D. Zhang, X.-Q. Luo, Y.-P. Wang, T.-F. Li, and J. You, "Observation of the exceptional point in cavity magnon-polaritons," *Nature communications*, vol. 8, no. 1, pp. 1–6, 2017.

Publications Published and Planned

Chapter 2:

- Saeid Vashahri-Ghamsari, B. He, and M. Xiao, "Continuous-variable entanglement generation using a hybrid $\mathscr{P}\mathscr{T}$-symmetric system", *Phys. Rev. A,* **96** 033806 (2017)

Chapter 3:

- Saeid Vashahri-Ghamsari, B. He, and M. Xiao,"Effects of gain saturation on the quantum properties of light in a non-Hermitian gain-loss coupler", *Phys. Rev. A,* **99** 023819 (2019)

Chapter 4:

- Saeid Vashahri-Ghamsari, Q. Lin, B. He, and M. Xiao, "Magnomechanical phonon laser beyond the steady-state approximation", (in preparation)